JOURNAL OF GEOMAGNETISM AND GEOELECTRICITY

VOL. III NO. 3-4

SOCIETY
OF
TERRESTRIAL MAGNETISM AND ELECTRICITY
OF
JAPAN

DEC. 1951

KYOTO

JOURNAL OF GEOMAGNETISM AND GEOELECTRICITY

The fields of interest of this quarterly Journal are as follows:

Terrestrial Magnetism	Aurora and Night Sky
Atmospheric Electricity	The Ozone Layer
The Ionosphere	Physical States of the Upper Atmosphere
Radio Wave Propagation	Solar Phenomena relating to the above Subjects
Cosmic Rays	Electricity within the Earth

The text should be written in English, German or French. The price is provisionally set as 180 yen per copy subject to change. We hope to exchange this Journal with periodical publications of any kind in the field of natural science.

The editor.

EDITORIAL OFFICE: Society of Terrestrial Magnetism and Electricity,
Geophysical Institute, Kyoto University, Japan

EDITORIAL STAFF: M. OTA and S. MATSUSHITA (Kyoto University)

Magnetic Susceptibility of Ferromagnetic Minerals Contained in Igneous Rocks.*

By Syun-iti AKIMOTO
Geophysical Institute, Tokyo University

Abstract

The thermal change in susceptibility of ferromagnetic mineral grains separated from igneous rocks was measured by a ballistic method in a weak magnetic field. The thermal change of susceptibility was classified into four types. These types were discussed in connection with the condition under which the original rock was formed. The dependency of the Curie-point and the magnitude of the susceptibility upon the chemical constitution was examined, the content of TiO_2 in ferromagnetic mineral being especially taken into account. Besides, the relation between the magnitude of susceptibility and the grain size was obtained from the viewpoint of the magnetic property of small particles.

§ 1. *Introduction*

The magnetic properties of igneons rocks have been examined fairly in detail by a number of investigators (1), (2), (3), (4), (5), (6), especially in connection with the local geomagnetic anomalies and their changes. The magnetic properties of rocks, however, are due to those of ferromagnetic minerals contained in them, the other minerals scarcely contributing to the magnetism of rocks. In other words, the magnetism of rocks is composed of the ensemble of magnetization of small grains of rock-forming ferromagnetic minerals. So that the fundamental problem in rock-magnetism will be the general description of rock-forming ferromagnetic minerals from the physical standpoint in reference to their chemical and mineralogical characteristics.

In the present study, the change with the temperature in magnetic susceptibility of rock-forming ferromagnetic minerals, which were separated from various kinds of mother igneous rocks, was measured, and the results were analysed in relation to the chemical composition, grain size and mineralogical characteristics of these grains of minerals. The aims of the present study are chiefly the following two.

(1) The natural ferromagnetic minerals contained in igneous rocks are generally of chemicel constitution different from a pure stoicheometric magnetite. It will be significant, therefore, to find the relations of the Curie-point and the magnitude of susceptibility to the chemical composition.

(2) On the other hand, it has been expected that the dimensions of grains play an important role upon the magnetic properties such as initial permeability and

---

* Contribution from Division of Geomagnetism and Geoelectricity, Geophysical Institute, Tokyo University. Series II. No. 20.

Table 1

No.	Locality	Petrological Descripion	Grain Size	Fe_2O_3+FeO	TiO_2
1	Niizima	Phenocryst magnetite in biotite liparie	410μ	63.01 31.46%	4.06 (*4.06)%
2	Lava in Asigara layer	Phenocryst magnetite in hyp. horn. dacite	130	67.60	10.81(13.73)
3	Zyobosi volc. Ito	Groundmass magnetite in olivine basalt	53	56.66	14.44(20.08)
4	Simohutagoyama, Hakone	Phenocryst magnetite in hyp. aug. andesite	120	75.80	10.86(12.46)
5	Kaziya Yugawara	Phenocryst magnetite in hyp. dacite	140	74.44	10.24(12.08)
6	Yugawara	Phenocryst magnetite in aug. hyp. andesite	130	69.84	8.73(11.05)
7	Karataki, Hakone	Phenocryst magnetite in aug. hyp. andesite	110	75.71	12.17(13.79)
8	Hiroawara	Phenocryst magnetite in aug. bearing hyp. dacite	130	83.28	11.40(12.02)
9	Odawara	Phenocryst magnetite in pumice	280	88.13	6.43(6.79)
10	Taga volc.	Phenocryst magnetite in oliv. aug. hyp. andesite	200	75.60	10.73(12.34)
11	Haruna volc.	Phenocryst magnetite in hyp. horn. dacite pumice	390	53.15 31.93	6.82(7.33)
12	Sukumogawa Hakone	Groundmass magnetite in andesite	43	65.05	16.59(20.18)
13	Okata Oosima	Groundmass magnetite in tholeiite	63	47.19 33.71	17.20(17.20)
14	Taga volc.	Groundmass magnetite in olivine basalt	46	36.03 43.89	18.02(18.02)
15	Taga volc.	Groundmass magnetite in oliv. aug. hyp. andesite	29	49.01	9.26(15.79)

* This value was calculated as 100% in total.

coercive force. (7) Since the grain sizes of those specimens which were dealt with in the present study range over some extent, the relation between the initial susceptibitity and the grain size was also examined.

§ 2. *Specimens*

The specimens examined here are 15 in total and each of them is the magnetite grains, petrologically so-called for the sake of simplicity, separated by an electromagnetic separator from original igneous rocks which were collected from volcanic localities in Kwanto District of Japan. The mean diameters of 50 grains of each sample were measured by means of a microscope. The result shows that the grain sizes vary from about 30μ to 400μ, the discrepancy depending on either they appear as phenocrysts or as microcrystals in groundmass in the original rocks. Their grain sizes. states of appearance in rocks and localities are shown in Table 1 together with the chemical constitutions which were analysed by I. Iwasaki and his colaborator. (3)

As will be assumed from the date of the chemical composition shown in

Θ_{a1}	Θ_{a2}	$\chi_{(T-20°C)}$	χ_0
575°C		9.66	9.66
565		7.41	8.21
455	320°C	2.72	3.28
570	520	4.27	4.47
600	390	5.18	5.70
530	440	6.60	7.31
500	420	6.70	7.54
540	450	7.84	8.70
580	450	4.22	4.35
550	460	5.44	5.80
570	540	7.67	7.72
580		2.39	2.96
580		1.29	1.54
500	400	1.36	1.67
550	450	1.74	2.24

this table, the ferromagnetic minerals concerned here are the ferromagnetic ferrites chiefly composed of FeO, Fe_2O_3 and TiO_2.

The petrological research of the original igneous rocks has been carried out by H. Kuno chiefly from a standpoint of analysis of pyroxenes contained in them. (9) According to his opinion, No. 1 and No. 2 specimens in Table 1 are the magnetite-grains in those rocks which were cooled slowly from a low temperature, being kept in the complete equilibrium, while No. 12, No. 13, No. 14 and No. 15 specimens are the magnetite-grains in those rocks which were cooled rapidly from a relatively high temperature and No. 4, No. 5, No. 6, No. 7, No. 8, No, 9, No. 10 and No. 11 specimens are the magnetite-grains in those rocks, the character of which lies between the above two cases.

§ 3. *Apparatus*

The apparatus for measuring the thermal change of the magnetic susceptibility of ferromagnetic mineral grains in a weak field is the same in its principle as that used in the previous studies upon igueous rock samples. (3), (4), (6) i.e. the maguetization of specimen was measured, by a ballistic method, at any temperature in a weak magnetic field a few times as much as that of geomagnetic field.

The test specimens were packed into a silica tube 3mm in inner diameter and 10cm in length. In the case of measuring the magnetization of the ferromagnetic minerals, the demagnetizing field is practically negligible in comparison with the applied magnetic field. The electric furnrce is a non-inductive and non-magnetic vacuum furnace, the air pressure in the furnace being always kept less than 1mm of mercury.

§ 4. *The Susceptibility-Temperature Curves*

The specimens were heated up to about 650°C in a vacuum furnace and then cooled down to the room temperature at the rate of 200°C/hour. During these processes, the change in specific magnetic susceptibility, χ, with temperature, T, was measured at every 20°C by means of the above mentioned apparatus in a weak field. The applied magnetic field in these experiments is 1.35 Oe in most cases except a few examples.

The results of these measurements are illustrated in Fig. 1. As will be seen

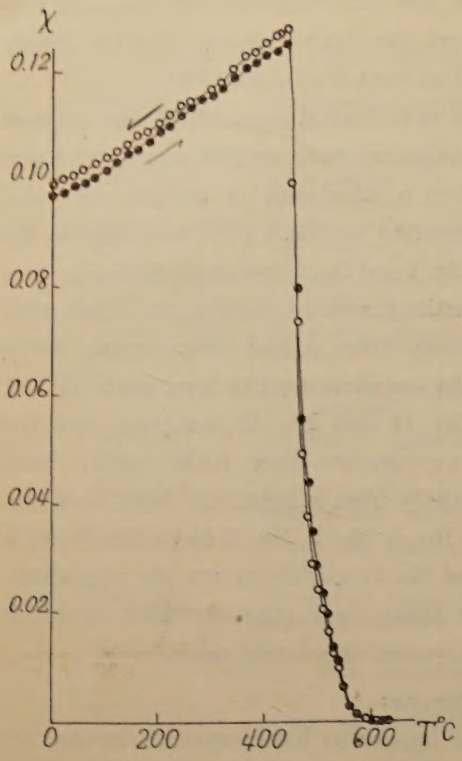

Fig. 1 No. 1 H=1.13 Oe

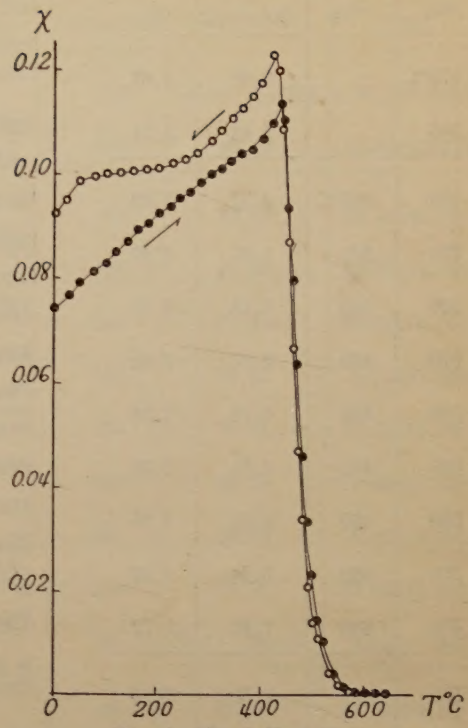

Fig. 1 No. 2 H=1.35 Oe

in this figure, the mode of thermal change of susceptibility of ferromagnetic minerals is similar so much to the previous results in the cases of the igneous rocks. It seems that there are four types of the mode of the thermal change of susceptibility. The first type is that the magnitude of susceptibility has a fairly large value and in heating

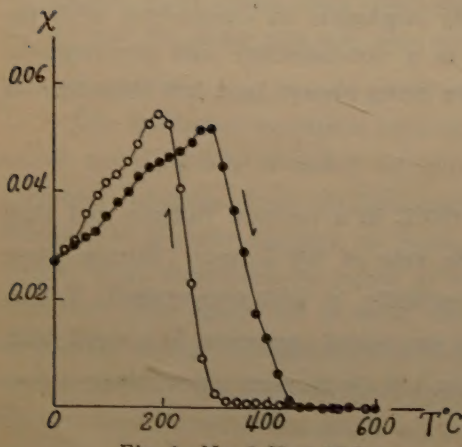

Fig. 1 No. 3 H=1.35 Oe

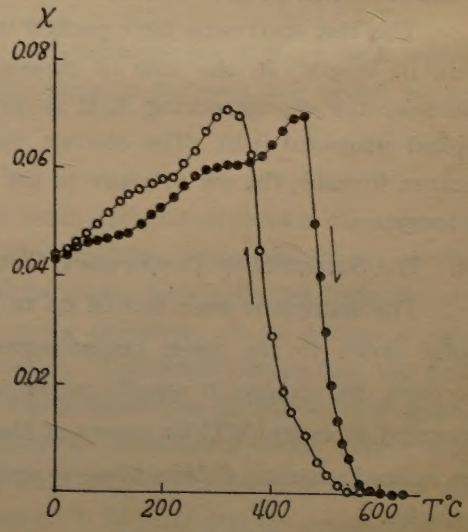

Fig. 1 No. 4 H=1.35 Oe

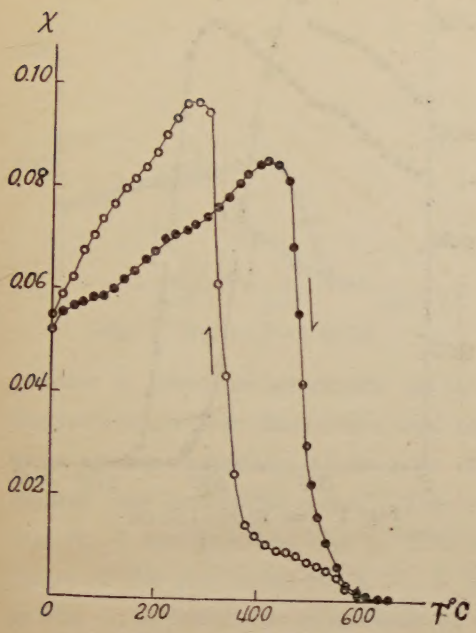

Fig. 1 No. 5 H=1.35 Oe

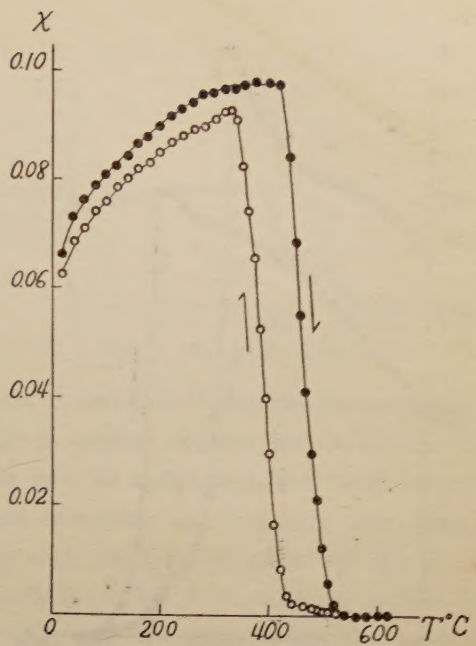

Fig. 1 No. 6 H=1.35 Oe

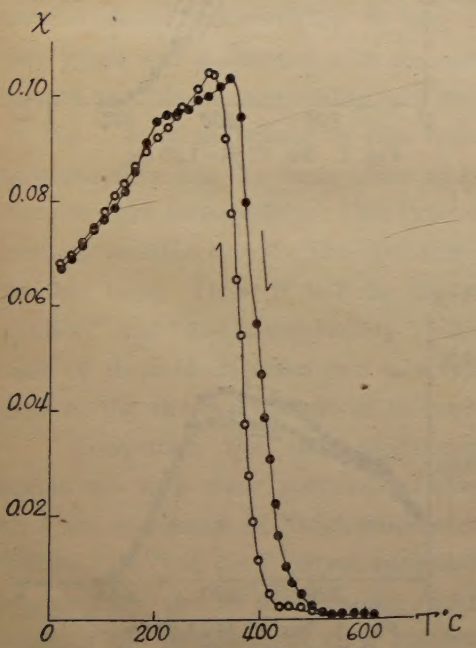

Fig. 1 No. 7 H=1.35 Oe

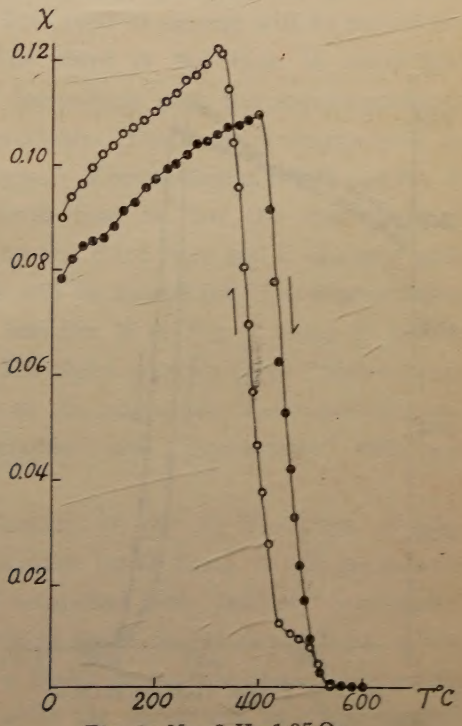

Fig. 1 No. 8 H=1.35 Oe

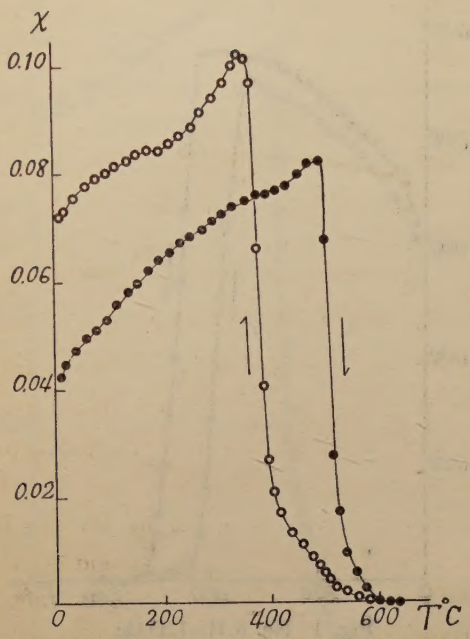

Fig. 1 No. 9 H=1.35 Oe

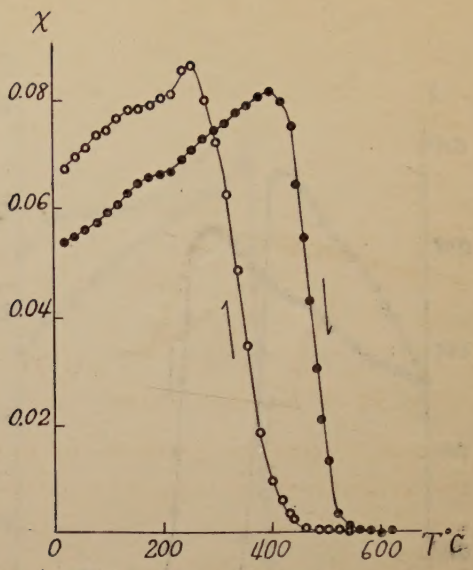

Fig. 1 No. 10 H=1.35 Oe

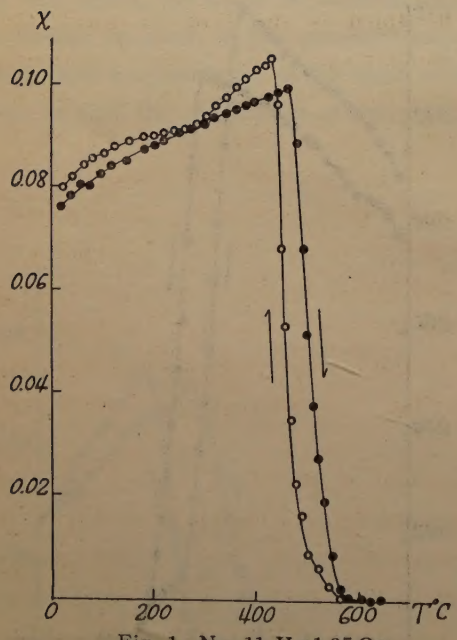

Fig. 1 No. 11 H=1.35 Oe

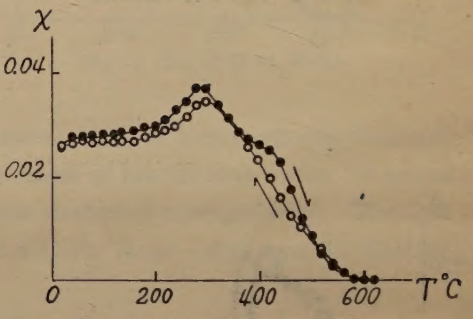

Fig. 1 No. 12 H=1.35 Oe

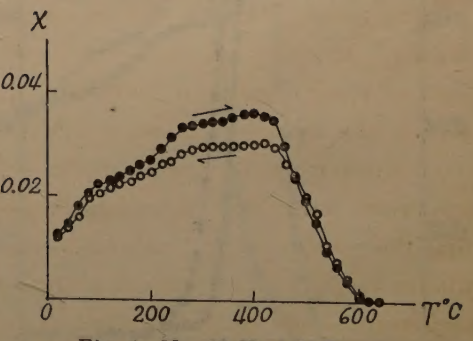

Fig. 1 No. 13 H=1.80 Oe

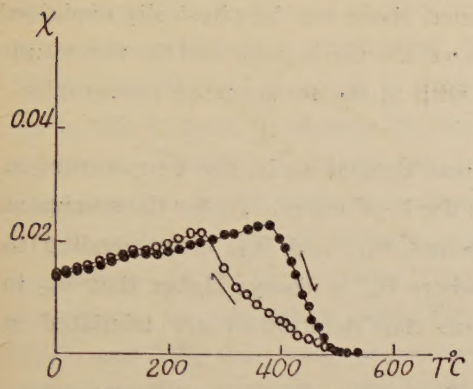

Fig. 1 No. 14 H=1.35 Oe

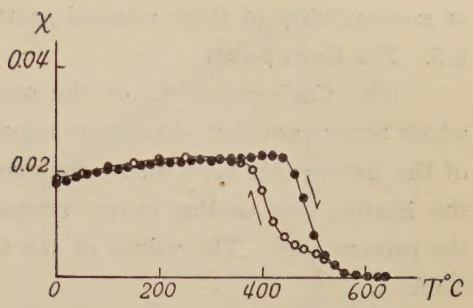

Fig. 1 No. 15 H=1.58 Oe

process it increases gradually up to about 450°C and then decreases abruptly until the ferromagnetism disappears, and the change in cooling process follows almost the same curve reversibly. This type of change will be called here the "high-susceptibility and reversible type." The specimens belonging to this type are No. 1 and No. 2 specimens in Fig. 1. The second is such the type as given by the $\chi-T$ curve of the specimens No. 3, No. 4, No. 5, No. 6, No. 7, No. 8, No. 9, No. 10 and No. 11 in Fig- 1, in which the magnitude of susceptibility has the same order of its value as the first type and the change in heating process is similar to that of the first type but the cooling curve differs distinctly from the heating one, and besides in re-heating and re-cooling processes the susceptibility changes reversibly along the same curve as that in the previous cooling curve. This type of change will be named the "high-susceptibility and irreversible type." The third is the type in which the magnitude of susceptibility is very small in comparison with the above-mentioned two types and it changes with temperature reversibly. This type of change will be named the "low-susceptibility and reversible type." The specimens No. 12 and No. 13 in Fig. 1 seem to belong to this type. The forth type is that the magnitude of susceptibility has the same order of its value as the third type and it changes with temperature irreversibly. This type of change will be named the "low-susceptibility and irreversible type." The specimens No. 14 and No. 15 in Fig. 1 seem to belong to this type. Thus, it will be summarized that there are two types "high-susceptibility" and "low-susceptibility" with respect to the magnitude of susceptibility and each of them is classified into two types "reversible" and "irreversible" with respect to the thermal change of susceptibility.

Comparing the above-mentioned classification of the $\chi-T$ curves of the specimens with their petrological classification made by H. Kuno, it will be noticed that the specimens of "high-susceptibility and reversible type" and of "low-susceptibility type" of $\chi-T$ curves correspond exactly to those cooled slowly from a low temperature and to those cooled rapidly from a high temperature respectively at the stage of the formation of their mother rocks, while the specimens of "high-susceptibility and irreversible type" correspond to those of petrologically intermediate type mentioned in § 2.

It seems that the correspondence mentioned above can be physically explained by taking into consideration the characteristics of the Curie-point and the magnitude of susceptibility of these mineral grains dealt with in the forthcoming paragraphs.

§ 5. *The Curie-points*

The Curie-point, Θ_a, of the specimens was defined to be the temperature at which ferromagnetism disappears apparently in the $\chi-T$ curve. As for the specimens of the irreversible type, there are two Curie-points, Θ_{a1}, and Θ_{a2}, corresponding to the heating and cooling curves respectively, where Θ_{a1} is always higher than Θ_{a2} in the present case. The values of the Curie-points thus determined are tabulated in Table 1.

The Curie-point is a physical constant of each ferromagnetic material. The Curie-point of pure magnetite, for example, has been determined to be at about 580°C. When FeO or TiO_2 makes a solid solution with Fe_3O_4, some amounts of decrease in the Curie-point will be observed. In order to examine the relation between the Curie-point and the chemical constitution of the specimens, Θ_a of fifteen specimens were plotted against the content of TiO_2 in them in Fig. 2. In the case of the irreversible type specimens, Θ_{a2} was taken as Θ_a, since it may be the more stable and consequently significant Curie-point. It will be seen in Fig. 2 that the Curie-point of the four reversible type specimens is always around 580°C and does not change with the content of TiO_2, while the Θ_{a2} of the irreversible type specimens decreases as the content of TiO_2 increases.

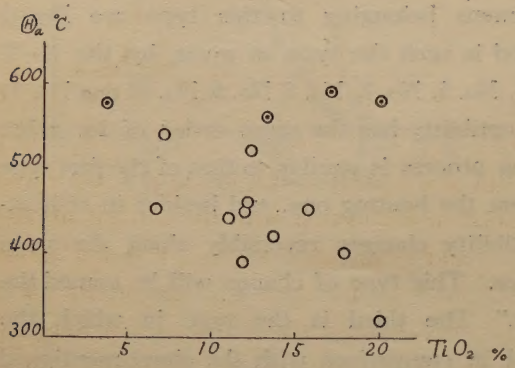

Fig. 2
◉ reversible type specimen
○ irreversible type specimen

The typical each two specimens among the two groups of the specimens of "reversible" and "irreversible" types were chemically separated into ferric and ferrous oxides and titan oxide. They are No. 1 and No. 13 in the "reversible" type specimens, and No. 11 and No. 14 in the "irreversible" type ones, the contents of FeO, Fe_2O_3 and TiO_2 in them being given in Table 1. In the two typical specimens of the "reversible" type, these three kinds of metalic oxides can be interpreted to compose FeO. Fe_2O_3 (magnetite) and FeO. TiO_2 (ilmenite) with very little excess. On the other hand, those of the two specimens of the "irreversible" type show a fair amount of FeO as an excess in the above-mentioned calculation of Norm of magnetite and ilmenite.

It may be assumed that the ferromagnetism of the "reversible" type specimens is practically that of magnetite alone, because the magnetism of ilmenite, which may simply be mixed with magnetite in this case, is far feebler compared with that of magnetite, tht Curie-point being kept around 580°C regardless of the content of ilmenite.

Fig. 3 shows $\chi-T$ curve of an artificial magnetite, where the Curie-point is 580°C, and the $\chi-T$ curve is reversible with respect to change in temperature. This $\chi-T$ curve can be considered to be the standard curve of small grain sample of almost pure magnetite. In the "irreversible" type specimens, on the other hand, FeO, Fe_2O_3 and TiO_2 may compose complex ferromagnetic minerals considerably different from a pure magnetite and consequently the Curie-point decreases with the increase in the apparent content of TiO_2.

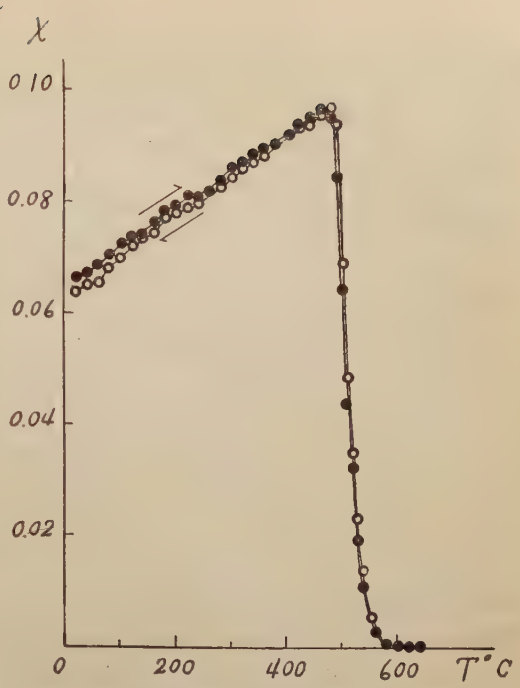

Fig. 3 H=1.35 Oe

§ 6. *Magnitude of susceptility*

It will be noticed that the specimens given in Fig. 1 have a wide variety of the magnitude of χ at room temperature. For the purpose of studying the effects of impurity and grain size upon the magnitude of χ, the values of χ at the room temperature were examined in connection with the content of TiO_2 and grain size, the result being shown in Fig. 4. That the magnitude of χ decreases as the grains become finer and as the content of TiO_2 increases will be fairly conceivable from the result given in this figure. However, there is also a close relation between the grain size and the TiO_2 content as will be seen in Fig. 4. Therefore, it becomes necessary to examine independently the dependency of the magnitude of χ on the above-mentioned two quantities. First, the dependency of χ on grain size was experimentally examined under the condition that the content of TiO_2 is kept constant. It has been already known that the initial permeability becomes smaller as the dimensions of the grains are diminished, since several experiments upon this subject have been reported.(10), (11) In the present study, the specimen No. 1, having the largest grain size, was pulverized into the smaller grains successively, and the susceptibility of their each step of grain size was measured. The results are shown in Fig. 5 together with those of the same test in an artificial magnetite and of R. Chevallier and S. Mathieu's similar work upon hematite. These three experiments

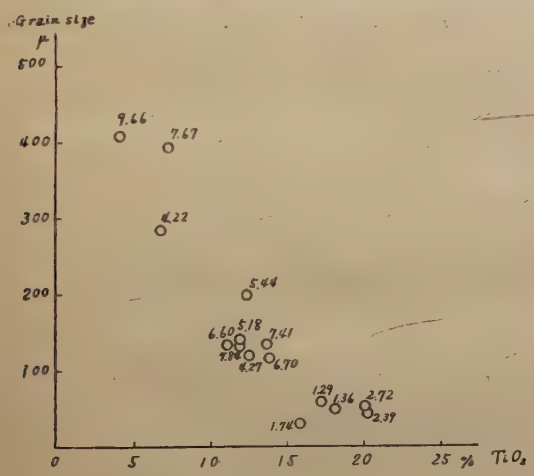

Fig. 4

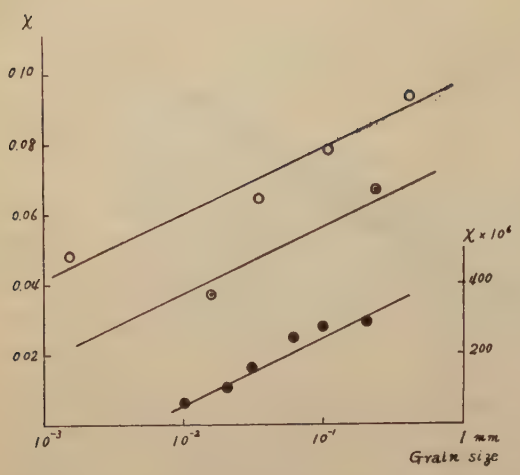

Fig. 5

may be considered to show nearly the same relation between the susceptibility and grain size. As the dimensions of the particle are diminished, the relative contribution of the various energy terms to the total energy are changed.(7) The wall energy of the boundary surfaces between domains is a surface energy and the magnetostatic energy is a volume energy, being proportional to r^2 and r^3 respectively, where r is the linedr dimension of representative grains.

For the small value of r, then, the surface energy becomes more dominant than the volume energy. Therefore, for the purpose of minimizing the total energy, the total area of the walls must decrease at the expense of the increase of volume energy. The magnetization change in a weak field is considered to be due to the reversible wall displacement, so that it is expected theoretically that the initial permeability becomes lower as the particle becomes smaller. The experimental results shown in Fig. 5 are considered to coincide with the above-mentioned theoretical expectation.

Now, the observed magnitude of χ of the fifteen specimens is plotted against the corresponding grain size in Fig. 6. It is obvious in this figure that the decreases of χ with the decrease of grain size is more rapid than that expected from the result given by Fig. 5. This fact will suggest that there is some other effect controlling the magnitude of susceptibility, which may be attributed to the content of TiO_2.

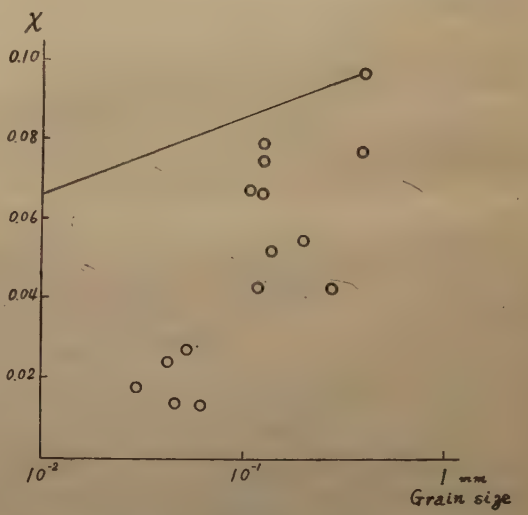

Fig. 6

It may be approximately assumed that the magnetic susceptibility, χ, of the ferrites of grain size, s, can be expressed by

$$\chi = \chi_0 \, g(s)$$

where $g(s)$ is the size factor, varying only with the size of grain, while χ_0 denotes the susceptibility of the material having a standard dimension. The functional form of $g(s)$ is given by the curve shown in Fig. 5. Then, the observed magnitude of χ was normalized by means of the above relation with respect to the grain size, where the standard dimension was taken to be 410μ in diameter i.e. the mean diameter of

the specimen No. 1.

The values of χ_0 thus obtained were plotted against the content of TiO_2 in Fig. 7. From these results it may be summarized that the magnitude of initial susceptibility depends on the content of TiO_2, the former decreasing with the increase of the latter. In the case of the reversible type specimens in which TiO_2 is assumed to appear chiefly as ilmenite, the effect of TiO_2 upon χ_0 may chiefly result from the change in the content of Fe_3O_4 in them. On the other hand, in the irreversible type specimens in which the Curie-point decreases with the increase of the content of TiO_2 and TiO_2 was assumed to be dissolved into Fe_3O_4 and to be present in a complex ferromagnetic mixed-crystal, the effect of TiO_2 upon χ_0 may be chiefly due to the magnetic property peculiar to that mixed-crystal itself.

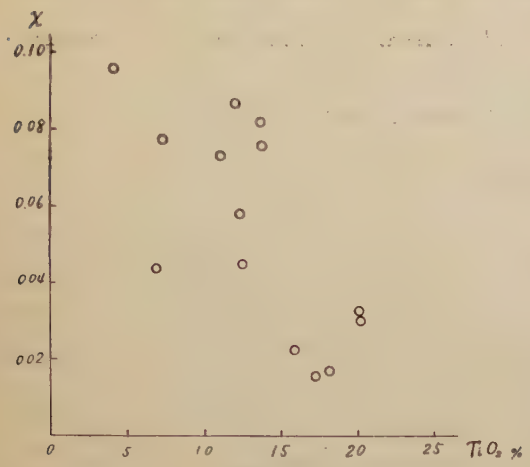

Fig. 7

§ 7. *Conclusion*

From the experimental facts obtained in the present study, the chemical constituion may be considered to play an important role on the magnetic properties, especially on the Curie-point and the initial susceptibility of the ferromagnetic minerals, though they used to be called simply "magnetite" in the broad sense of the word in petrology. The grain size seems to influence the rather secondary effect upon the magnitude of susceptibility.

The reversible and irreversible properties of the thermal change of susceptibility also seem to be closely connected with the condition under which the original rock was formed from an original magna.

If such problems as mentioned above are resolved completely in the future, it could make a contribution not only to geomagnetism but also to petrology.

In concluding this paper, the writer wishes to express his sincere thanks to Dr. T. Nagata for his detailed direction throughout this study, and to Dr. H. Kuno for his kindness of putting the specimens at the writer's disposal and of offering many valuable suggestions from the petrological point of view.

References

(1) J.G. Koenigsberger, Terr. Mag., **43**, 119 (1938)
(2) R. Chevallier et J. Pierre, Ann. Physique, **18**, 353 (1932)
(3) T. Nagata, Bull. Earthq. Res. Inst., **19**, 579 (1941)
(4) T. Nagata, Bull. Earthq. Res. Inst., **21**, 1 (1943)
(5) H. Manley, Thesis (Univ. of London), June 1946
(6) T. Nagata and S. Akimoto, Jour. Geomag. Geoel, **2**, 29 (1950)

(7) C. Kittel, Phys. Rev., **70**, 965 (1946)
(8) I. Iwasaki, Personal Communication.
(9) H. Kuno, Personal Communication.
(10) V.H. Gottschalk and F.S. Wartman, U.S. Bureau of Mines Report of Investigations, **3298**, 67 (1935)
(11) R. Chevallier et S. Mathieu, C.R. Ac. Sc. Paris., **204**, 854 (1937)

Development and Decay Processes of the Bay Disturbances in Geomagnetic Field*

By Naoshi FUKUSHIMA
(Geophysical Institute, Tokyo University)

Abstract

In this study, the progressive change in the current system for the bay disturbance was chiefly examined in four examples with the aid of the world-wide magnetogram copies. The average current system corresponding to the maximum stage of the bay disturbance, which is given in Fig. 3, can be approximated as a result of the dynamo-theoretical calculation under the assumption on the distribution of the electric conductivity in the upper atmosphere such as that the ratio of the conductivity in the auroral zones to that in the equatorial region is about 14 in the dark hemisphere and about 4 in the sunlit hemisphere. The development and decay processes of individual bay disturbances are not a simple intensification and diminution of the mean current system such as given in Fig. 3. It was noticed that the westward auroral zone current in the dark hemisphere seems to become most intense nearly at the same time when the disturbance force at most part of lower latitude regions reaches its maximum magnitude, and the eastward auroral zone current in the sunlit hemisphere does not yet fully develope by that time and becomes most intense a few tens minutes later.

§ 1. *Introduction*

The average characteristics of the bay disturbance in geomagnetic field have been investigated by many authorities, for example by L. Steiner [1], H. Hatakeyama [2], H.C. Silsbee and E.H. Vestine [3], J.M. Príncep [4] and others. Some of them introduced the current system equivalent to the distribution of the disturbance force of the bay disturbance with the aid of the world-wide data [2][3]. On the other hand, it has been shown by T. Rikitake [5] and further extended by the present writer [6] [7] that the current system corresponding to the bay disturbance or to the S_D-field can be approximately derived from the dynamo-theory under the appropriate assumption on the distribution of the electric conductivity in the earth's upper atmosphere. The investigations of the bay disturbance hitherto, however, concern chiefly the average state of the bay disturbance, and so the conclusion obtained ought to correspond to its quasi-stationary state.

---

* Contribution from Division of Geomagnetism and Geoelectricity, Geophysical Institute, Tokyo University. Series II, No. 21.

The polar magnetic disturbances such as S_D and bay disturbance have been considered to be caused by the corpuscular stream impinging upon the earth's upper atmosphere after the travel from the sun. Trials for detecting directly the impinging particles have been made by many observers. The recent results by L. Vegard [8], A.B. Meinel [9] and C.W. Gartlein [10] show a strong evidence of the presence of protons incoming into the upper atmosphere in high latitude regions at the time of intense auroral display. Then, the electric conductivity in the upper atmosphere will be fairly affected by such particles at that time, or at the time of polar magnetic disturbance. Since the geomagnetic disturbance at high latitude regions is considered to be closely related to the ionization of upper atmosphere there, knowledges of the characteristics of the polar magnetic disturbances will give a clue to research the nature of the corpuscular stream from the sun as well as the effect of the impinging particles in the earth's upper atmosphere. It will be significant at the present stage of the study of the mechanism of the bay disturbance, to trace the progressive change in the bay field, or in other words, to know the dynamical behaviour of the development and decay of the bay disturbance.

In the present study, therefore, the whole process of four bay disturbances were examined in detail, especially with respect to the characteristics of development and decay of their equivalent current systems.

§ 2. *Data used in the analysis*

Examined data were chosen from those occurred in April 1933, during the Second International Polar Year Observation, since many magnetograms over the world in the equinoctial season could be obtained only for those in this epoch. Dates and times of the bay disturbances are

April 3, 1933, 10—13 h G.M.T.,
April 9, 1933, 9—12 h G.M.T.,
April 10, 1933, 14—17 h G.M.T.,
April 23, 1933, 5— 8 h G.M.T.

The world-wide magnetogram copies at the time of the above four bay disturbances were prepared by Prof. T. Nagata at Department of Terrestrial Magnetism, Carnegie Institution of Washington, and from U.S. Coast and Geodetic Survey. The number of the observatories amounts to 33, 26 of which are in the northern hemisphere and 7 in the southern one. Besides these data, the tables of hourly values in the Polar Year publications could be utilized for reference at 15 observatories.

The former 33 observatories will be called here the first kind observatories, and the latter 15 observatories the second kind ones. The abbreviation and the position of the stations and other elements are tabulated in Table I, in which the stations written in italic mean those of the second kind. The distribution of the observatories is shown in Fig. 1, in which the stations of the first kind are given by full circles and those of the second kind by hollow circles.

Table I

Observatory	Abbreviation	Φ	Λ	φ	λ	ψ	D	D-ψ
Thule	TH	88°.0	0°.0	76°.5	291°.1	0°.0	-81°.2	-81°.2
Godhavn	GO	79.8	32.5	69.2	306.5	-17.5	-57.2	-39.7
Scoresby Sund	SS	75.8	81.8	70.5	383.0	-36.2	-34.5	1.7
Angmagssalik	AN	74.3	52.7	65.6	37.6	-22.6	-39.8	-17.2
Sveagruvan	SV	73.9	130.7	77.9	16.8	-46.2	- 4.9	41.3
Calm Bay	CB	71.5	153.3	80.3	52.8	-32.2	21.1	53.3
Björnöja	BJ	71.0	124.7	74.5	19.2	-37.9	- 1.9	36.0
Julianehaab	JU	70.8	35.6	60.7	314.0	-13.8	-43.4	-29.6
Fort Rae	FR	69.0	290.9	62.8	243.9	24.1	37.5	13.4
Tromsö	TR	67.1	116.7	69.7	18.9	-30.8	- 3.7	27.1
Petsamo	PE	64.9	125.8	69.5	31.2	-27.6	5.8	33.4
Matotchkin Shar	MS	64.8	146.5	73.3	56.4	-22.4	21.7	44.1
College	CO	64.5	255.4	64.9	212.2	27.0	30.4	3 4
Sodänkylä	SO	63.8	120.0	67.4	26.6	-26.7	3.0	29.7
Dickson	DI	63.0	161.5	73.5	80.4	-12.8	28.5	41.3
Kandalkcha	KN	62.5	124.2	67.1	32.4	-25.0	6.7	31.7
Lerwick	LE	62.5	88.6	60.1	358.8	-23.6	-13.6	10.0
Dombås	DO	62.3	100.0	62.1	9.1	-23.6	- 8.5	15.1
Meanook	ME	61.8	301.0	54.6	246.7	17.2	26.4	9.2
Sitka	SI	60.0	275.4	57.0	224.7	21.4	30.0	8.6
Eskdalemuir	ES	58.5	82.9	55.3	356.8	-20.4	-14.2	6.2
Lovö	LO	58.1	105.8	59.4	17.8	-22.1	- 2.6	19.5
Agincourt	AG	55.0	347.0	43.8	280.7	3.6	- 7.6	-11.2
Abinger	AB	54.0	83.3	51.2	359.6	-18.4	-11.5	6.9
Gross Raum	GR	53.3	105.3	54.8	20.5	-19.5	- 1.0	18.5
Yakutsk	YA	51.0	193.8	62.0	129.7	5.8	-16.2	-22.0
Cheltenham	CH	50.1	350.5	38.7	283.2	2.4	- 7.1	- 9.5
San Miguel	SM	45.6	50.9	37.8	334.4	-11.3	-18.2	- 6.9
Ebro	EB	43.9	79.7	40.8	0.5	-15.0	- 9.8	5.2
San Fernando	SF	41.0	71.3	36.5	353.8	-13.6	-12.2	1.4
Tucson	TU	40.4	312.2	32.2	249.2	10.1	13.9	3.8
Toyohara	TY	36.9	203.5	47.0	142.8	6.7	- 9.0	-15.7
San Juan	SJ	29.9	3.2	18.4	293.9	- 0.7	- 5.2	- 4.5
Teoloyucan	TE	29.6	327.0	19.8	260.8	6.6	9.5	2.9
Helwan	HE	27.2	106.4	29.9	31.3	-12.7	0.0	12.7
Kakioka	KA	26.0	206.0	36.2	140.2	6.2	- 5.8	-12.0
Aso	AS	22.0	198.0	32.9	131.0	4.2	- 3.8	- 8.0
Honolulu	HO	21.1	266.5	21.3	201.9	12.3	10.2	- 2.1
Antipolo	AT	3.3	189.8	14.6	121.2	2.0	0.5	- 1.5
Huancayo	HU	- 0.6	353.8	-12.0	284.7	1.3	7.2	5.9
Mogadiscio	MO	- 2.7	114.3	2.0	45.4	-10.5	- 0.8	9.7
Elisabethville	EL	-12.7	94.0	-11.7	27.5	11.7	- 9.0	-20.7
Apia	AP	-16.0	260.2	-13.8	188.2	11.7	10.7	- 1.0
Tananarive	TN	-23.7	112.4	-18.9	47.5	-11.2	8.3	19.5
Cape Town	CT	-32.7	79.9	-33.9	18.5	-13.7	-23.8	-10.1
Watheroo	WA	-41.8	185.6	-30.3	115.9	1.3	- 3.6	- 4.9
Toolangi	TO	-46.7	220.8	-37.5	145.5	9.5	8.5	- 1.0
Orcades de Sud	OS	-49.9	18.2	-60.7	315.2	- 7.2	3.1	10.3

Notes
- Φ Geomagnetic latitude (The position of north geomagnetic pole assumes φ=78.°5N, λ=291°E)
- Λ Geomagnetic longitude
- φ Geographic latitude
- λ Geographic longitude
- ψ The angle formed by the great circle joining the station and the geomagnetic pole with the geographical meridian of the station (eastward positive)
- D Declination (for April 1933)

WORLD, NORTHERN HEMISPHERE IN GEOMAGNETIC COORDINATE

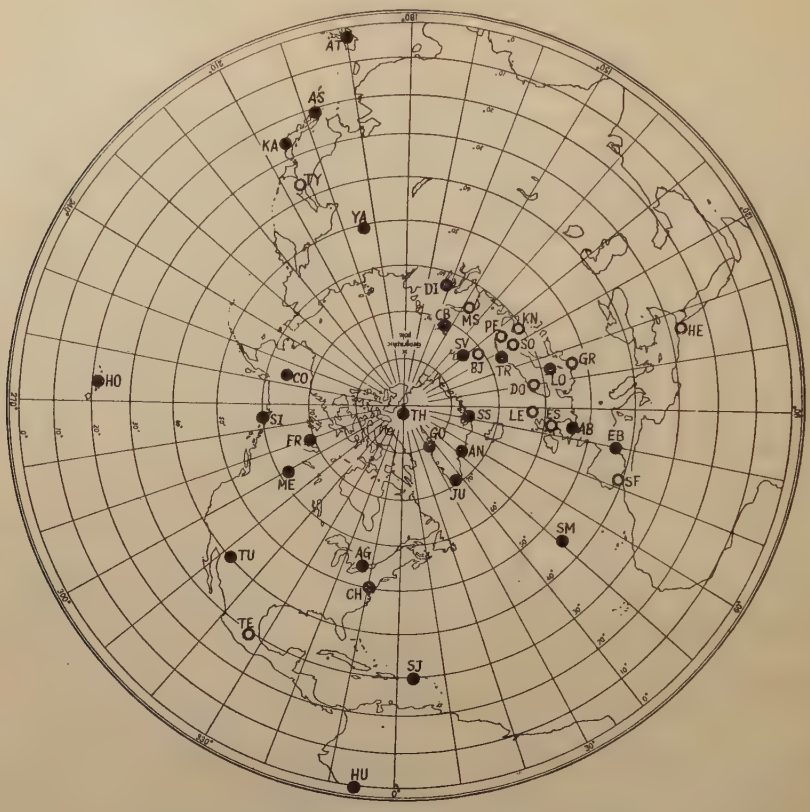

WORLD IN GEOMAGNETIC COORDINATE, MERCATOR PROJECTION

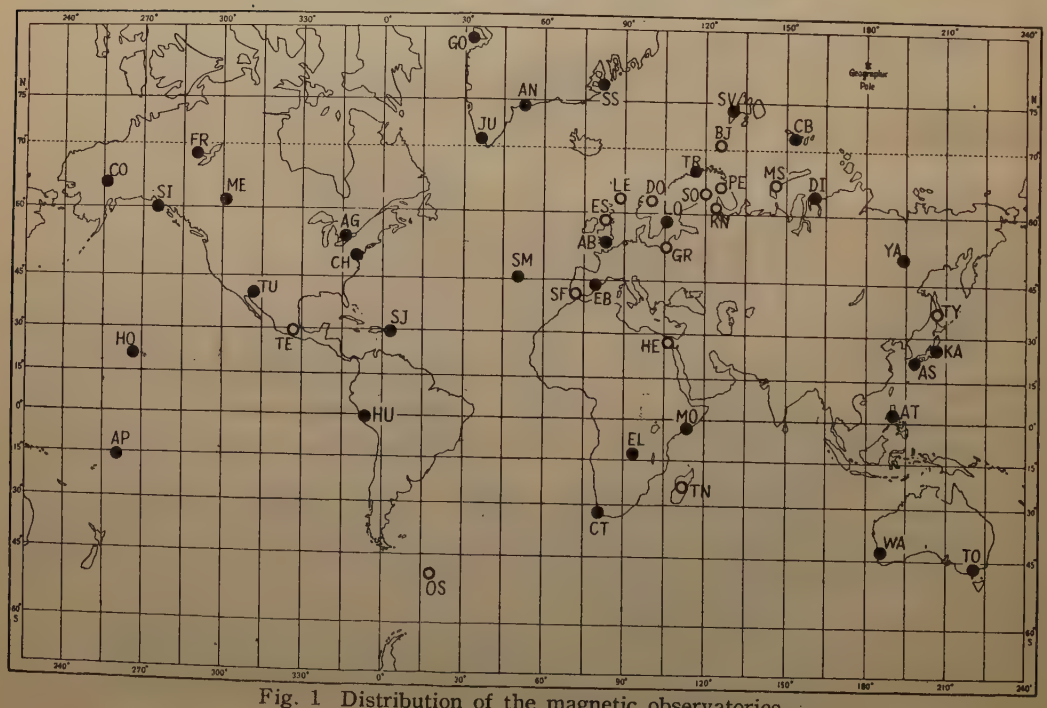

Fig. 1 Distribution of the magnetic observatories.

§ 3. *General description of the geomagnetic condition of the days, on which the bay disturbances occurred*

The international daily magnetic character figure *C*, and *Kp*-indices on April 3, 9, 10 and 23, 1933, are given below, where the *Kp*-indices written in Gothic type correspond to the bay disturbances.

Date	*C*	G.M.T.	*Kp*-indices							
		00–03h	03–06h	06–09h	09–12h	12–15h	15–18h	18–21h	21–24h	Sum
1933 April 3	0.9	2+	3+	3–	**4–**	4–	1+	2+	2_0	21+
9	0.7	3–	2–	3_0	**4–**	3_0	3–	1_0	1+	19_0
10	0.7	1+	2+	2+	2_0	**3–**	$\mathbf{3_0}$	3–	0+	17–
23	1.1	3–	4_0	4+	2_0	4–	2+	4–	3–	25+

The mean values of *C* and daily sum of *Kp* on international quiet days in April 1933 are 0.12 and 7 respectively, while those on international disturbed days are 1.28 and 26. The geomagnetic condition on the above four days was not so calm, but rather moderately disturbed on the whole. *Kp*-indices at the time of the bay disturbances show a slight increase as will be seen in the above table.

Some examples of the magnetograms at the time of the bay disturbances are reproduced in Fig. 2 (*a*)–(*d*). As will be seen in the figure, the bay disturbance observed in high latitude regions is much more complicated in its mode of variation. Moreover, the geomagnetic field is not in undisturbed state before and after the very time of the bay disturbance in high latitude regions. So that there may be a little uncertainty in defining the normal geomagnetic variation which ought to take place if the bay disturbance concerned did not occur. It was assumed here that the form of the normal geomagnetic variation is a linear change from the value before the beginning of a bay to that after the bay. Practically, the said definition of the normal variation was applied for 10–13 h G.M.T. on April 3, 9–12 h G.M.T. on April 9, 14–17 h G.M.T. on April 10, and 5–8 h G.M.T. on April 23. The deviation from the above-mentioned normal variation curve was defined as the disturbance force of the geomagnetic field due to the bay disturbance.

§ 4. *Character of the mean current system of the four bays at their maximum stage*

The disturbance force of the magnetic field at the time of the bay disturbance in the low and middle latitude regions seems to increase and decrease simultaneously over the world in a first approximation, though the variation in the disturbance force is fairly complicated in high latitude regions. The times at which the disturbance force in the low and middle latitude regions reaches its maximum value were determined to be 11 h 52 m G.M.T. on April 3, 10 h 00 m on April 9, 15 h 00 m on April 10 and 06 h 20 m on April 23 for respective bay disturbances. The overhead current system corresponding to the average distribution of disturbance fields at the above-mentioned times is given in Fig. 3, while each current systems at four respective times are illustrated later in Figs. 7–10. The overhead current system was derived in the

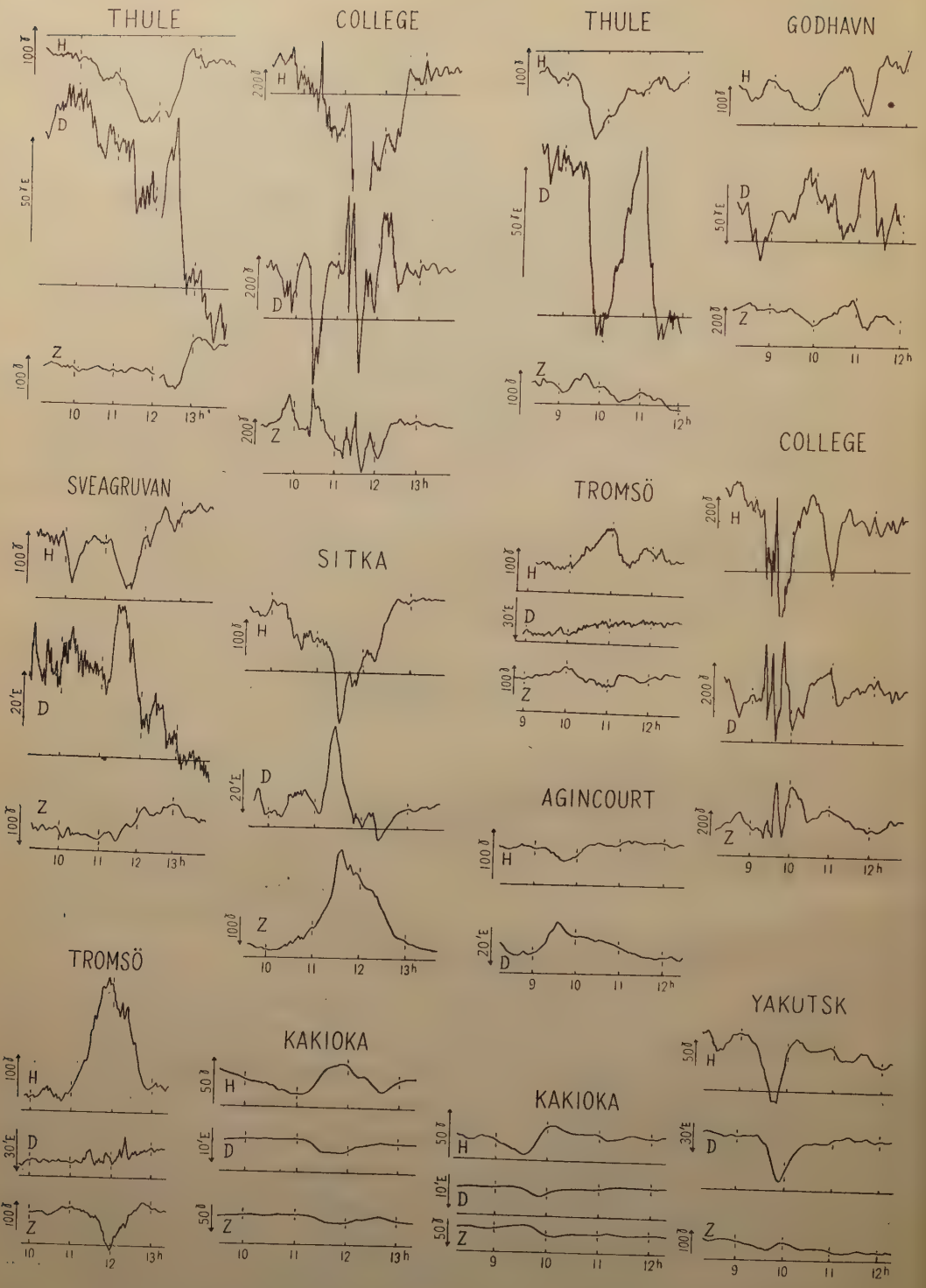

(*a*) April 3, 1933 (*b*) April 9, 1933

Fig. 2 Examples of magnetogram at the time of bay disturbance.

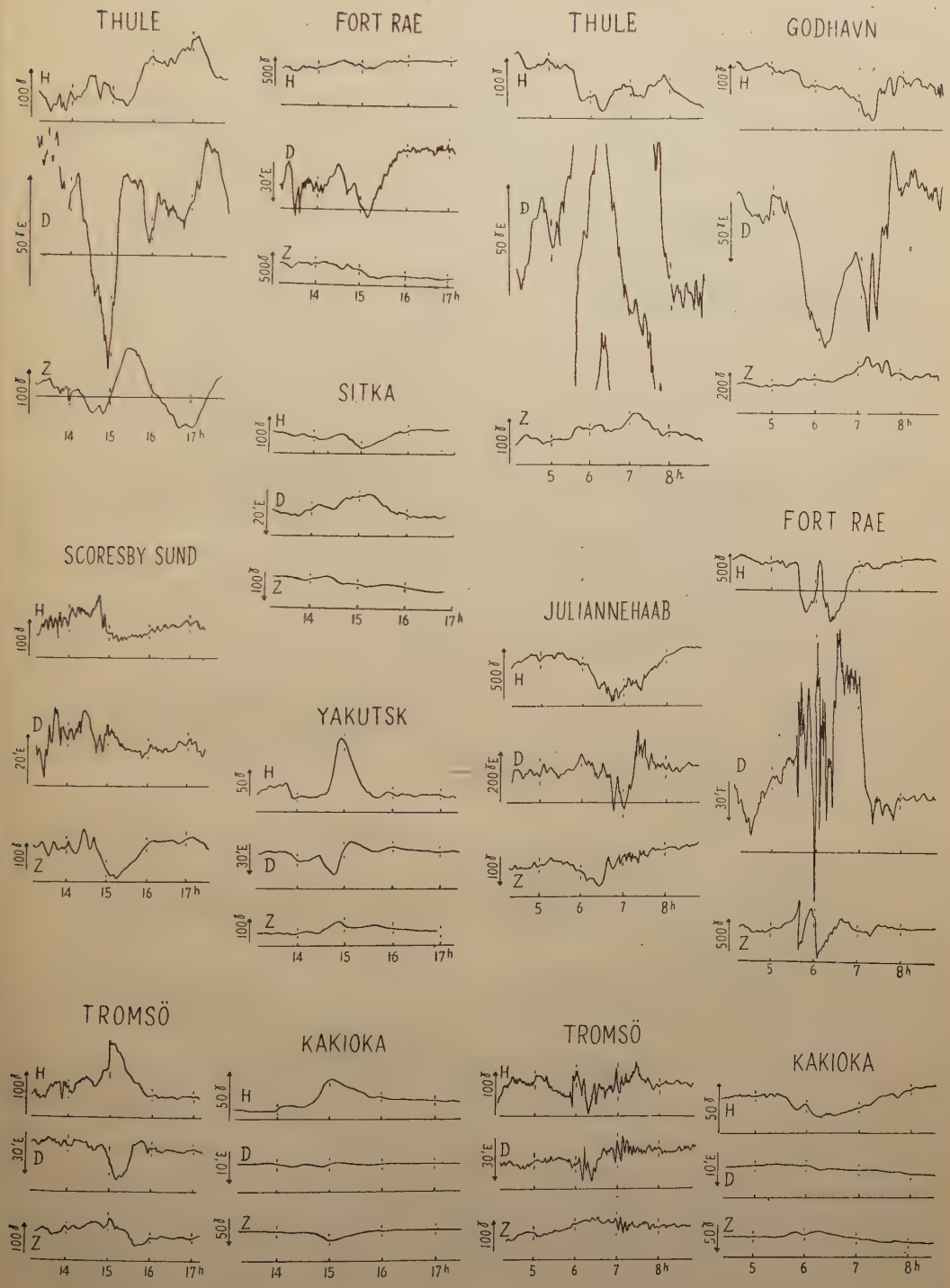

(*c*) April 10, 1933 (*d*) April 23, 1933

Fig. 2 Examples of magnetogram at the time of bay disturbance.

following way. According to T. Rikitake's result [11], the internal origin part of the magnetic disturbance force due to the induced electric current within the earth, is nearly a half as much as the external origin part in its magnitude, and the phase lag between these two parts is negligibly small. Hence, the overhead current system equivalent to the external origin part of the bay disturbance was so derived that the overhead current intensity is responsible for two-thirds of the horizontal component of the disturbance force at respective stations, while the external origin part of the vertical component, evaluated to be twice the observed value, being taken into account only qualitatively in the present study. The current system in Fig. 3 is in good agreement with Silsbee and Vestine's one [3], though there is a little discrepancy in the phase of the current system with respect to the direction towards the Sun, which amounts to about 30° in angle.

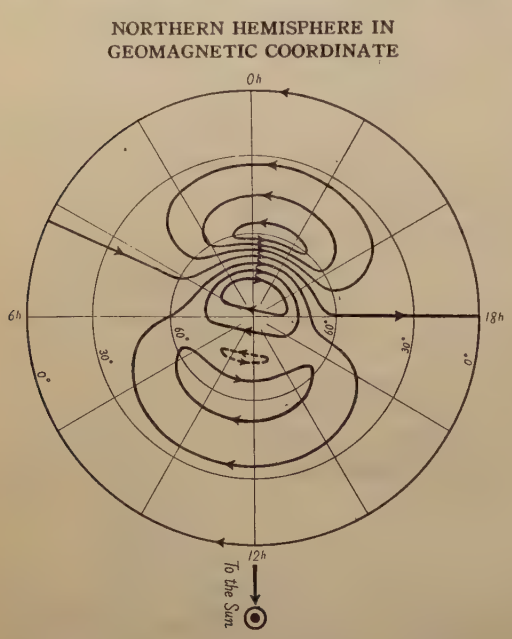

Fig. 3. Average current system of four bay disturbances at their maximum stage. Electric current of 1.0×10^5 amp. flows between successive stream lines in the direction indicated by arrow.

The above current system was compared with the theoretical one calculated by the dynamo-theory [7] [12]. The calculation was made under the following assumptions. The distribution of the electric conductivity in the earth's upper atmosphere is assumed to be expressed in the geomagnetic coordinate by

$$K=aK_0 \quad \text{in the polar caps} \quad (\theta=0°\sim20° \text{ and } 160°\sim180°),$$

$$K=bK_0\,(1+\gamma\cos\varphi) \quad \text{in the auroral zones} \quad (\theta=20°\sim25° \text{ and } 155°\sim160°),$$

$$K=K_0 \quad \text{in the equatorial region} \quad (\theta=25°\sim155°),$$

where K_0 is a constant value, and the constants a, b and γ are so chosen that

$$a\sim1, \quad b\gg1 \quad \text{and} \quad 0<\gamma<1.$$

φ in the expression of the conductivity in the auroral zones denotes the geomagnetic longitude measured from the midnight meridian, so that the conductivity at midnight is $\frac{1+\gamma}{1-\gamma}$ times that at noon in the auroral zones. The above-mentioned assumption on the distribution of the conductivity in the auroral zones will be a reasonable one, if we take into account the result of the actual geomagnetic data by M. Hasegawa [13]. The main magnetic field of the earth is replaced by that of a centred dipole and the velocity potential of the air motion at the level of the conductive layer was put to be in the form of that

$$\psi=\sum_n\sum_m k_n^m P_n^m(\cos\theta)\sin(m\varphi+\alpha_n^m).$$

In the numerical calculation, only the most predominant term of $n=1$ and $m=1$ was adopted, and α_1^1 was assumed $-\frac{3}{2}\pi$ for convenience [6]. Then, the current function J derived from the dynamo-theory has a form

$$J=J_q+J_D,$$

where J_q corresponds to S_q-field, and J_D to S_D-field attributed to the anomalous large conductivity in the auroral zones. J_D in the above relation can be separated as

$$J_D=J_{D0}+\gamma J'_D,$$

where J_{D0} corresponds to the case when $\gamma=0$, and $\gamma J'_D$ is a perturbation term due to the longitudinal inequality of the conductivity in the auroral zones. The details of the calculation has already been described in a previous paper [7], together with the results of computation.

The observed currret system of bay disturbance given in Fig. 3 was compared with the J_D current systems derived theoretically by varying the magnitude of a, b and γ. It was concluded then that the distribution of the conductivity in the upper atmosphere at the time of the maximum deviation of the bay disturbance force in the low and middle latitude regions can be best expressed by

$$a=1.2,\quad b=9\quad \text{and}\quad \gamma=0.6$$

in the present model, or in other words, the conductivity of the auroral zone is about 14 times that of the equatorial region near midnight and about 4 times near noon, while the conductivity in the polar cap is comparable or somewhat large compared with the equatorial one. In Fig. 4, the current system calculated under the assumption that $a=1.2$, $b=9$ and $\gamma=0.6$ is given for comparison. Since the current intensity in the calculation is determined by the product of k_1^1 and K_0, the value of $k_1^1K_0$ is appropriately chosen, so that the numerical difference of current function between the pole and the equator in the both current systems in Fig. 3 and Fig. 4 agrees with each other. The calculated current system shows good agreement with the observed oue. The distribution of the values of the current function with respect to latitude in the noon and midnight meridians is compared in Fig. 5 in the both observed and calculated ones. It will be noticed that the width of the auroral zone, which is taken to be 5° in latitude in the calculation, may be somewhat wider in the observed one. The neglection of the obliquity of the earth's magnetic axis with its rotation axis, and some other simple assumptions on the air motion and the

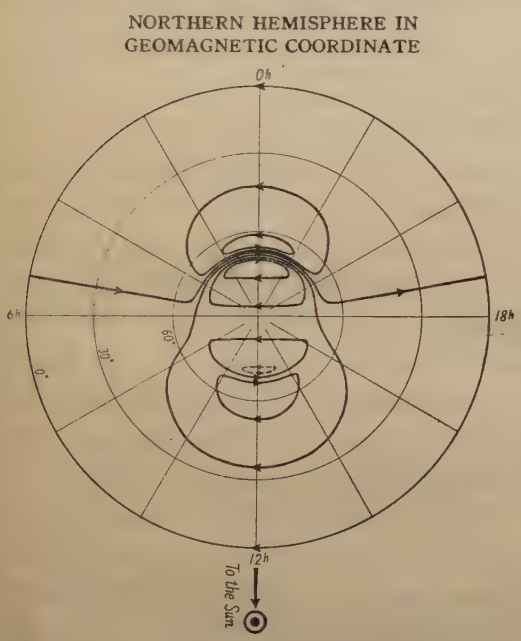

Fig. 4 Current system calculated from dynamo-theory under the assumption $a=1$, $b=9$ and $\gamma=0.6$.

distribution of the electric conductivity in the conductive shell would not result in significant difference in the conclusion for the present purpose of approximate estimation of the value of the electric conductivity in the upper atmosphere.

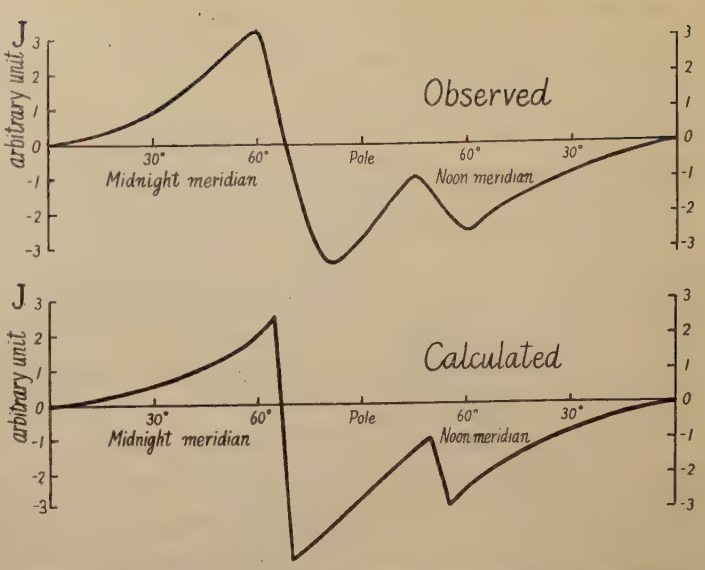

Fig. 5 Change in the value of current function with latitude in the noon and midnight meridians. The top and the bottom of the figure correspond to the average current systems given in Fig. 3 and to the calculated one in Fig. 4, respectively.

§ 5. *The variation in the disturbance force with the progress of time*

As already mentioned in § 4 and shown in Fig. 2, the variation in the disturbance force in high latitude regions with time is fairly complicated, while it seems that the disturbance forces observed at various localities in the low and middle latitude regions increase and decrease almost simultaneously with each other. The times at which the horizontal intensity and declination of the disturbance force at all stations showed their optimum values during respective bay disturbances are plotted in Fig. 6, where the circles show those of the horizontal intensity and the squares those of declination. The full circles and the black squares correspond to the maximum values of horizontal intensity and eastward declination respectively, while the hollow circles and the white squares to the minimum values. Large circles or squares and small ones correspond to major and minor optimum values. It will be seen in Fig. 6 that the circles and squares do not always concentrate around a few definite time-lines, especially for the cases of the observatories in high latitudes. This fact shows that the variation in the disturbance forces in high latitude regions is so complicated that some of the maximum and minimum of magnetic disturbances at different places take place at different times. However, there are a few time-lines around which are concentrated most number of the optimum symbols, though not all of them. These times are, for example,

on April 3, 11 h 06 m, 11 h 30 m, 11 h 52 m, 12 h 05 m, 12 h 40 m,
on April 9, 09 h 40 m, 09 h 50 m, 10 h 00 m, 11 h 00 m,
on April 10, 14 h 30 m, 15 h 00 m, 15 h 10 m, 15 h 30 m,
on April 23, 05 h 48 m, 06 h 00 m, 06 h 10 m, 06 h 20 m, 06 h 40 m, 07 h 20 m.

The change in the current system during a course of the bay disturbance will be described for respective bays in the followings, and the common characteristics are summarized later.

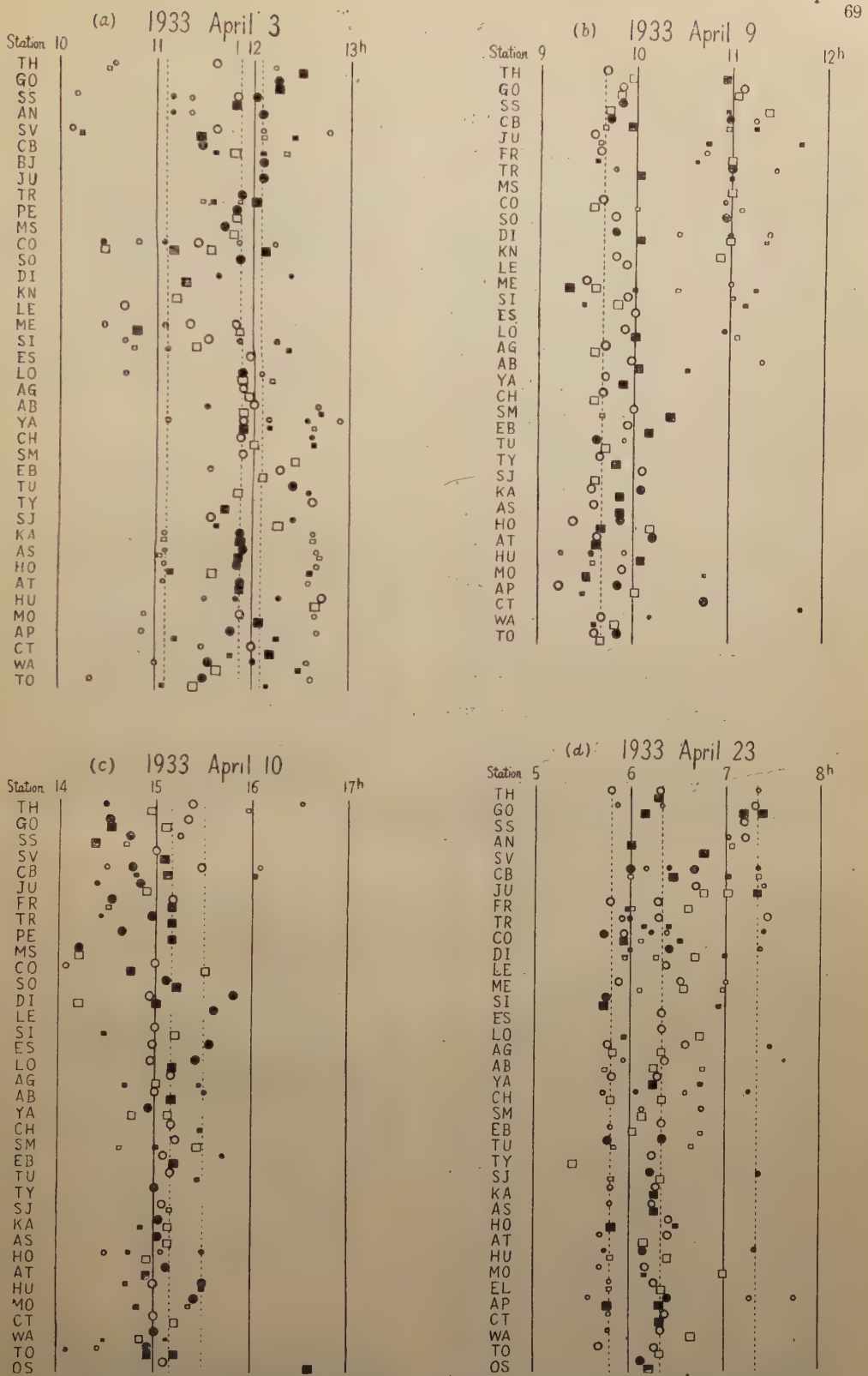

Fig. 6 Distribution of the times, at which the disturbance forces of the horizontal intensity and declination take their optimum values. (● $\Delta H>0$, ○ $\Delta H<0$, ■ $\Delta D>0$, □ $\Delta D<0$)

(i) The bay disturbance on April 3, 1933, 10 h – 13 h G.M.T.

The current systems at 11h 06 m, 11h 52 m and 12h 05 m are illustrated in Fig. 7 (*a*)–(*c*). In Fig. 7 and also in Figs. 8 – 10, the eletcric current of 1.0 $\times 10^5$ *amp.* flows between successive stream lines in the direction indicated by the arrow. At 11 h 06 m, the intense westward auroral zone current in the dark hemisphere could be clearly seen, while no distinct eastward auroral zone current appeared in the opposite hemisphere. In the most part of the low and middle latitude regions, the disturbance force in horizontal intensity was negative in its sign, namely the westward zonal current was predominant there. At 11h 52 m, the intensity of the westward auroral zone current reached its maximum. The easward auroral zone current in the sunlit hemisphere was formed by that time. In the low and middle latitude regions, the disturbance force took its maximum value at that time in general, and the positive bay was observed in almost 40% of the whole regions. During 11 h 52m—12 h 05 m, the eastward auroral zone current scarecely decreased in its intensity, while the intensity of the westward one fairly dimished. In the low and middle latitude regions, the area of the region in which the positive disturbance force of horizontal intensity observed, seemed to become a little wider during the interval of time. This tendency of the broadening of the positive bay area, which is first noticed by H. Hatakeyama (reference [2], p. 24) and later discussed by the present writer [14], was clearly recognized in this bay disturbance.

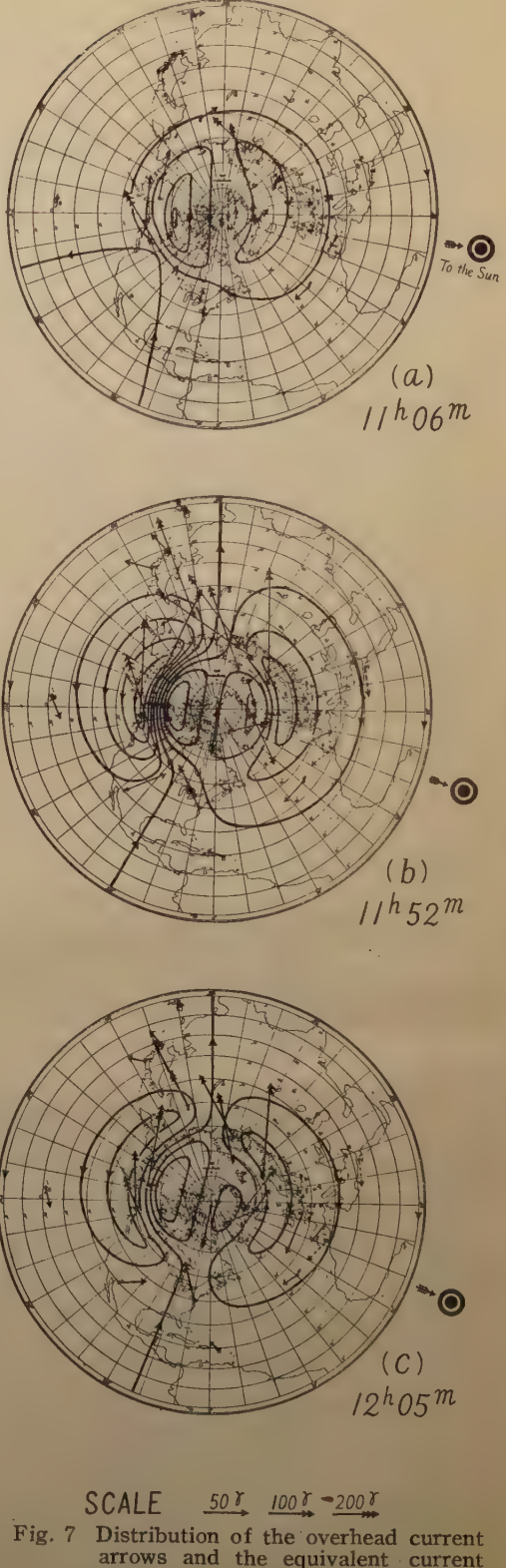

Fig. 7 Distribution of the overhead current arrows and the equivalent current system for the bay disturbance on April 3, 1933.

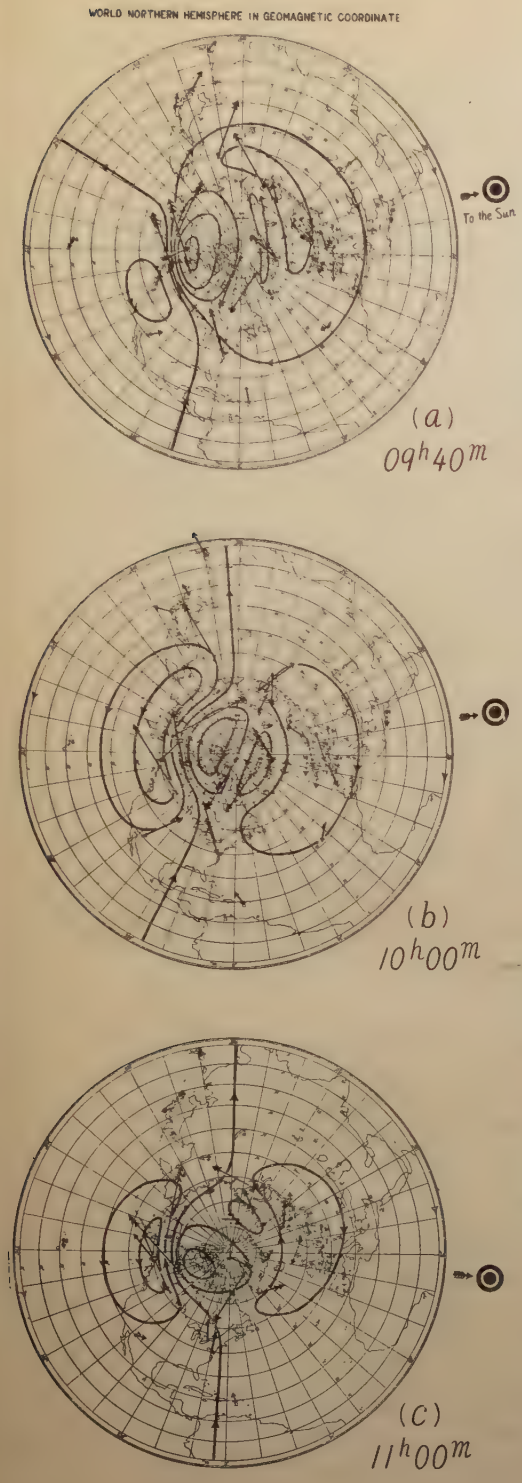

Fig. 8 Distribution of the overhead current arrows and the equivalent current system for the bay disturbance on April 9, 1933.

(ii) The bay disturbance on April 9, 1933, 09 h – 12 h G.M.T.

The current system at 09 h 40 m, 10 h 00 m and 11 h 00 m are illustrated in Fig. 8 (*a*)–(*c*). At 09 h 40 m, the westward auroral zone current in the dark hemisphere had developed by that time, while the eastward one in the sunlit hemisphere was not so definite, just similar as in the preceding example. During 09 h 40 m–10h 00 m, the westward auroral zone current became a little weak in the intensity and the eastward current appeared near the auroral zone of the sunlit hemisphere, though not so intense. The disturbance forces in the low and middle latitude regions took their maximum values about that time. Until 11 h 00 m, the intensity of the current system dimished as a whole, while the westward auroral zone current became again intense. The broadening tendency of the positive bay area, which is mentioned with respect to the case of the preceding bay, was remarkable in this case, too.

(iii) The bay disturbance on April 10, 1933, 14 h – 17 h G.M.T.

The current systems at 15 h 00 m, 15 h 10 m and 15 h 30 m are illustrated in Fig. 9 (*a*)–(*c*). The disturbance force reached its maximum value at 15 h 00 m over the whole world except near the auroral zone in the sunlit hemisphere, where the disturbance at 15 h 10 m was a little large than that at 15 h 00 m. In other words, the disturbance force began to diminish after 15 h 00 m everywhere over the world except only near the auroral zone in the sunlit hemisphere. The current system at 15 h 30 m showed no distinct vestige of the intense

auroral zone current. On the other hand, it was also derived that there was no intense current system corresponding to the distribution of the disturbance force at 14 h 30 m. Therefore, the bay disturbance on April 10 had comparatively short life, among the four bays examined in this study.

(iv) The bay disturbance on April 23, 1933, 05 h–08 h G.M.T.

The geomagnetic condition in the high latitude regions before and after the bay disturbance is not so calm in general. Among the four examples of bay disturbance dealt with in this study, the one of April 23 was in the most good condition, namely the geomagnetic field did not show large perturbation in high latitude regions before and after the bay disturbance. The mode of the variation in the geomagnetic field, however, was a rather complicated one. As already shown in Fig. 2 (*d*), the magnetogram in the low and middle latitude regions reveals that as if two bay disturbances took place successively. The record obtained at Fort Rae showed also the same character, and the decrease in horizontal intensity was anomalously large, namely it exceeded 1000γ at 06 h 17 m G.M.T. On the other hand, the records at Godhavn and Angmagssalik, which situate south of Greenland, showed no remarkable change at that time, and the maximum disturbance force took place at about 07 h 20 m, at which any corresponding variation could scarecely be observed at Fort Rae and other stations of lower latitude.

The current systems at 05 h 48 m, 06 h 20 m and 07 h 20 m are illustrated in Fig. 10 (*a*)–(*c*), where the former two times correspond to the occurrence of the optimum disturbance force in the auroral zone of American side and in the lower latitude regions, and the later one to the occurrence of the maximum

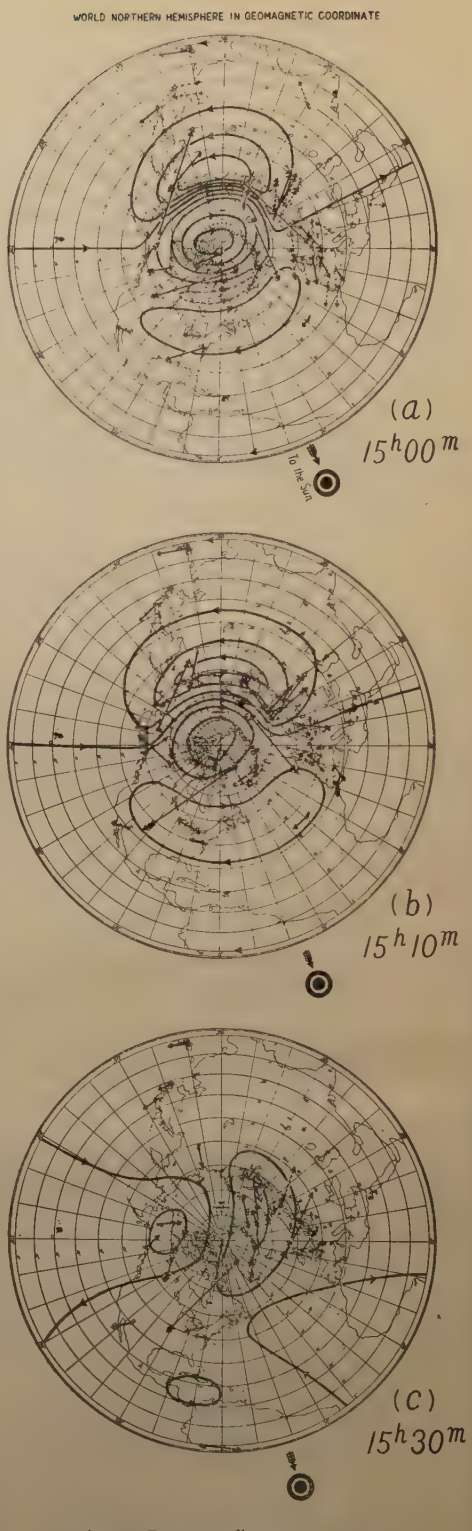

Fig. 9 Distribution of the overhead current arrows and the equivalent current system for the bay disturbance on April 10, 1933.

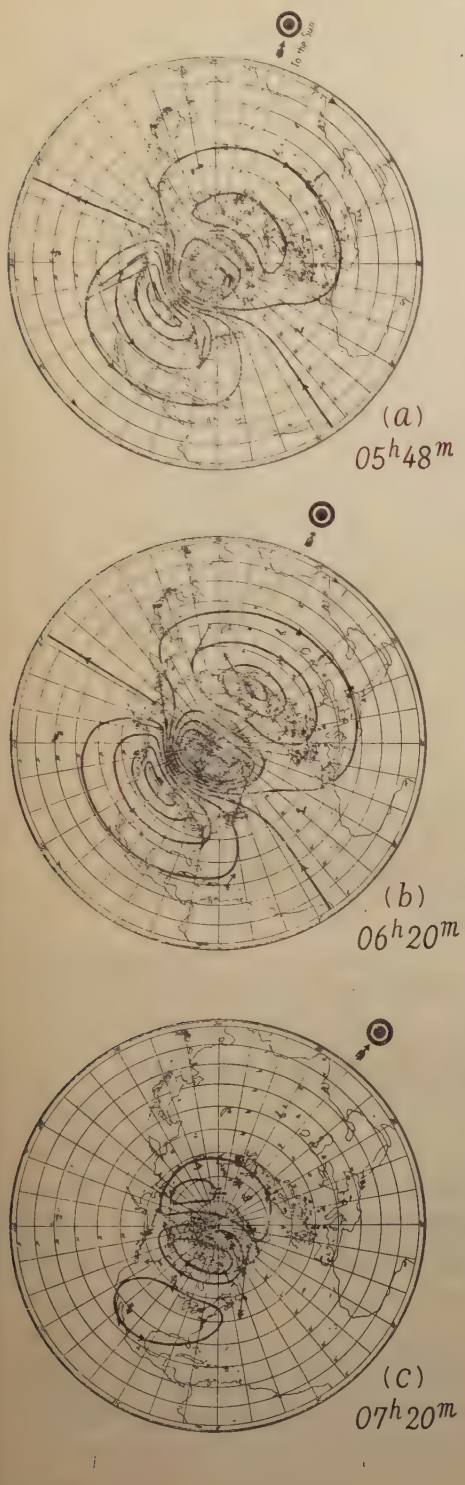

Fig. 10 Distribution of the overhead current arrows and the equivalent current system for the bay disturbance on April 23, 1933.

disturbance force at the south of Greenland. In the current systems of (*a*) and (*b*) of Fig. 10, we see at once the presence of greatly intense auroral zone current in the dark hemisphere, while the eastward one in the sunlit hemisphere was not yet formed at 05h 48 m and not so distinct even at 06 h 20 m. The current system at 07 h 20 m showed the fadeaway of the so-called S_D-current system, and there could be seen the presence of some disturbance only in the polar region.

The increase and decrease of the disturbance force over the world in every 15 minute intervals during 05 h 30 m – 07 h 00 m is schematically shown in Fig. 11 (*a*)–(*f*). The stations at which the magnitude of the disturbance increased in 15 minute interval are plotted by full circles, and those at which the decrease in the magnitude of the disturbance force was observed are plotted by hollow circles, and the stations at which no significant increase or decrease took place are marked by the hollow circle with small full circle in it. There can be seen a rather systematic distribution of these circles. The variation of the disturbance force during 05 h 45 m – 06 h 00 m given in Fig. 11 (*b*) chiefly concerns the decrease in the intensity of the westward auroral zone current after its maximum at 05 h 48 m. The next figure (*c*) is chiefly due to the second increase in the westward auroral zone current. Fig. 11 (*d*), (*e*) and (*f*) are of the intervals at which the westward auroral zone current diminished after the second maximum of its intensity at 06 h 20 m, and the disturbance force became larger at the south of Greenland. This series of figure illustrates the fact that the disturbance force of the bay disturbance does not increase or decrease simultaneously over the world. The is to say, there are cases, in which the

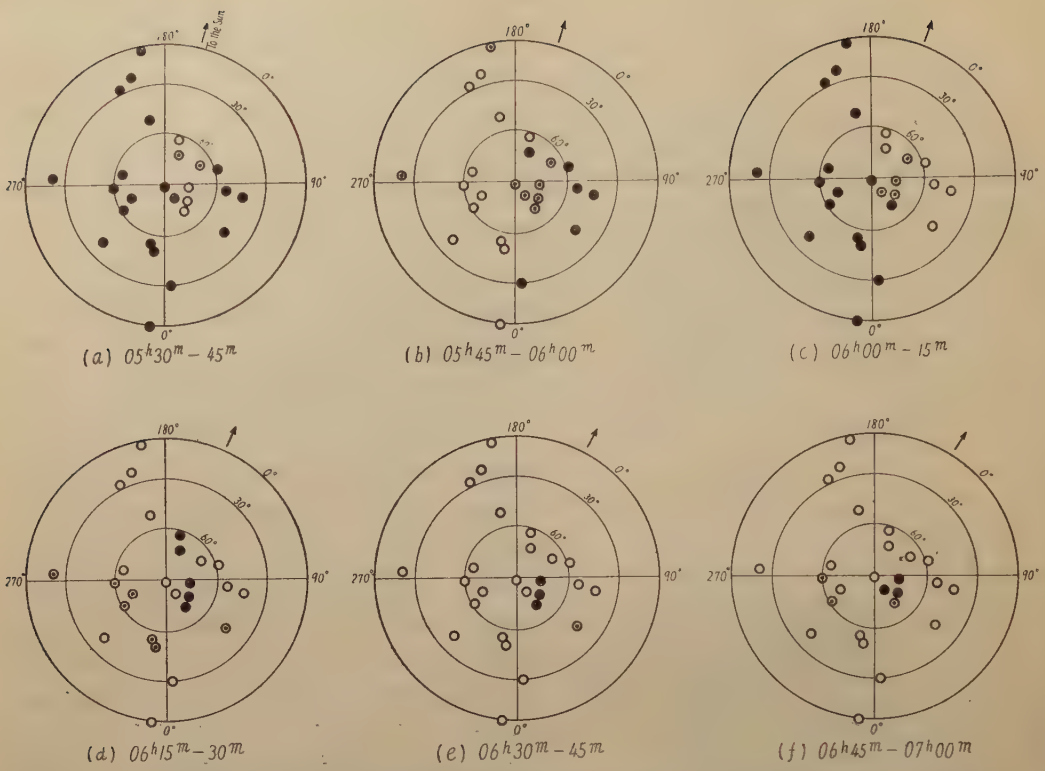

Fig. 11 Distribution of the increasing and decreasing areas in the disturbance force. Stations at which the disturbance force became larger or smaller with time are plotted by ● and ○ respectively. ⊙ means the station at which no significant increase or decrease in the disturbance force was observed.

disturbance force at some region increase or decrease contrary to the variation in most part of the whole earth's surface. The variation in the intensity of the westward and the eastward auroral zone currents, which were already explained in the preceding three examples of the bay disturbances, are of course the case.

Taking a general survey of the progressive change in the current system of the bay disturbance during its development and decay process, one may notice that the westward auroral zone current in the dark hemisphere became most intense at the same time with the occurrence of the maximum disturbance force in lower latitude regions, while the intensity of the eastward auroral zone current in the sunlit hemisphere did not yet reach its maximum, but it did about 10 or 20 minutes later. This result is illustrated in Fig. 12, where the change in the total amouut of the westward current flow in high latitudes in the dark hemisphere as well as that of the eastward current in the sunlit hemisphere with the progress of time is shown.

§ 6. *Results obtained in this study*

It will be said that the equivalent current system for the bay disturbance at its maximum stage, which was statistically derived from the analysis of many bays, can be approximated as a result of the dynamo-theoretical calculation under the

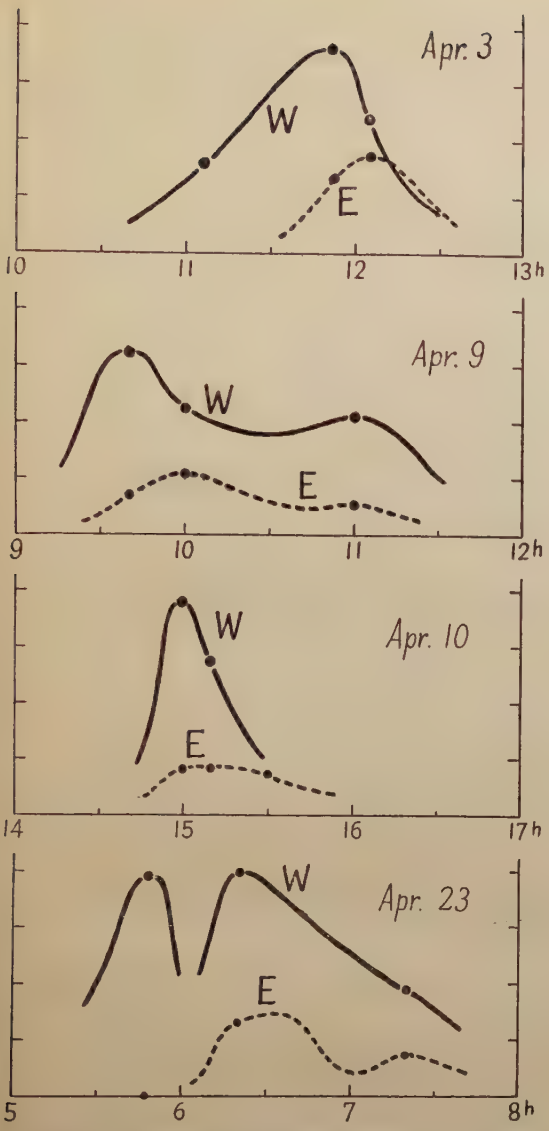

Fig. 12 Change in the total amount of the westward electric current in the auroral zone in the dark hemisphere (denoted by W) and the eastward one in the sunlit hemisphere (denoted by E).

appropriate assumption on the distribution of the electric conductivity in the earth's upper atmosphere. The result of the examination of the progressive change in the current system for the respective bay disturbances, however, shows that the development and decay of individual bay disturbance is not a simple intensification and diminution of the mean current system. Summarizing the mode of progressive change in the current system of four examples of bay disturbances, the following facts will be especially marked:

(i) The disturbance force does not always increase or decrease simultaneously over the whole world, especially in high latitude regions.

(ii) The westward auroral zone current seems to become most intense nearly at the same time when the disturbance force at most part of lower latitude regions reaches its maximum magnitude, and the eastward auroral zone current does not yet fully develope by that time, and becomes most intense a few tens minutes later.

(iii) In the low and middle latitude regions, the area in which the positive bay is observed, becomes wider with time.

For the purpose of establishing the above-mentioned results, further examination by means of many other examples of bay disturbances will be necessary, especially with respect to the character (ii). The more detailed examination of the progressive change in the current system and consequent conclusions will be reported in the future.

In concluding, the writer wishes to express his hearty thanks to Prof. T. Nagata, who kindly arranged the world-wide data for the present study and gave him kind

direction and encouragement throughout the work. Prof. T. Nagata and the writer thank to Directors of Department of Terrestrial Magnetism, Carnegie Institution of Washington and U.S. Coast and Geodetic Survey, through whose courtesy these data were prepared.

(Read: Oct. 21, 1951)

References

[1] L. Steiner, Terr. Mag., **26**, 1 (1921).
[2] H. Hatakeyama, Geophys. Mag., **12**, 15 (1938).
[3] H.C. Silsbee and E.H. Vestine, Terr. Mag., **47**, 195 (1942).
[4] J.M. Príncep, Memorias del Observatorio del Ebro, No. 10 (1949).
[5] T. Rikitake, Rep. Ionosphere Res. Japan, **2**, 57 (1948).
[6] N. Fukushima, Geophysical Notes, Tokyo Univ., Vol. 2, No. 21 (1949).
[7] N. Fukushima, Journ. Geomag. Geoele., **2**, 103 (1950).
[8] L. Vegard, Nature, **144**, 1089 (1939).
[9] A.B. Meinel, Phys. Rev., **80**, 1096 (1950).
[10] C.W. Gartlein, Phys. Rev., **81**, 463 (1951).
[11] T. Rikitake, Bull. Earthq. Res. Inst., **28**, 45 (1950).
[12] N. Fukushima, Rep. Ionosphere Res. Japan, **4**, 113 (1950).
[13] M. Hasegawa, Trans. Oslo Meeting, I.A.T.M.E., 507 (1949).
[14] N. Fukushima, Geophysical Notes, Tokyo Univ., Vol. 3, No. 22 (1950).

The Effects Of Atmospheric Motion And Dynamo Current On The Electron Density Of The Ionosphere

Ken-ichi MAEDA

(Electrical Communication Laboratory, Ministry of Telecommunications.)

Summary

The paper deals with the possibility that the ionospheric electron density is affeted by the flow of the charged particles (electrons, negative and positive ions) associated with the atmospheric mass motion and dynamo current from dynamo-theoretical aspect. The theoretical relationships among the electron density, atmospheric motion and dynamo current are deduced and some numerical examples as applied to the F2-layer are given. The effect of dynamo current is small in comparison to that of atmospheric mass motion, which must account for the dynamo current corresponding to the *Sq* field of geomagnetic variation.

I. Introduction.

According to the dynamo theory the ionosphere will be the sheet of overhead current system, which must be accountable for the diurnal variation field (*Sq*) of the terrestrial magnetism and the theory can be applied to interpret the S_D field with some assumptions on the conductivity of the ionosphere in the polar regions.

In the dynamo theory it is considered that the horizontal mass motion of the upper atmosphere exists and it produces in the ionosphere under the influence of the vertical field of permanent magnetism of the earth a system of electric current, which is responsible for the *Sq* field.

By this theory we are led to the idea that the charged particles (electrons, negative and positive ions) are made to move with velocities corresponding to the mass motion and the overhead current and as the result the ionospheric electron density will be affected by such flows of the charged particles.

Concerning the vertical ionic drift due to a horizontal air current and its effect on the ionosphere D.F. Martyn[1] studied the problem on the dynamo theoretical view.

It is the aim of the present writer to clarify the theoretical relation among the electron density of the ionosphere, the horizontal mass motion of the upper atmosphere and the overhead current and to show some examples of a deformation of the diurnal variation curve of electron density by estimating the order of magnitude of the above-mentioned effects on the basis of informations hitherto known in the field of geomagnetism and ionosphere.

II. Fundamental equations for the variation of the charged particles.

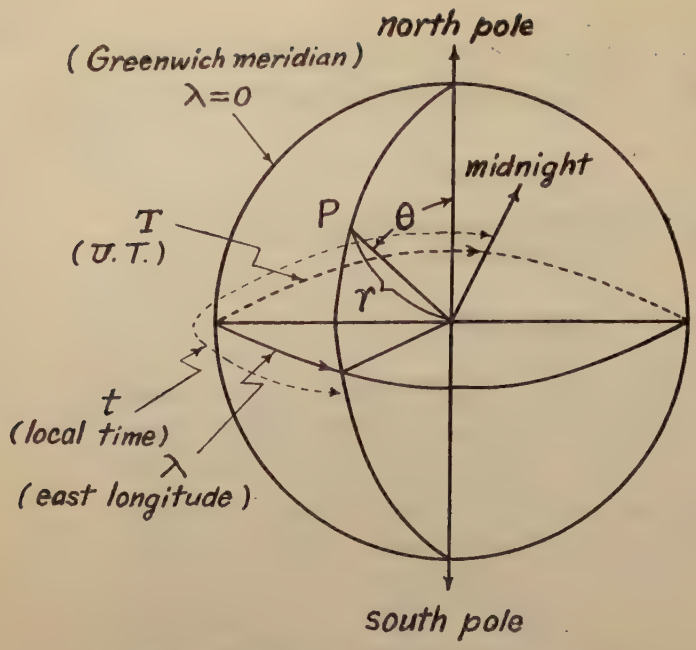

Fig. 1 Polar coordinates
P : r, θ, $t(=\lambda+T)$, t is reckoned from midnight.

Fig. 1 shows the spherical coordinates to be used in this report and the universal time (T), longitude (λ), colatitude (θ) and local time (t) are also shown there. The following notations are used.

u, v: southward and eastward velocities of mass motion respectively, (vertical motion is neglected.)

u', v': southward and eastward velocities of the charged particles associated with the current system respectively, (vertical current in neglected.)

$r=R+h$, R: the radius of the earth,

h: the height of the layer,

n, n_1, n_2: the number density of the electron, the negative and the positive ions respectively.

Suffices 1 and 2 mean the quantity concerning the negative and positive ions respectively and no suffix the electron.

q: the rate of ion production,

α: the coefficient of recombination,

β: the coefficient of attachment,

γ: the coefficient of detachment.

Then the differential equations connecting the n, n_1 and n_2 can be written as follows.

$$(1)\qquad \frac{\partial n}{\partial t}=q-\alpha n_2 n-\beta n+\gamma n_1-\frac{\partial}{r\partial\theta}\{n(u+u')\}-\frac{\partial}{r\sin\theta\,\partial\lambda}\{n(v+v')\},$$

$$(2)\qquad \frac{\partial n_1}{\partial t}=\beta n-\gamma n_1-\frac{\partial}{r\partial\theta}\{n_1(u+u_1')\}-\frac{\partial}{r\sin\theta\,\partial\lambda}\{n_1(v+v_1')\},$$

$$(3)\qquad \frac{\partial n_2}{\partial t}=q-\alpha n_2 n-\frac{\partial}{r\partial\theta}\{n_2(u+u_2')\}-\frac{\partial}{r\sin\theta\,\partial\lambda}\{n_2(v+v_2')\}.$$

If we put the current function for Sq field as J and the effective thickness of the ionosphere as z_d, we get the following relations.

$$(4)\qquad \text{southward}:\quad \frac{\partial J}{ez_d r\sin\theta\,\partial\lambda}=n_2u_2'-n_1u_1'-nu'\simeq n_2u_2'-n_1u_1'=-(n_1+n_2)\,u_1',$$

$$(5)\qquad \text{eastward}:\quad -\frac{\partial J}{ez_d r\partial\theta}=n_2v_2'-n_1v_1'-nv'\simeq n_2v_2'-n_1v_1'=-(n_1+n_2)\,v_1'.$$

Here the contribution of electron to the overhead current is neglected as the electronic conductivity is negligibly small in comparison to the ionic conductivity.(2) Also u_2' and v_2' are put to be equal to $-u_1'$ and $-v_1'$ respectively and e is the absolute value of the charge of an electron.

If we assume the total conductivity of E and F layers or the contribution of the both layers as the current sheet to be roughly equal (this point is discussed in the later section), we get the following relations from (4) and (5) for one layer.

$$(6)\qquad n_1u_1'=-\frac{1}{2ez_d}\frac{n_1}{n_1+n_1}\frac{\partial J}{r\sin\theta\partial\lambda},\quad n_1v_1'=\frac{1}{2ez_d}\frac{n_1}{n_1+n_2}\frac{\partial J}{r\partial\theta},$$

$$(7)\qquad n_2u_2'=\frac{1}{2ez_d}\frac{n_2}{n_1+n_2}\frac{\partial J}{r\sin\theta\partial\lambda},\quad n_2v_2'=-\frac{1}{2ez_d}\frac{n_2}{n_1+n_2}\frac{\partial J}{r\partial\theta}.$$

Next we consider on some approximations concerning the divergence terms in (1), (2) and (3). For instance, in the case of $\partial(nv)/r\sin\theta\partial\lambda$, the term of space derivative of the density n (that is $v\partial n/r\sin\theta\partial\lambda$) is equal to $(\partial n/\partial t)(v/c_0)$, where $c_0(r\sin\theta\partial\lambda/\partial t)$ is the peripheral velocity of the point under consideration in the ionosphere by earth's rotation. As v/c_0 can be assumed as much less than unity, the term of space derivative of n will give a small change to the left hand side of (1) and therefore can be neglected. Also in other cases the terms of space derivatives of n, n_1 and n_2 can be neglected. Therefore the equations (1), (2) and (3) can be written as follows, putting $s_1=n_1/(n_1+n_2)$ and $s_2=n_2/(n_1+n_2)$,

$$(8)\qquad \frac{dn}{dt}=q-\alpha n_2n-\beta n+\gamma n_1-nf,$$

$$(9)\qquad \frac{dn_1}{dt}=\beta n-\gamma n_1-n_1f+s_1g,$$

$$(10)\qquad \frac{dn_2}{dt}=q-\alpha n_2n-n_2f-s_2g,$$

where

$$(11)\qquad f=\frac{\partial u}{r\partial\theta}+\frac{\partial v}{r\sin\theta\partial\lambda},$$

$$(12)\qquad g=\frac{1}{2ez_dr^2}\left\{\frac{\partial}{\partial\theta}\left(\frac{\partial J}{\sin\theta\partial\lambda}\right)-\frac{1}{\sin\theta}\left(\frac{\partial^2J}{\partial\lambda\partial\theta}\right)\right\}.$$

The equations (8), (9) and (10) together with (11) and (12) are the fundamental equations connecting n, n_1 and n_2 (density of the charged particles), u, v (mass velocity) and J (current function).

III. g, the effect of ionic flow associated with overhead current.

The magnetic potential (V) and the current function (J) for Sq are given by the following equations.(3)

$$(13)\qquad V=\sum_{n=1}^{\infty}\sum_{m=0}^{n}e_n^m\left(\frac{r}{R}\right)^nRP_n^m(\theta)\cos\{m(\lambda+T)+\epsilon_n^m\},$$

$$(14)\qquad J=-\frac{1}{4\pi}\sum_{n=1}^{\infty}\sum_{m=0}^{n}\frac{2n+1}{n+1}\left(\frac{r}{R}\right)^nRe_n^mP_n^m(\theta)\cos\{m(\lambda+T)+\epsilon_n^m\}.$$

e_n^m and ϵ_n^m are given in the following table 1, where the values(3) are the mean of those in 1902 and 1905 and the value of r was taken as 6,630 km (h=260 km) for F2 layer.

Table I. (e_n^m in 10^{-5} emu and ϵ_n^m in degree)

m \ n	1		2		3		4		5		6	
	e_n^m	ϵ_n^m	e_n^m	ϵ_n^m	e_n^m	ϵ_n^m	e_n^m	ϵ_n^m	e_n^m	ϵ_n^m	e_n^m	ϵ_n^m
1	±3.2	23	6.1	26	±1.8	341						
2			±1.8	241	3.4	204	±0.7	197				
3					±0.9	87	1.5	39	±0.2	220		
4							±0.4	2	0.4	228	±0.9	84

values underlined: equinox, others: solstitial inequality.

Using the above values J is written as follows, where $\lambda+T$ is replaced by ωt. (t is in second and ω is $0.728\times10^{-4}\text{sec}^{-1}$.)

$$
\begin{cases}
\text{Equinox: } J\ (\text{emu}) = -9.7\times10^3 \sin\theta\cos\theta\{\cos(\omega t+26)+0.68\sin\theta\cos(2\omega t+204) \\
\qquad +0.35\sin^2\theta\cos(3\omega t+39)+0.10\sin^3\theta\cos(4\omega t+228)\}, \\
\text{Solstitial inequality: } J\ (\text{emu}) = -9.7\times10^3 \sin\theta\{0.26\cos(\omega t+23) \\
\qquad +0.15\sin\theta\cos(2\omega t+241)+0.07\sin^2\theta\cos(3\omega t+87)+0.03\sin^3\theta\cos(4\omega t+2) \\
\qquad +0.11(5\cos^2\theta-1)\cos(\omega t+341)+0.04\sin\theta(7\cos^2\theta-1)\cos(2\omega t+197) \\
\qquad +0.01\sin^2\theta(9\cos^2\theta-1)\cos(3\omega t+220)+0.06\sin^3\theta(11\cos^2\theta-1)\cos(4\omega t+84)\}.
\end{cases} \tag{15}
$$

For the calculation of g, z_d must be evaluated. z_d is defined with the total conductivity (K) and the specific conductivity (σ) at the height under consideration, that is 260 km for F2 layer, where σ is maximum and the current sheet is assumed to be concentrated.

$$z_d = \frac{K}{\sigma}.$$

For F2 layer z_d is roughly estimated as 50 km.[2] Thus we obtain the following equation for g.

$$
\begin{cases}
\text{Equinox: } g\ (\text{ions/cm}^3/\text{sec}) = -0.14\cos^2\theta\left\{\frac{1}{\sin\theta}\sin(\omega t+26)+1.36\sin(2\omega t+204)\right. \\
\qquad \left. +1.05\sin\theta\sin(3\omega t+39)+0.42\sin^2\theta\sin(4\omega t+228)\right\}, \\
\text{Solstitial inequality: } g\ (\text{ions/cm}^3/\text{sec}) = -0.14\cos\theta\left\{\frac{0.26}{\sin\theta}\sin(\omega t+23)\right. \\
\qquad +0.29\sin(2\omega t+241)+0.22\sin\theta\sin(3\omega t+87)+0.13\sin^2\theta\sin(4\omega t+2) \\
\qquad +\frac{0.11(5\cos^2\theta-1)}{\sin\theta}\sin(\omega t+341)+0.09(7\cos^2\theta-1)\sin(2\omega t+197) \\
\qquad \left. +0.04\sin\theta(9\cos^2\theta-1)\sin(3\omega t+220)+0.22\sin^2\theta(11\cos^2\theta-1)\sin(4\omega t+84)\right\}.
\end{cases} \tag{16}
$$

Calculated examples are shown in Fig. 2 in the case of $\theta=54°$ (colatitude of Tokyo).

IV. f, the effect of mass flow by atmospheric motion.

The velocity potential (Ψ) and the velocity of atmospheric motion are put as follows.[3]

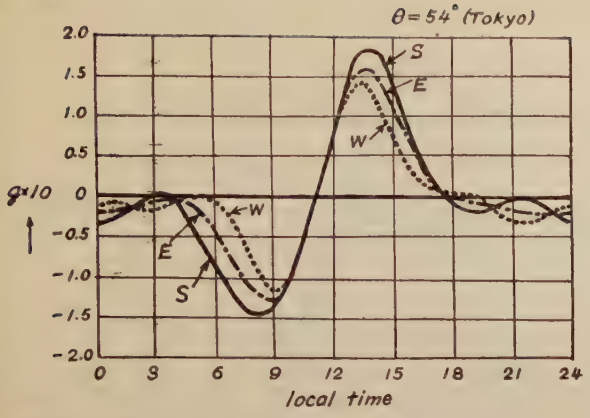

Fig. 2 Time variation of $g\times10$ (ions/cm³/sec).
S: summer solstice,
E: equinox,
W: winter solstice.

(17) $$\Psi=\sum_{n=1}^{\infty}\sum_{m=0}^{n}k_n^m P_n^m(\theta)\cos\{m(\lambda+T)+\alpha_n^m\},$$

(18) southward velocity:
$$u=-\frac{\partial\Psi}{r\partial\theta}=-\frac{1}{r}\sum\sum k_n^m\frac{d}{d\theta}(P_n^m(\theta))\cos\{m(\lambda+T)+\alpha_n^m\},$$

(19) eastward velocity:
$$v=-\frac{\partial\Psi}{r\sin\theta\partial\lambda}=\frac{1}{r}\sum\sum k_n^m\frac{m\cdot P_n^m(\theta)}{\sin\theta}\sin\{m(\lambda+T)+\alpha_n^m\}.$$

The current function (J), velocities (u, v) and the vertical magnetic field (Z) are connected by the following equation,[3] assuming the total conductivity (K) as constant.

(20) $$\frac{\partial^2 J}{\sin\theta\partial\lambda^2}+\frac{\partial}{\partial\theta}\left(\sin\theta\frac{\partial J}{\partial\theta}\right)=rK\left\{\frac{\partial}{\partial\lambda}(vZ)+\frac{\partial}{\partial\theta}(uZ\sin\theta)\right\},$$

(21) $$Z=-2G\cos\theta.$$

Here we assumed the axis of geomagnetism as coincident with that of the earth's rotation. (this point is discussed in the later section.) The both sides of (20) are calculated as shown below and then k_n^m and α_n^m are evaluated.

(22) $$\frac{\partial^2 J}{\sin\theta\partial\lambda^2}+\frac{\partial}{\partial\theta}\left(\sin\theta\frac{\partial J}{\partial\theta}\right)=\frac{\sin\theta}{4\pi}\sum_{n=1}^{\infty}\sum_{m=0}^{n}n(n+1)\frac{2n+1}{n+1}\left(\frac{r}{R}\right)^n Re_n^m P_n^m(\theta)\cos\{m(\lambda+T)+\epsilon_n^m\},$$

(23) $$rK\left\{\frac{\partial}{\partial\lambda}(vZ)+\frac{\partial}{\partial\theta}(uZ\sin\theta)\right\}=-2GK\sin\theta\sum_{n=1}^{\infty}\sum_{m=0}^{n}\frac{k_n^m}{2n+1}\left\{n(n+2)\sqrt{(n+m+1)(n-m+1)}\,P_{n+1}^m(\theta)+(n-1)(n+1)\sqrt{(n+m)(n-m)}P_{n-1}^m(\theta)\right\}\cos\{m(\lambda+T)+\alpha_n^m\}.$$

For the harmonics P_{m+1}^m of J corresponds to P_m^m of Ψ and k_m^m and α_n^m are obtained. Next for the harmonics P_m^m of J corresponds to P_{m+1}^m of Ψ and k_{m+1}^m and α_{m+1}^m are obtained. Finally for the harmonics P_{m+2}^m of J corresponds to P_{m+1}^m and P_{m+3}^m of Ψ and k_{m+3}^m and α_{m+3}^m must be calculated by using k_{m+1}^m and α_{m+1}^m determined beforehand. The equations for k's and α's are given as follows.

(24) $$k_m^m=-\frac{R}{8\pi GK}\left(\frac{r}{R}\right)^{m+1}\frac{(m+1)(2m+3)\sqrt{2m+1}}{m(m+2)}e_{m+1}^m,\quad \alpha_n^m=\epsilon_{m+1}^m,$$

(25) $$k_{m+1}^m=-\frac{R}{8\pi GK}\left(\frac{r}{R}\right)^{m}\frac{(2m+3)\sqrt{2m+1}}{m+2}e_m^m,\quad \alpha_{m+1}^m=\epsilon_m^m,$$

(26) $$-\frac{R}{8\pi GK}\left(\frac{r}{R}\right)^{m+2}\cdot(m+2)(2m+5)e_{m+2}^m\cos\{m(\lambda+T)+\epsilon_{m+2}^m\}=k_{m+1}^m\frac{(m+1)(m+3)\sqrt{m+1}\cdot2}{2m+3}\cos\{m(\lambda+T)+\alpha_{m+1}^m\}+k_{m+3}^m\frac{(m+2)(m+4)\sqrt{2m+3}\sqrt{3}}{2m+7}\cos\{m(\lambda+T)+\alpha_{m+3}^m\}.$$

The following table is obtained for k_n^m and α_n^m. In the calculation $2G$ was put as $\frac{2}{3}$ emu and K as 10^{-7} emu.

Table II. (k_n^m in emu and α_n^m in degree) $k_1^1 = -2.90\times10^{11}$ emu (K=10^{-7} emu)

J side			Ψ side		
P_n^m	e_n^m	ϵ_n^m	P_n^m	k_n^m/k_1^1	α_n^m
P_2^1	6.1	26	P_1^1	1	26
P_3^2	3.4	204	P_2^2	0.59	204
P_4^3	1.5	39	P_3^3	0.29	39
P_5^4	0.4	228	P_4^4	0.09	228
P_1^1	3.2	23	P_2^1	0.25	23
P_3^2	1.8	241	P_3^2	0.20	241
P_3^3	0.9	87	P_4^3	0.13	87
P_4^4	0.4	2	P_5^4	0.07	2
P_3^1	1.8	341	P_2^1	0.25	23
			P_4^1	0.13	269
P_4^2	0.7	197	P_3^2	0.20	241
			P_5^2	0.11	90
P_5^3	0.2	220	P_4^3	0.13	87
			P_6^3	0.11	258
P_6^4	0.9	84	P_5^4	0.07	2
			P_7^4	0.13	108

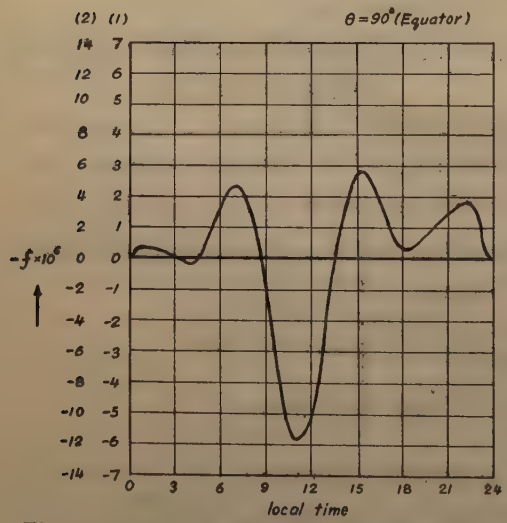

Fig. 3-A Time variation of $-f\times10^6$ (sec^{-1}). scale (1): $K=10^{-7}$emu, scale (2): $K=0.5\times10^{-7}$emu. (The curve is same for three seasons upon the equator.)

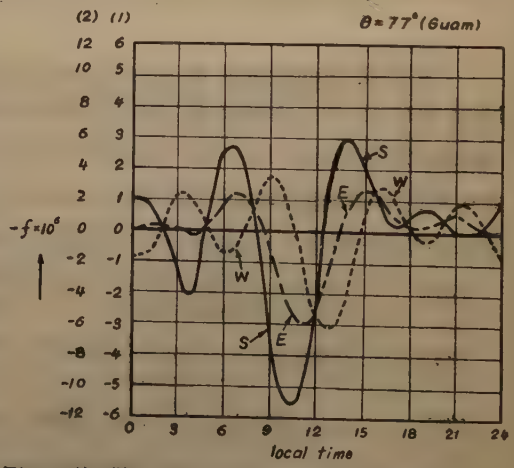

Fig. 3-B Time variation of $-f\times10^6$ (sec^{-1}). S: summer solstice, scale (1): $K=10^{-7}$emu, E: equinox, scale (2): $K=0.5\times10^{-7}$emu. W: winter solstice.

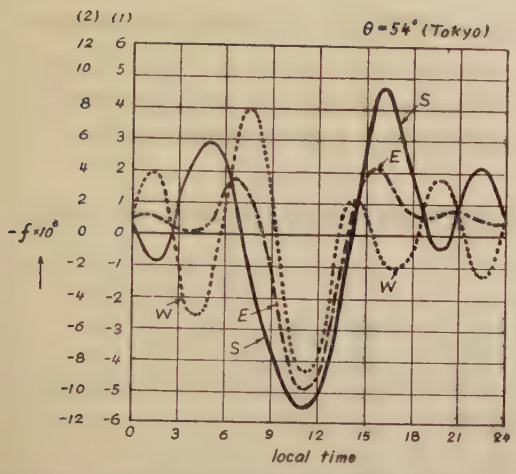

Fig. 3-C Time variation of $-f\times10^6$ (sec^{-1}).
S: summer solstice, scale (1): $K=10^{-7}$emu,
E: equinox, scale (2): $K=0.5\times10^{-7}$emu.
W: winter solstice.

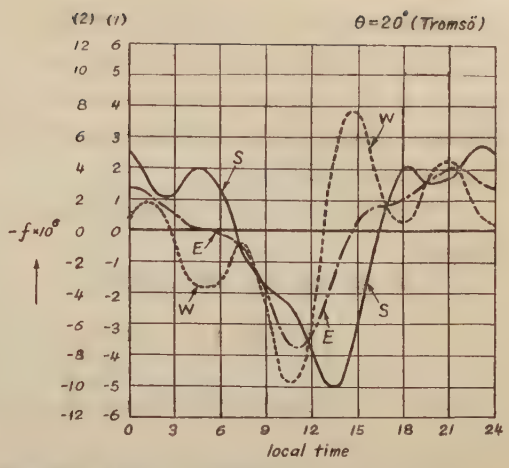

Fig. 3-D Time variation of $-f\times10^6$ (sec^{-1}).
S: summer solstice, scale (1): $K=10^{-7}$emu,
E: equinox, scale (2): $K=0.5\times10^{-7}$emu.
W: winter solstice.

Then we can calculate f (sec^{-1}) by (11), (18) and (19) using the above table.

$$
\begin{cases}
\text{Equinox:}\quad f(\text{sec}^{-1})=-\dfrac{0.66\times10^{-13}}{K}\left\{\left(\sin\theta+\dfrac{1}{\sin\theta}\right)\cos(\omega t+26)+1.02(3-2\cos^2\theta)\right. \\
\left.\cos(2\omega t+204)+0.69\sin\theta(4-3\cos^2\theta)\cos(3\omega t+39)+0.26\sin^2\theta(5-4\cos^2\theta)\cos(4\omega t+228)\right\}, \\
\text{Solstitial inequality:}\quad f(\text{sec}^{-1})=-\dfrac{0.66\times10^{-13}}{K}\cos\theta\left\{\dfrac{0.44}{\sin\theta}(5-4\cos^2\theta)\cos(\omega t+23)\right. \\
+0.39(11-9\cos^2\theta)\cos(2\omega t+241)+0.26\sin\theta(19-16\cos^2\theta)\cos(3\omega t+87) \\
+0.15\sin^2\theta(29-25\cos^2\theta)\cos(4\omega t+2)-\dfrac{0.10}{\sin\theta}(112\cos^4\theta-173\cos^2\theta+57)\cos(\omega t+269) \\
-0.27(75\cos^4\theta-108\cos^2\theta+29)\cos(2\omega t+90)-0.31\sin\theta(132\cos^4\theta-181\cos^2\theta \\
\left.+41)\cos(3\omega t+258)-0.12\sin^2\theta(637\cos^4\theta-842\cos^2\theta+165)\cos(4\omega t+108)\right\}.
\end{cases}
\tag{27}
$$

Calculated examples are shown in Fig.3 for various colatitudes.

The calculated equations for u (cm/ sec) and v (cm/sec) are added in the following.

$$
\begin{cases}
\text{Equinox:}\quad u\,(\text{cm/sec})=\dfrac{4.37\times10^{-5}}{K}\cos\theta\{\cos(\omega t+26)+1.02\sin\theta\cos(2\omega t+204)\right. \\
\left.+0.69\sin^2\theta\cos(3\omega t+39)+0.26\sin^3\theta\cos(4\omega t+228)\right\}, \\
v\ (\text{cm/sec})=-\dfrac{4.37\times10^{-5}}{K}\{\sin(\omega t+26)+1.02\sin\theta\sin(2\omega t+204)+0.69\sin^2\theta\sin(3\omega t \\
+39)+0.26\sin^3\theta\sin(4\omega t+228)\}, \\
\text{Solstitial inequality:}\quad u\,(\text{cm/sec})=\dfrac{4.37\times10^{-5}}{K}\{0.44(2\cos^2\theta-1)\cos(\omega t+23) \\
+0.39\sin\theta(3\cos^2\theta-1)\cos(2\omega t+241)+0.26\sin^2\theta(4\cos^2\theta-1)\cos(3\omega t+87) \\
+0.15\sin^3\theta(5\cos^2\theta-1)\cos(4\omega t+2)+0.10(28\cos^4\theta-27\cos^2\theta+3)\cos(\omega t+269) \\
+0.27\sin\theta(15\cos^4\theta-12\cos^2\theta+1)\cos(2\omega t+90)+0.31\sin^2\theta(22\cos^4\theta-15\cos^2\theta \\
+1)\cos(3\omega t+258)+0.12\sin^3\theta(91\cos^4\theta-54\cos^2\theta+3)\cos(4\omega t+108)\}, \\
v\,(\text{cm/sec})=-\dfrac{4.37\times10^{-5}}{K}\cos\theta\{0.44\sin(\omega t+23)+0.77\sin\theta\sin(2\omega t+241)+0.79\sin^2\theta \\
\sin(3\omega t+87)+0.60\sin^3\theta\sin(4\omega t+2)+0.10(7\cos^2\theta-3)\sin(\omega t+269)+0.55\sin\theta(3\cos^2\theta \\
-1)\sin(2\omega t+90)+0.31\sin^2\theta(11\cos^2\theta-3)\sin(3\omega t+258)+0.49\sin^3\theta(13\cos^2\theta \\
-3)\sin(4\omega t+108)\}.
\end{cases}
\tag{28}
$$

V. Differential equation of the electron density (F layer) and its approximate solution.

The diurnal variation of the electron density (n) is given by solving simultaneously (8), (9) and (10), using (16) and (27) for g and f. But as it is difficult to obtain a perfect solution for n, we must be satisfied with rough estimations for some limited times of day.

In order to discuss in some detail, some mathematical approximations must be devised.

n, n_1 and n_2 are put as follows.

$$(29)\qquad \begin{cases} n=n_0+x, & n_0=\sqrt{\dfrac{q_0}{\alpha}}\sqrt{\dfrac{\gamma}{\beta+\gamma}}, & \dfrac{dn}{dt}=\dfrac{dx}{dt}, \\ n_1=n_{10}+y, & n_{10}=\dfrac{\beta}{\gamma}\sqrt{\dfrac{q_0}{\alpha}}\sqrt{\dfrac{\gamma}{\beta+\gamma}}, & \dfrac{dn_1}{dt}=\dfrac{dy}{dt}, \\ n_2=n_{20}+z, & n_{20}=\sqrt{\dfrac{q_0}{\alpha}}\sqrt{\dfrac{\beta+\gamma}{\gamma}}, & \dfrac{dn_2}{dt}=\dfrac{dz}{dt}. \end{cases}$$

n_0, n_{10} and n_{20} were defined as the steady state values of electron, negative and positive ion densities respectively in the case when f and g are put to zero. q_0 is the above-mentioned steady state value of q. Then the equations (8), (9) and (10) can be written as follows, considering that f is of the order of less than 1/10 of β or γ. (product terms of x, y, z and f are neglected.)

$$(30)\qquad \begin{cases} \dfrac{dx}{dt}=a_1x+b_1y+c_1z+h_1, \\ \dfrac{dy}{dt}=a_2x-b_1y+h_2, \\ \dfrac{dz}{dt}=a_3x+c_1z+h_3, \end{cases}$$

where

$$(31)\qquad \begin{cases} a_1=-\alpha n_{20}-\beta, \quad b_1=\gamma, \quad c_1=-\alpha n_0, \\ a_2=\beta, \quad a_3=-\alpha n_{20}, \quad h_1=q-q_0-fn_0, \\ h_2=s_1g-fn_{10}, \quad h_3=q-q_0-fn_{20}-s_2g. \end{cases}$$

The differential equation for x is given below.

$$(32)\qquad \begin{cases} \dfrac{d^3x}{dt^3}+A\dfrac{d^2x}{dt^2}+B\dfrac{dx}{dt}=C, \\ A=\alpha(n_{20}+n_0)+\beta+\gamma, \\ B=\alpha\{n_0(\beta+\gamma)+\gamma n_{20}\}, \\ C=q''+\gamma q'-n_0f''-(\gamma n_{20}-\alpha n_0n_{10})f'+(s_1\gamma+s_2\alpha n_0)g'+\gamma\alpha n_0g. \end{cases}$$

The primes attached to q, f and g mean their time derivatives. If we neglect g, (32) becomes as follows.

$$(33)\qquad \begin{cases} \dfrac{d^2x}{dt^2}+A\dfrac{dx}{dt}+Bx=C', \\ C'=q'+\gamma(q-q_0)-n_0f'-(\gamma n_{20}-\alpha n_0n_{10})f. \end{cases}$$

In the equations (32) and (33) A and B are independent of time and C add C' are a constant term plus linear combinations of sinusoidal functions if q, q' and q'' are

put approximately for daytime not far from noon as follows.

We assume the Chapman distribution for q and consider q at the level of its maximum value. If we denote q_m as q at $\chi=0$, we get

$$
(34)\quad \begin{cases} q=q_m\cos\chi=q_0\dfrac{\cos\chi}{\sin(\theta+\delta)}, \\ q-q_0=-I(1+\cos\omega t), \quad (t \text{ is reckoned from midnight}) \\ q'=\omega I\sin\omega t, \\ q''=\omega_2 I\cos\omega t, \\ I=\cos\delta\sin\theta\, q_m=\dfrac{\cos\delta\sin\theta}{\sin(\theta+\delta)}q_0, \end{cases}
$$

where δ is the declination of the sun. Then the equations (32) and (33) can be solved and the solution consists of a constant term, two exponential terms and a group of sinusoidal function terms, but it is necessary to know at least three quantities concerning n and/or $\frac{dn}{dt}\left(\text{or } \frac{d^2n}{dt^2}\right)$ at certain times in order to determine the integral constant.

For a rough estimation, neglecting the term of g or g', the particular solution for the following equation

$$
(35)\quad \frac{d^2x}{dt^2}+A\frac{dx}{dt}+Bx=-n_0f'-(\gamma n_{20}-\alpha n_0 n_{10})f
$$

will give the part corresponding the effect of f, which should be superposed to the usual results (x_0) in the case of sole existence of q and q', that is the general solution of

$$
(36)\quad \frac{d^2x}{dt^2}+A\frac{dx}{dt}+Bx=q'+\gamma(q-q_0).
$$

For this purpose a particular solution of (35) is presented in the following.

$$
(37)\quad x=\sum_{m=1}^{4}C_m\frac{(B-m^2\omega^2)\cos(m\omega t+\delta_m)+m\omega A\sin(m\omega t+\delta_m)}{(m\omega A)^2+(B-m^2\omega^2)^2} \\ +\sum_{m=1}^{4}C'_m\frac{(B-m^2\omega^2)\sin(m\omega t+\delta'_m)-m\omega A\cos(m\omega t+\delta'_m)}{(m\omega A)^2+(B-m^2\omega^2)^2},
$$

where C_m and C'_m are put as follows,

$$
(38)\quad -n_0f'-(\gamma n_{20}-\alpha n_0 n_{10})f=\sum_{m=1}^{4}C_m\cos(m\omega t+\delta_m)+\sum_{m=1}^{4}C'_m\sin(m\omega t+\delta'_m).
$$

(37) can also be used for a particular solution of (36), if C_m and C'_m are put equal to the amplitudes of cosine and sine components of $q'+\gamma(q-q_0)$.

As n is equal to n_0+x_0+x, we can evaluate a rough variation curve of the electron density for the daytime not too far from the noon.

For the night time variation of the electron density the foregoing method is not applicable. For an approximate treatment we assume the positive ion density (n_2) as constant for the time under consideration. Then the differential equation for n is written below.

$$
(39)\quad \frac{d^2n}{dt^2}+(\beta+\gamma+\alpha n_2+2f)\frac{dn}{dt}+\{\gamma\alpha n_2+f(\beta+\gamma+\alpha n_2+f)+f'\}n=s_1\gamma g.
$$

When we notice that in the coefficients of the above equation the terms containing f and f' are very small in comparison to $\beta+\gamma+\alpha n_2$ and $\gamma\alpha n_2$, and that the former terms are sinusoidal functions of the first order (f^2 is neglected), the following solution is obtained for the first approximation. The term of g serves for the final value of n, but as it is very small, we neglect it for the brevity.

$$(40)\quad n = A_1 e^{-(\beta+\gamma+\alpha n_2)t}\left\{1-\frac{(\beta+\gamma+\alpha n_2)f-f'}{\omega^2+j\omega(\beta+\gamma+\alpha n_2)}\right\}+A_2 e^{-\frac{\gamma\alpha n_2}{\beta+\gamma+\alpha n_2}t}\left\{1+\frac{(\beta+\gamma+\alpha n_2)f+f'}{\omega^2-j\omega(\beta+\gamma+\alpha n_2)}\right\},$$

where A_1 and A_2 are the constants, which are to be determined from the actual conditions. In the above calculations the followings are assumed.

$$(\beta+\gamma+\alpha n_2)^2 \gg 4\gamma\alpha n_2.$$

Unless γ at night is neglected (here γ will denote the coefficiect of detachment by some non-photoelectric processes), the decay of n consists of two trends (exponential terms) generally, and under the influence of f each trend involves a small wavy component, the period and phase of which depend upon those of f and f' and other constants.

As seen from (40), the first term is the rapidly decaying component and its wavy component becomes insignificant soon after sunset. The second term decays slowly and its wavy component does not fade out too rapidly.

VI. Numerical examples.

The curves of g and f were shown in Fig. 2 and Fig. 3 in each foregoing section, and as the curves show, g can be neglected for most cases owing to its small order of magnitude.

In order to know the variation of n we must determine the values of q_0, α, β, γ, s_1 and s_2. As examples for F2 layer the following three sets of values were adopted for calculation.

(1) $q_0=70$ ions/cm^3/sec, $\alpha=10^{-11}$cm^3/sec, $\beta=10^{-4}$ sec^{-1}, $\gamma=3\cdot10^{-4}$ sec^{-1}, $s_1=0.2$, $s_2=0.8$,

(2) $q_0=70$, $\alpha=10^{-11}$, $\beta=10^{-4}$, $\gamma=10^{-4}$, $s_1=0.33$, $s_2=0.67$,

(3) $q_0=70$, $\alpha=10^{-11}$, $\beta=1.4\times10^{-4}$, $\gamma=0.7\times10^{-4}$ $s_1=0.4$, $s_2=0.6$.

For the above values x of (38) was calculated for the period around noon, putting $\theta=54°$ (colatitude of Takyo). Fig. 4 shows the results for three seasons, that is equinox, summer and winter solstices. If we put K as 0.5×10^{-7} emu[6] rather than 10^{-7} emu, the magnitude of x becomes twice as large.

As easily accepted by these curves, the variation curve of n near noon is flattened as compared with the usual curve of n_0+x_0, where x_0 is the solution of (36), that is, in the case of neglection of f and g. The flattening effect is greatest in summer solstice and in some cases for large amplitudes of x as in summer the curve becomes

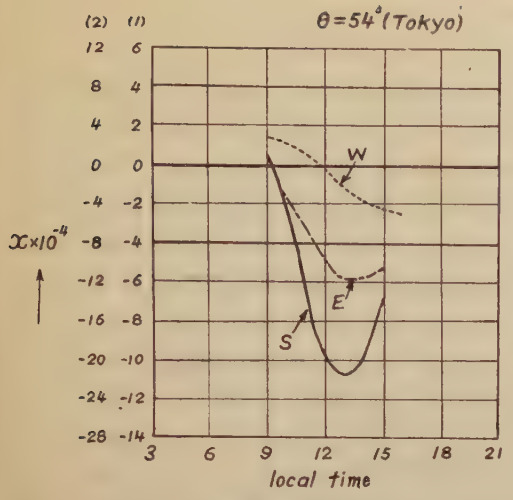

Fig. 4-A Time variation of $x\times10^{-4}$ (electrons/cm³).
case 1. $\beta=10^{-4}$, $\gamma=3\times10^{-4}$.
S: summer solstice, scale (1): $K=10^{-7}$emu,
E: equinox, scale (2): $K=0.5\times10^{-7}$emu.
W: winter solstice.

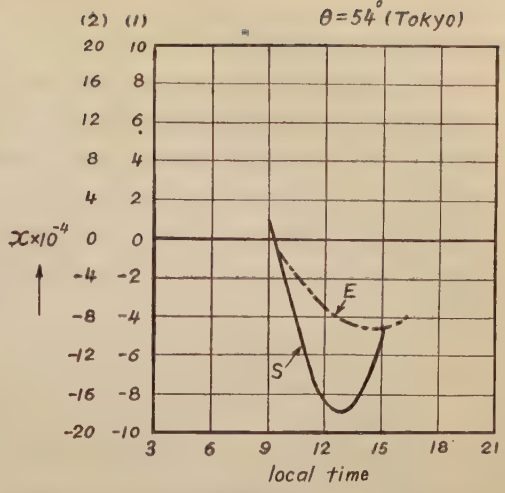

Fig. 4-B Time variation of $x\times10^{-4}$ (electrons/cm³).
case 2. $\beta=\gamma=10^{-4}$.
S: summer solstice, scale (1): $K=10^{-7}$emu.
E: equinox, scale (2): $K=0.5\times10^{-7}$emu,
W: winter solstice.

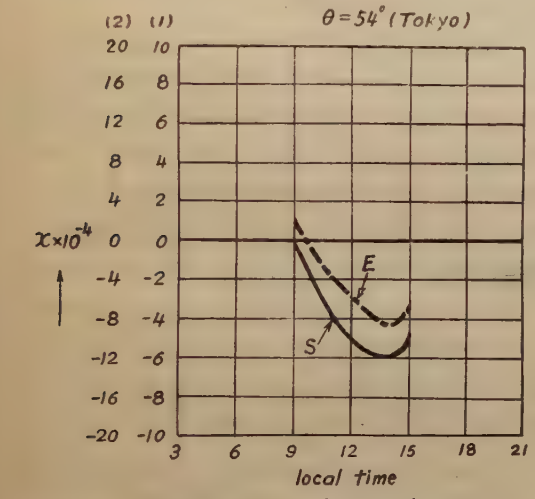

Fig. 4-C Time variation of $x=10^{-4}$ (electrons/cm³).
case 3. $\beta=1.4\times10^{-4}$, $\gamma=0.7\times10^{-4}$.
S: summer solstice, scale (1): $K=10^{-7}$emu,
E: equinox, scale (2): $K=0.5\times10^{-7}$emu.
W: winter solstice.

concave upward with two peaks in the daytime and the bottom of the curve comes near noon. For comparatively small x such as in winter, the single peak of n exists and its time can fall in the forenoon, though the usual curve without f and g has generally its peak in the afternoon.

For the night time variation the wavy components of slowly decaying term, that is the second term of (40), is significant. The exponent of the slowly decaying term $(\gamma\alpha n_2/(\beta+\gamma+\alpha n_2))$ is of the order of $(0.3\sim0.5)\times10^{-4}$ for the above three cases and the magnitude of the wavy component is about $(1.3\sim1.4)\times(2\sim3)\%$. If f for the night is taken as three times as great, as discussed in (iii) of the next section, the percentage will rise to about 10% of the slowly decaying term. This point is expected to account for the night time variation of n in the F layer.

As for the E layer the similar effects as in the F layer are expected, but the order of magnitude of the effects is comparatively less than that in the case of F layer. The considerations about this are left for future study.

VII. Notes and discussions on some associated problems.

It must be mentioned here that there are some points to be discussed in the

course of this study, which are directly connected to the physical nature of the dynamo theoretical phenomena.

(i) In the foregoing sections the velocities of electrons, negative and positive ions in the mass flow of the upper atmosphere were assumed as all equal (u and v), but there may be some questions regarding the velocity of electron flow. If we take into consideration the suggestion that the electrons lag behind the general flow of of atoms and molecules under the extremely low pressure of the ionosphere, the term of f in (8) should be neglected and consequently C and C' in (32), (33) become as follows.

$$(41) \qquad \begin{cases} C=q''+\gamma q'-(\gamma n_{10}-\alpha n_0 n_{20})f'+\gamma\alpha n_0^2 f+(s_1\gamma+s_2\alpha n_0)g'+\gamma\alpha n_0 g, \\ C'=q'+\gamma(q-q_0)-(\gamma n_{10}-\alpha n_0 n_{20})f+\gamma\alpha n_0^2\int f dt. \end{cases}$$

And (39) for the night time equation becomes as follows.

$$(42) \qquad \frac{d^2n}{dt^2}+(\beta+\gamma+\alpha n_2+f)\frac{dn}{dt}+\{\gamma\alpha n_2+f(\beta+\alpha n_2)\}n=s_1\gamma g.$$

As seen from the comparison of the above equations with (32), (33) and (39), there will be no substantial differences in the contents of consideration of n in the foregoing sections, even if u and v for the electrons are neglected.

(ii) Dynamo theory assumes a single layer as the overhead current sheet. It seems however to be accepted according to our recent study[2] that the F layer can serve as a sheet as well as the E layer. If the horizontal mass velocities in the both layers are of the same order of magnitude and the same phase, their contributions will be roughly equal, as their total conductivities are of the same order of magnitude, although a strict treatment of dividing their parts of contribution is difficult.

If we adopt the hypothesis by N. Fukushima,[4] that there exist double sheets of current system and the velocities at each sheet is different in magnitude and opposite in phase, the velocities u and v, and consequently f, become greater than those treated in the foregoing sections. Also the ionic flow (g) is made greater, and may not be simply neglected in some cases.

(iii) T. Nagata and M. Sugiura[5][6] explained the longitudinal inequality of solar diurnal variation of geomagnetic field by taking into account the non-coincidence of the axes of earth's rotation and geomagnetism. By this work it can be suggested that similar considerations as the above may lead us to a theoretical explanation of longitudinal inequality of electron density variation of the ionosphere (F layer). It was not difficult to extend the present study on this line, but this idea had to face the difficulty that the order of magnitude of g is not sufficient enough to discuss the above inequality of the electron density of F layer. In case of the hypothesis of double sheets with opposite velocities, a freedom of choice of each velocity is given, but it is not allowed to make g too great independently, because f becomes too great for each layer at the same time and its effect on the electron density grows unreasonably great.

It was tried to extend the study to the effect of solar disturbed current system

for S_D, taking into account the non-coincidence of the both axes, but for the same reason as above it will not be reported here.

(iv) In the equation (20) connecting J, u, v and Z, the total conductivity (K) is assumed as constant. But K varies actually in time and space, though its variation may not so great as the electron density (n) itself. We put

$$K=K_0/\xi, \tag{43}$$

where ξ is a function of λ (or t) and θ, and if we neglect the term of space derivatives of ξ, we can rewrite the equation (20) as follows.

$$\frac{\partial^2 J}{\sin\theta\partial\lambda^2}+\frac{\partial}{\partial\theta}\left(\sin\theta\frac{\partial J}{\partial\theta}\right)=rK_0\left\{\frac{\partial}{\partial\lambda}\left(\frac{v}{\xi}Z\right)+\frac{\partial}{\partial\theta}\left(\frac{u}{\xi}Z\sin\theta\right)\right\}. \tag{44}$$

Therefore the velocities u and v hitherto obtained in the foregoing sections are vertual or effective ones and equivalent to $\frac{u}{\xi}$ and $\frac{v}{\xi}$ respectivly. When we denote the former u and v as u_{eq} and v_{eq}, then follow the equations for the actual velocities u and v,

$$\begin{cases} u=\xi u_{eq}\,, \\ v=\xi v_{eq}\,. \end{cases} \tag{45}$$

According to our study ξ is roughly evaluated as 1 at daytime and about 3 at night in the middle latitude, with 10^{-7} emu of K_0, which was adopted in our foregoing treatments.

According to this consideration the value of f at night becomes simply 3 times as great as that in the foregoing treatments.

(v) It is to be noticed that by the presence of g and f the electricity can not be strictly neutral in the ionosphere. The relation is expressed by the following equation from (8), (9) and (10).

$$\frac{d}{dt}\{n_2-(n_1+n)\}=-f\{n_2-(n_1+n)\}-g. \tag{46}$$

If g and f are negligibly small, the electricity is practically neutral.

References

1. D.F. Martyn; Proc. Roy. Soc. A, Vol. 189, No. 241 (1947).
2. K. Maeda; J. Geomag. Geoelec., Vol. 2, No. 2 (1950), pp. 45~53.
3. S. Chapman & J. Bartels; Geomagnetism, Oxford Press (1940).
4. N. Fukushima; Geophys. Notes, Tokyo Univ., Vol. 2, No. 21 (1949).
5. T. Nagata & M. Sugiura; Geophys. Notes, Tokyo Univ., No. 36 (1948).
6. T. Nagata, N. Fukushima & M. Sugiura; J. Geomag. Geoelec., Vol. 2, No. 2 (1950) pp. 35~44.

Acknowledgements

The author wishes to express his sincere thanks to Prof. T. Nagata, Messers N. Fukushima and M. Sugiura of Tokyo University for their valuable discussions and kind help in the course of this study.

On the Effect of the Earth's Magnetic Field on the Virtual Height of the Ionosphere

By Teruo SATO

Geophysical Institute, Kyoto University.

Abstract

In this paper we calculate the virtual height of the reflection point of a radio wave incident in the ionosphere at a frequency of 0.834 fc, where fc is the critical frequency of the ionosphere, in the presence of the earth's magnetic field. We also calculate the magnitude of the retardation of the wave resulting from the transmission in the lower ionized layer. In these calculations, we take three cases that the inclination of the magnetic field vector respectively is 0°, 30° and 90°. It is found that the virtual height of the reflection point of the wave at a frequency of 0.834 fc, which is equal to the actual height of the ionosphere in the case of no magnetic field, does not indicate the actual height in the presence of the earth's magnetic field, and the value of the retardation depends on y, which is the ratio of the gyro-frequency to the wave frequency, and on f_1/f_2, where f_1 and f_2 are the critical frequency of the lower and upper ionized layers respectively.

Further, it is also found that the effect of the earth's magnetic field on both virtual height and retardation is maximum, when the inclination of the earth's magnetic field vector is 0°, that is, on the magnetic equator; and minimum when the inclination is 90°, that is, on the magnetic pole.

1. Introduction.

It is well known that the height of the reflection point of an incident radio wave in the ionosphere, is generally shown as virtual height. It is difficult to calculate this height theoretically in the presence of the earth's magnetic fiield. Usually, in order to avoid complexity of the effect of the earth's magnetic field, it is expressed by an integral for $H\int_{\mu=1}^{\mu=0}\frac{dz}{\mu}$ in the case of the vertical incidence, where μ is the refractive index, z is the height in the unit of the scale height, and H is the scale height of the ionosphere. Appleton[1] calculated this integral by assuming a relation between the electron density and the height, and deduced the formula of the virtual height of the reflection point of the wave at frequencies below the critical frequency. Booker and Seaton[2] showed that the actual height of the maximum electron density is equal to the virtual height of the vertically incident wave at a frequency of 0.834 fc,

using Appleton's formula.

In these studies the effect of the earth's magnetic field is not considered. If this effect is not great, the results of these studies hold. In general, this effect has been considered to be small.

In this paper we calculate the virtual height of the reflection point of the wave at a frequency of 0.834 fc, in the case of vertical incidence in the presence of the earth's magnetic field by the numerical operation, assuming a parabolic electron density distribution, and for some typical cases of inclinations of the earth's magnetic field. Further, we calculate, for the assumed ratio of the critical frequency of the lower ionized layer to that of the upper layer, the magnitude of retardation of the incident wave in the F_1 and F_2 layers resulting from the transmission of the wave in the lower ionized layers.

2. Calculation of Virtual Height in the Presence of the Earth's Magnetic Field.

The virtual height of a vertical incident wave in the presence of the earth's magnetic field is clearly given by

$$h_m' = H\int_{\mu=1}^{\mu=0} \frac{\partial(f\mu)}{\partial f}\,dz = H\int_{\mu=1}^{\mu=0}\left(f\frac{\partial\mu}{\partial f}+\mu\right)dz, \qquad (1)$$

where f is the frequecy of the incident wave. The distance between the earth and the base of the ionized layer is omitted for simplicity.

In order to calculate this integral, it is more convenient to use the relation between the refractive index and the electron density and also the electron density and the height, than to use the refractive index itself which contains earth's magnetic field in a complicated form. From the definition of the height, this height is equal to the half-thickness of the ionized layer. At first, the relation between the electron density and the refractive index is given by Booker[3] as follows;

$$x^3+Ax^2+Bx+\Gamma=0, \qquad (2)$$

$$A=-u\{1+2(C^2-q^2)\}, \qquad (3)$$

$$B=(C^2-q^2)\}(2u^2-y^2)+(S_1y_1+S_2y_2+qy_3)^2+u^2(C^2-q^2)\}, \qquad (4)$$

$$\Gamma=-u\{u^2-y^2\}(C^2-q^2)^2, \qquad (5)$$

where $x=4\pi e^2N/mp^2$,

$p=2\pi f$, N=electron density, e, m=change and mass of electron.

$u=1-iz\fallingdotseq 1$,

$z=\nu/p$,

S_1, S_2, C=components of a unit vector in the direction of incidence along the rectangular axes 1, 2, 3. In the vertical incidence, $S_1=S_2=0$, $C=1$.

$q=$ upward vertical component of phase-propagation vector. This equals to the refractive index in the vertical incidence.

$y=f_H/f$,= ratio of gyro-frequency to wave frequency.

y_1, y_2, y_3,=component of the earth's magnetic field vector along the axes 1, 2, 3.

If we take the axis 3 in the direction of propapation of the wave, the direc-

tions of the axes 1 and 2 are arbitrary. Because the components of the earth's magnetic field vector is contained in $(S_1y_1+S_2y_2+qy_3)$ in (4), and this is the scalar product of the phase propagation vector and the earth's magnetic field vector. In other words, the effect of the earth s magnetic field depends only on an angle between the direction of the phase-propagation and the earth's magnetic field vector. In the vertical incidence, $S_1=S_2=0$, $q=\mu$, and the effect of the earth's magnetic field depends on an inclination of the field vector. As the component y_3 is contained in the form of y_3^2, results of calculations in the north hemisphere are equal to results of calculations in the south hemisphere. In this study we take three cases in which the inclination of the earth's magnetic field vector is 0°, 30° and 90°. The inclination 0° and 90° are the value on the magnetic equator and magnectic pole. In these places, the solution of (2) shows a kind of a singular solution. Therefore, it seems to be appropriate to start from the calculation in the inclination of 30°.

A, Case of Inclination 30°.

Equation (2) has three roots. One of them refers to the ordinary wave and other two roots to the extraordinary waves. One of the two roots corresponding to the extraordinary waves is of no practical interest, because its does not show $x=0$ for the value $\mu=1$, but the other chracterises that the wave is reflected from the point $x=1-y$. For a root corresponding to the ordinary and extraordinary wave $\frac{\partial\mu}{\partial f}$ and $f\frac{\partial\mu}{\partial f}$ is given by

$$\frac{\partial\mu}{\partial f}=\frac{-\left[\frac{\partial A}{\partial f}x^2+\frac{\partial B}{\partial f}x+\frac{\partial \Gamma}{\partial f}+\frac{\partial x^3}{\partial f}+A\frac{\partial x^2}{\partial f}+B\frac{\partial x}{\partial f}\right]}{\frac{\partial A}{\partial \mu}x^2+\frac{\partial B}{\partial \mu}x+\frac{\partial \Gamma}{\partial \mu}}, \tag{6}$$

$$f\frac{\partial\mu}{\partial f}=\frac{2y^2(1-\mu^2)+(1-\mu^2)(6-4y^2-2\mu^2+\mu^2y^2)x+4x^2(2\mu^2-3)+6x^3}{\mu[4x^2+\{2.5y^2-8+(4-y^2)\mu^2\}x+4(1-y^2)(1-\mu^2)]}. \tag{7}$$

For a particular value of y, (7) is evaluated by substitution of the value of x and μ which is related by equation (2). If we substitute (7) into (1), then (1) is calculated, assuming electron density distribution, by numerical operation for the difficulty of the integration. Curves of $\mu+f\frac{\partial\mu}{\partial f}$ are shown in Fig. 1 for $y=$ 1/4 and 1/10 for ordinary and extraordinary and extraordinary waves by a full and dotted lines respectively. The curves indicate that the value for the ordinary wave is smaller than that for the extraordinary for the same electron density. This is because the penetration frequency of the extraordinary wave is greater

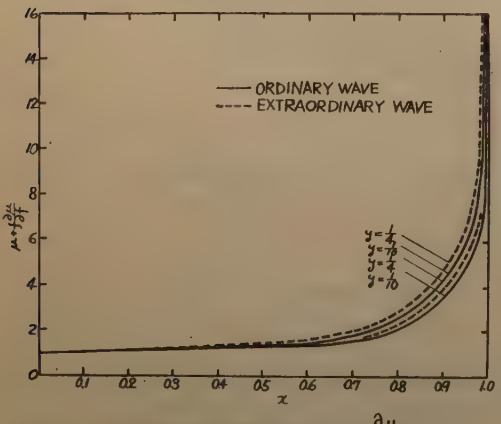

Fig. 1 The relation between $\mu+f\frac{\partial\mu}{\partial f}$ and x for ordinary and extraordinary wave for $y=1/4$ and $1/10$ in the case of inclination 30°.

than that of the ordinary wave for the same layer. Curves also indicate that as y increases, $\mu+f\frac{\partial\mu}{\partial f}$ increases for the same x. This implies that the effect is great as the wave frequency is small. Further, it is known that as the electron density approaches the maximum value, this value rapidly increases. Therefore, the effect of the earth's magnetic field is great in the neighbourhood of the reflction point and not in the region of the small electron density.

As the electron distribution, we take a parabolic form given by the expression

$$s=100\{1-(1-x)^{\frac{1}{2}}\}, \qquad (8)$$

where s is the height in km (that is, the distance from the base of the layer), and $x=4\pi e^2N/mp^2$.

This expression shows that at $x=1$ the height is 100km and at $x=0$ the height is 0. As above mentioned, the sending and receiving station of the wave are situated at $x=0$.

The electron density at a height of the reflection point of the wave at a frequency of 0.834 fc in an ionized layer, is equal to $0.695\,N_0$, where N_0 is the maximum electron density of the layer. Therefore, the distribution of the electron density to be applied to the calculation is the part below this level. Thus we can integrate numerically (1) by use of (7) and (8). These results of calculations for the ordinary and extraordinary waves are shown in Fig. 1. h_m and h_a show the virtual height of the wave at a frequency of 0.834 fc in the presence of the earth's magnetic field and that in no magnetic field respectively. (h_m-h_a) is the value to be corrected in the calculation in no magnetic field. As we presume,these curves explain that the virtual height of the wave at a frequency of 0.834 fc in the presence of the earth's magnetic field, is greater than that in the case of no magnetic field. For example, in the case of $y=1/4$ for an ordinary wave, the actual height should be smaller by 20.5km than that calculated in no magnetic field. Therefore, when we calculate the actual height of the maximum electron density, we must take the virtual height of the wave at a freqnency less than 0.834 fc. Curves also show that the quantity (h_m-h_a) is greater for small value of $1/y$ than for great value, and greater for the extraordinary wave than for the ordinary wave. It is well known that the difference between the critical frequency of the ordinary wave and that of the extraordinary wave, is about 0.6 Mc/sec. in practical observation for middle latitude. Thus (h_m-h_a) for the ordinary wave, for example, at a 4 Mc/sec. corresponds to (h_m-h_a) for tne extraordinary wave at a frequency of about 4.6 Mc/sec., and $(h_m$

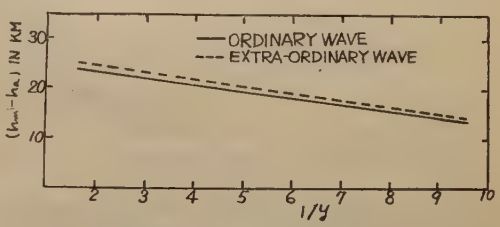

Fig. 2 The difference of the height of the reflection point of the wave incident in the ionosphere in the presence of the earth's magnitic field and in no magnetic field. h_m shows the height in the presence of magnetic field and h_a in no magnetic field.

$-h_a$) from the two waves is equal. It is sufficient to calculate for only one kind of wave.

These results are proportional to the semi-thickness of the ionized layer.

B. Case of Inclination 90°.

Equation (2) has three roots. In this case one of them is 1. This implies that the refractive index is independent of the electron density. Then this root cannot be taken in our study. Two other roots are $(1-\mu^2)(1+y)$, $(1-\mu^2)(1-y)$. Waves characterized by these roots are the wave reflected from the point of $x=1+y$ and $x=1-y$ respectively. These refer to the extraordinary wave. $f\frac{\partial\mu}{\partial f}$ for two waves is given by

$$f\frac{\partial\mu}{\partial f}=\frac{2y^2(1-\mu^2)+(1-\mu^2)2x(3-\mu^2-2y^2\mu^2)-4x^2(3-2\mu^2)+6x^3}{(x-1)[x-(1-y^2)(1-\mu^2)]} \qquad (9)$$

Curves $\mu+f\frac{\partial\mu}{\partial f}$ for two waves, after a similar operation with that in A, are given in Fig. 3 for $y=1/4$ and $1/10$. Full lines show the wave reflected from $x=1+y$, and dotted lines show the wave reflected from $x=1-y$. It is easily clear that the form of curves are similar with those in Fig. 1, and $\mu+f\frac{\partial\mu}{\partial f}$ for the wave reflected from $x=1-y$ is greater than that for the wave reflected from $x=1+y$. Comparing the dotted line for $y=1/4$ and that for $1/10$ in Fig. 1 and 3, it is found that the value $\mu+f\frac{\partial\mu}{\partial f}$ is greater for lines in Fig. 1 than that in Fig. 3. This implies that the effect of the earth's magnetic field becomes greater as the inclination decreases. This tendency is indicated over all x, and specially remarkable near $x=1$.

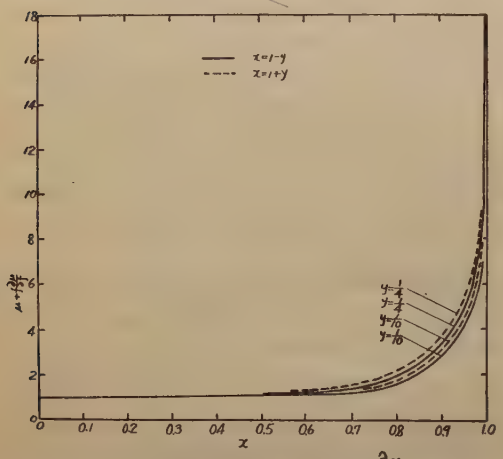

Fig. 3 The relation between $\mu+f\frac{\partial\mu}{\partial f}$ and x for the waves reflected from the point $x=1-y$ and $x=1+y$ for $y=1/4$ and $1/10$ in the case of inclination 90°.

Integrated height is given in Fig. 4. The full line shows (h_m-h_a) for the wave reflected from $x=1+y$, and the dotted line shows that for the wave reflected from $x=1-y$. (h_m-h_a) for the two waves are small compaced with those in Fig. 2, and become smaller as $1/y$ increases.

C. Case of Inclination 0°.

Equation (2) has three roots. But in this case two of them are of no practical interest, because, for one of the two x does not become 0 when μ is 1, and for the other $x=1-\mu^2$, which is the relation used in the calculation in no magnetic field. A root to be taken in our study is

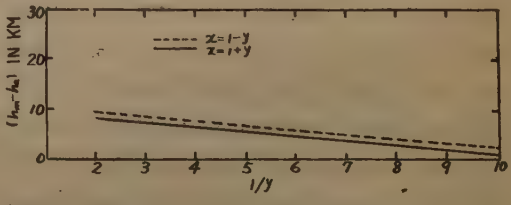

Fig. 4 (h_m-h_a) for the waves reflected from the point $x=1-y$ and $x=1+y$ in the case of inclination 90°.

$$x=\frac{2-\mu^2-\sqrt{4y^2(1-\mu^2)+\mu^4}}{2}. \tag{10}$$

For the wave characterized by this root, $f\frac{\partial\mu}{\partial f}$ is given by

$$f\frac{\partial\mu}{\partial f}=\frac{\mu^2x^2+(1-\mu^2)(y^2-\mu^2)x+y^2(1-\mu^2)}{\mu y^2x}. \tag{11}$$

Curves for $\mu+f\frac{\partial\mu}{\partial f}$ are shown in Fig. 5 for $y=1/4$ and $1/10$. The wave characterized by (10) is that reflected from the point of maximum electron density defined by $x=1-y$. Thus comparing the curves in Fig. 5 with those in Fig. 1 and 3, $\mu+f\frac{\partial\mu}{\partial f}$ in Fig. 5 is the greatest in three cases for the same electron density and the same value of y. Especially, the difference is great near $x=1$.

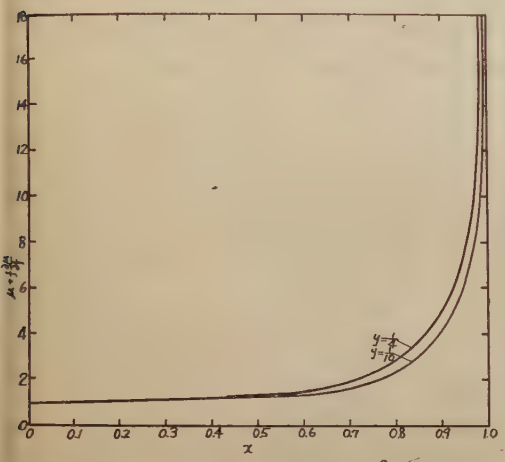

Fig. 5 The relation between $\mu+f\frac{\partial\mu}{\partial f}$ and x for $y=1/4$ and $1/10$ in the case of inclination 0°.

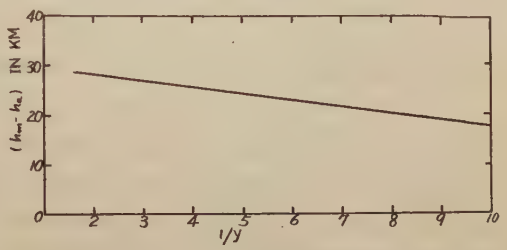

Fig. 6 (h_a-h_m) for wave reflected from the point $x=1-y$ in the case of inclination 0°.

Integrated height is given in Fig. 6. (h_m-h_a) for the same $1/y$, is the greatest in three cases.

After all, the effect of the earth's magnetic field is maximum in the case that the inclination of the magnetic field vector is 0°, that is, on the magnetic equator and minumum on the magnetic pole.

3. Calculation of Retardation.

By use of the above mentioned numerical we will consider the magnitude of the retardation of the wave in the lower ionized layer. It is pointed out that in the case of vertical incidence of the wave, for example, in the F_2 layer, the wave is affected by the F_1 and E layers. In the calculation of this kind it is necessary to know the electron density and the thickness of each layer and the form of the valley between two layers. The form of the valley between F_1 and F_2 and that between F_1 and E are not distant. These are not detected by the wave observation. Manning[4] assumed this form in his work. Therefore, we must, too, assume the form of the valley in the calculation. We classify this form into two cases, that is;

(a) the case where the electron density over the valley is the same as the maximum electron density of the lower ionized layer, and

(b) the case where is no another electron distribution particularly defined between the two layers, which is superposed on the electron distribution of two largers.

A. Case of Inclination 30°.

(i) Case of the crititical frequency of the F_2 layer.

In this case, as the electron density in the E layer is too small compared with that in F_1 layer, we can neglect the effect of the retardadation in the E layer. The electron density of the F_1 layer is not much great but two times of that of the E layer. Concerning the case (b), the effect is small compared with the case (a), so that the calculation in the case (b) is omitted. The electron distribution of F_1 and F_2 layer is assumed to be Chapman's and parabolic respectively. The scale height and the height of the maximum electron deusity in the F_1 and F_2 layer are 30km, 70km and 220km, 320km respectively. Results of these numerical calculations only for the ordinary wave for $y=1/6$, 1/8, and 1/10 are shown in Fig. 7, as the magnitude of the retardation for the ordidary and extraordinary waves is almost equal.

These curves indicate that the retardation of the wave depeuds on the ratio of the critical frequency of F_1 layer to that of F_2 layer. As the ratio increases the retardation increases. Therefore, if the ratio of the electron density of the F_1 layer to that of F_2 layer is small, the effect of the retardation can be neglected. From the wave observation, it is found that the maximum electron density of the F_1 and F_2 layer in day-time is about $2\sim 3\times10^5$/c.c. and $1\sim2\times10^6$/c.c.. Then the effect of the retardation on the virtual height can be neglected in practice.

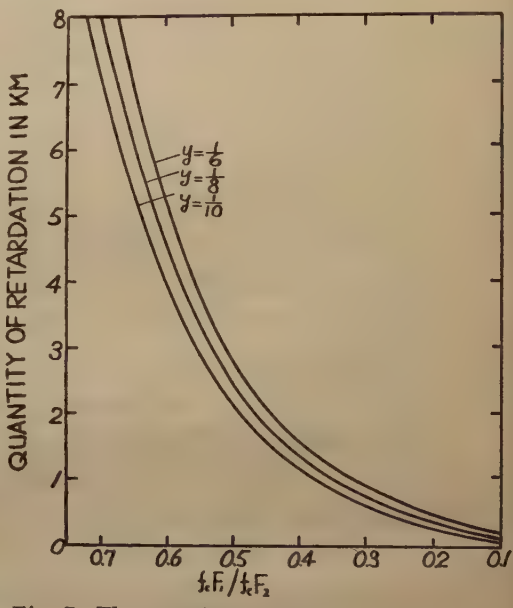

Fig. 7 The magnitude of the retardation of the wave at the critical frequency of the F_2 layer in the case of inclination 30°.

(ii) Case of the critical frequency of the F_1 layer.

In this case the scale height of the E layer is taken to be 10km, and as the difference between the electron density in two layers is small, it appears that the retardation is considerable. From the wave observation, it is found that the maximum electron density of the E layer in day-time is $1\sim1.5\times10^5$/c.c..

case (a)

Results are shown in Fig. 8 for $y=1/3$ and 1/4 by full lines. It is found that as the ratio of the critical frequency of the E layer to that of the F_1 layer increases, the retardation in E layer rapidly increases as in the case (i), and reaches to 18.5km for 0.7.

case (b)

Results are shown in Fig. 8 for $y=1/3$ and 1/4 by dotted lines. It is clear that the effects are smaller than those in case (a). In the practical observations the

possibility may be greater in the case (b) than in the case (a). Thus when we are concerned with a measurement of the height of the maximum electron density of F_1 layer, it is necessary to correct.

B. Case of Inclination 90°.

(i) Case of the critical frequency of the F_2 layer.

As the quantity of retardation for the two waves are equal, operation for the wave reflected from the point $x=1-y$, is carried out for $y=1/6$, $1/8$ and $1/10$. The quantity of the retardation in Fig. 9 is small for all y compared with Fig. 7. When the ratio of the critical frequency of F_1 layer to that of the F_2 layer is small, the retardation does not change for the increase of the inclination of the earth's magnetic field, and it becomes greater for the smaller inclination when the rotio increases

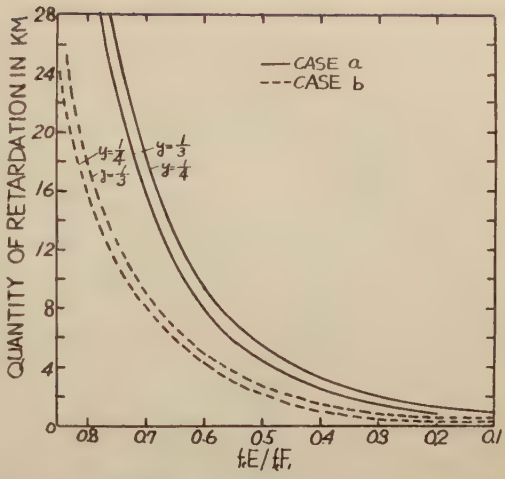

Fig. 8 Quantity of the retardation of the wave at a critical frequency of the F_1 layer. Full lines show the case (a) and dotted lines the case (b) in the case of inclination 30°.

(ii) Case of the critical frequency of the F_1 layer.

Curves for retardation for two cases (a) and (b) are shown in Fig. 10. Full and dotted lines show case (a) and case (b) respectively. When ratio of the critical frequency of the E layer to that of the F_1 layer is great, the decrease of the quantity

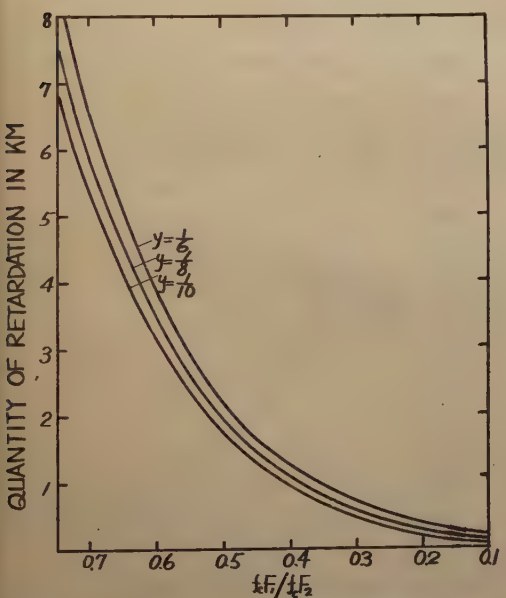

Fig. 9 Quantity of the retardation of the wave at a critical frequency of the F_2 layer in the case of inclination 90°.

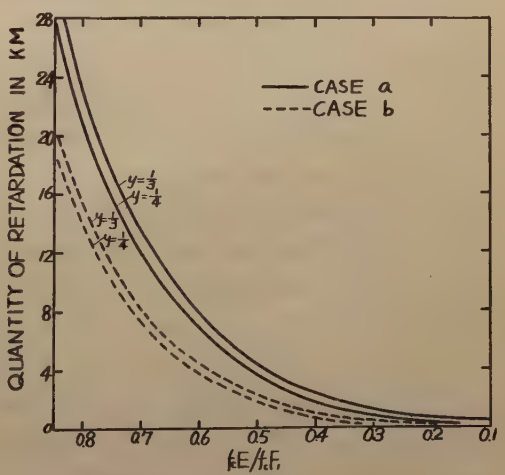

Fig. 10 Quantity of the retardation of the wave at a critical frequency of the F_1 layer in the case of inclination 90°.

of the retardation, comparing with Fig. 8, is remarkable. This decrease is mainly due to the decrease of retardation above the maximum electron density of the E layer.

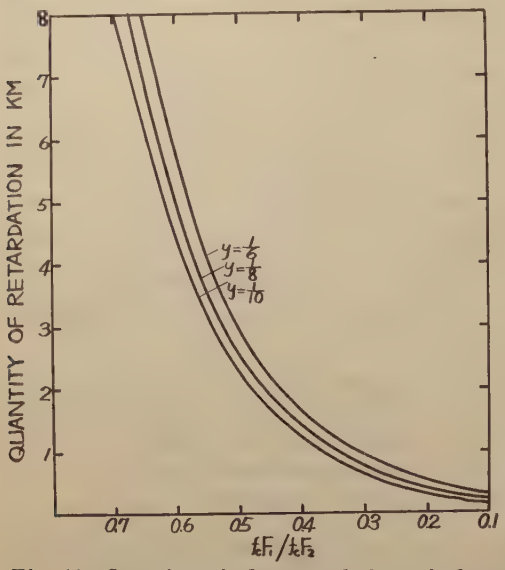

Fig. 11 Quantity of the retardation of the wave at a critical frequency of the F_2 layer in the case of inclination 0°.

C. Case of Incliuation 0°.

(i) Case of the critical frequency of the F_2 layer.

In this case, the quantity of the retardation is great compared with A aud B. Fig. 11 shows these quantities. Shapes of curves are similar with (i) in A aud B.

(ii) Case of the critical frequency of the F_1 layer.

Retardation of the wave in the E layer is greatest of the three cases. Even in the case (b) the retardation reaches, in Fig. 12, about 10km for $y=1/3$ and $1/4$ when the ratio of the critical frequency of the E layer to that of F_1 layer is 0.7. Therefore, the correction is necessary in a measurement of the virtual height of the F_1 layer near the magnetic equator. When the ratio is below 0.4, the retardation is small.

4. Conclusion.

It is found that the effect of the earth's magnetic field and the retardation of the wave, by which the virtual height of the reflection point of the wave is affected, increase as the frequency of the wave incident in the ionosphere decreases and also the retardation of the wave increases as the ratio of the critical frequency of the lower ionized layer to that of the upper ionized layer increases. Further, it is pointed out that the effect of the earth's magnetic field and the retardation of the wave increase when the inclination of the magnetic field vector decreases, and reach the maximum on the magnetic equator and the minimum on the magnetic pole.

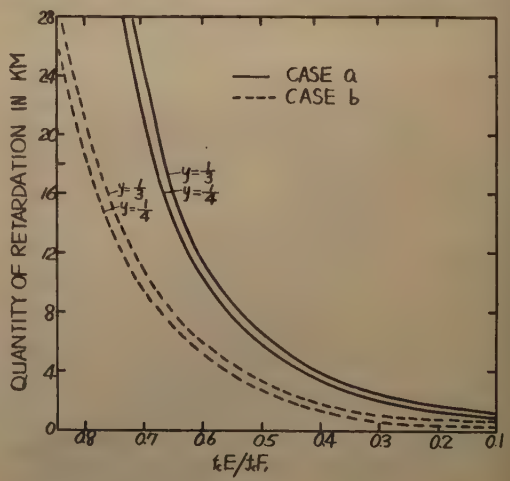

Fig. 12 Quantity of the retardation of the wave at a critical frequency of the F_1 layer in the case of inclination 0°.

In the practical operation of correction to the virtual height of the reflection point of the wave at a frequency of 0,834 fc, it is necessary to consider two corrections. The one is the correction for the

effect of the earth's magnetic field in the layer itself, and the other for the retardation of the wave resulting from the trausmission in a lower ionized layer. These corrections are to be taken in a measurement conceruiug the F_1 layer, but one of the two, the retardation in the lower ionized layer, can be neglected concerning the F_2 layer.

In conclusion, the writer wishes to express his hearty thanks to Prof. M. Hasegawa, Dr. M. Ota and Mr. Hirono for their kind advice, aud to Dr. K. Maeda for helpful suggestions during the course of this study.

References

(1) E.V. Appleton, Proc. R. Soc., A. **162**, 451 (1937)
(2) H.G. Booker and M.J. Seaton, Phys. Rev. **57**, 87 (1940)
(3) H.G. Booker, J. Geophys. Resear. **54**, 243 (1949)
(4) L.A. Manning, Proc. I.R.E. **137**, 599 (1949)

On the Relation between the Cosmic Ray Intensity and the Geomagnetic Storm

By Kazuo NAGASHIMA
Geophysical Institute, Kyoto University

Abstract

Many investigators made various attempts which were calculated to explain the decrease of cosmic ray intensity during a magnetic storm in the maguetic field of the ring current, suggested by S. Chapman.[1] Unfortunately their results seemed to contain many qualitative faults.

In this paper, I do not try to search for the cause of the decrease in the magnetic field, but in the electric field, connected with the magnetic storm. From such a standpoint, the shape of the westward current system which is appropriate to account for the cosmic ray phenomena during the maguetic storm, is discussed. Qualitatively, the results, obtained, seem to be adequate enough to explain quite reasonably the observed phenomena of cosmic rays, although, quantitatively, there still remain somewhat questionable points.

In this paper, I also discuss relative merits between the magnetic field hypothesis and this electric one.

§ 1. *Introduction*

The decrease of cosmic ray intensity during the magnetic storm is a world-wide phenomenon, which was first discovered by S.E. Forbush[2] and thereafter confirmed by many others.[3]

Its principal characteristics are as follows:

(A) Decrease of cosmic ray intensity:[2],[3] —When a magnetic storm breaks out, the intensity of cosmic rays begins to decrease, the curve of which is similar to that of the earth's magnetic horizontal component.

(B) Latitude effect of the decrease of cosmic ray intensity:[4]—S.E. Forbush, investigating the latitude effect of the decrease of cosmic ray intensity during the magnetic storm by using the data obtained from several observatories, found it to be only several per cent.

(C) Decrease of cosmic ray intensity at high latitudes well above the "knee" of the latitude effect:[5]—During their voyage, D.H. Loughridge and P.H. Gast found this fact. This phenomenon also appears at Godhavn (Geomagnetic Latitude 80°N.).

(D) No variation of cosmic ray intensity during some large magnetic storm:[4] —It is frequently reported that in spite of large decreases of magnetic horizontal

component during some magnetic storms, the intensities of cosmic rays do not vary at all.

(E) Increase of the amplitude of the diurnal variation of cosmic rays during the magnetic storm:[6]—Y. Sekido pointed out that the amplitude of cosmic rays increased during the magnetic storm and the curve of this increase had no similarity with that of the earth's magnetic horizontal component or that of the cosmic ray intensity.

(F) Advancement of the phase of the diurnal variation of cosmic rays during the magnetic storm:[6]—At the same time, Y. Sekido showed that the phase of the diurnal variation of cosmic rays advanced during the magnetic storm and the curve of this advancement had some similarity with that of the earth's magnetic horizontal component or that of the cosmic ray intensity.

S. Chapman concluded that the axially symmetric part of the magnetic storm field was due to the electric current which flowed westward above the earth, a few earth radii apart. At the same time, he[1] suggested that, in the inner region of such current system, the earth's magnetic field was weakened, while it was strengthened in the outer region. This can be regarded as the increase of the earth's magnetic dipole moment in the outer region, so that the cosmic ray intensity was decreased during the magnetic storm, by the well known theory of Lemaitre and Vallarta.[7]

Accepting this assumption as true, let us examine in what follows whether this magnetic hypothesis is suitable in explaining reasonably the above mentioned phenomena.

(i) T.H. Johnson,[8] analyzing this storm effect, concluded that the magnetic storm effect of cosmic rays was of the order three hundred times too large to be accounted for as an increase of the magnetic dipole moment according to Chapman's hypothesis.

(ii) As for experimental evidence (B), there is nothing to be said about the propriety of this theory, as the motion of a charged particle is not clear at present in the earth's magnetic dipole field and the magnetic field produced by the west-ward current system.

(iii) We cannot explain the experimental evidence (C) because the increase of the earth's magnetic dipole moment seems to give no influence in a region well above the "knee" of the latitude cut-off which is supposed to be due to the presence of the sun's magnetic dipole field, suggested by L. Jánossy.[9] But, as there is at present no agreement about Jánossy's suggestion, it may be unsuitable to judge from this phenomenon that this hypothesis encounters with a serious difficulty.

(iv) Experimental evidence (D) seems to be explained by this hypothesis as follows: The larger the distance to the current system (for example Ring Current) from the earth's centre, the larger the magnetic dipole moment of the earth. Then the decrease of cosmic ray intensity becomes larger. That is to say, this phenomenon depends upon the dimension of the current system.

(v) Experimental evidence (F) seems to be explainable by this hypothesis.[10] But it is difficult to acount for experimental evidence (E), because it is low energy

region of cosmic rays, that is prevented to arrive at the earth by the increase of the earth's magnetic dipole moment, and therefore the amplitude of the diurnal variation of cosmic ray during the magnetic storm must be decreased.

Some criticism against this Chapman's hypothesis is brought forward as follows: As pointed out by T.H. Johnson,[11] and J. Clay and E.M. Bruin,[12] the magnetic field of the region, in which cosmic rays suffer extremely the influence of the earth's magnetic field, is weakened by the ring current of the magnetic storm, and therefore there must result an increase of cosmic ray intensity. This idea is inferred from the Bruche's experiment[13] of the ring current model, which indicates the southward shifting of auroral zone.

T. Nagata,[14] treating mathematically the problem of charged particles in the magnetic fields of the earth's dipole and a ring current, confirmed the Bruche's experiment.

From these considerations, we cannot understand why the cosmic ray intensity is decreased by such a ring current which causes the southward shifting of auroral zone, because cosmic rays are only different in energy from auroral particles, and their motions in such a magnetic field must have some similarity.

Recently, all attempts by many investigators,[15] following Chapman's suggestion, resulted in failures.

From the above discussions, it is not appropriate to account for the decrease of cosmic ray intensity by this hypothesis. But, supposing from their similarity in phase between the decrease of magnetic horizontal component and that of cosmic ray intensity, we cannot suppose, these phenomena are produced by quite different causes.

On the other hand, H. Alfvén[24] advocated a hypothesis that the intensity of cosmic rays was decrease during the magnetic storm by the electric field produced in the stream which was emitted from the sun. In the next, I will state the outline of this hypothesis and attempt to examine the validity of it.

A neutral ionized stream emitted from the sun, passing through the solar magnetic field, positive and negative charges are accumulated at the boundary of this stream by the influence of the magnetic field and then an electric field is produced in the stream, as shown in Fig. 1. As pointed out by H. Alfvén, the charges accumulated on the sides of the stream tend to produce a current, for example along the line AEB. However, the inductance of this loop is so big that its time constant τ is very long, possibly of the order of years. When the time during which the stream has been on is short compared to τ, there is no appreciable electric field outside the stream, because the field from the charges on the sides of the stream is neutralized by an induced field. Then, before the magnetic storm, for example when the earth locates at a point B in Fig. 1, the cosmic rays, which arrive on the earth passing through the stream, gain energies corresponding to the potential difference of the stream. While the cosmic rays, not passing through it, do not change in energies. Therefore the intensity of cosmic rays becomes higher than the normal

state on the average. After the storm, when the earth locates at a point A in Fig. 1, the cosmic rays, passing through the stream lose their energies, and not passing through it, they make no change in energies. So that the intensity of cosmic rays becomes lower than the normal state, on the average. He stated also that the electric field of the order of about 10^8 volts was necessary in order to produce a variation of 1 per cent of the intensity. This is a rough review of his hypothesis. According to this hydothesis, the intensity of cosmic rays must increase before and decrease after the storm, and the quantity of the increase must be almost the same as that of the decrease. However, in the cases of the cosmic ray storms, commonly observed, the increase does not occur so that this is a difficult point of this hypothesis. Moreover, the data of cosmic ray storm which he cited in order to explain his hypothesis, is that of the extraordinary increase of cosmic ray intensity which seldom occurs. Even in this case, the cause of the increase is not the same as that of the decrease, because the increases produces extremely the latitude effect at various observatories, while the decrease does not. So that, although his hypothesis is very suggestive, it must encounter with a serious difficulty. Moreover, he did not calculate accurately the influence of the electric field upon the cosmic ray intensity.

From the above various considerations, it is possible to say that the cosmic ray storm is produced by some cause growing with the west-ward current system, if this cause will explain reasonably the above mentioned phenomena. The magnetic field of the current system may become this cause if Chapman's hypothesis will be improved, but I will attempt in what follows at explaining these phenomena by the electric field (which differs from that of the stream).

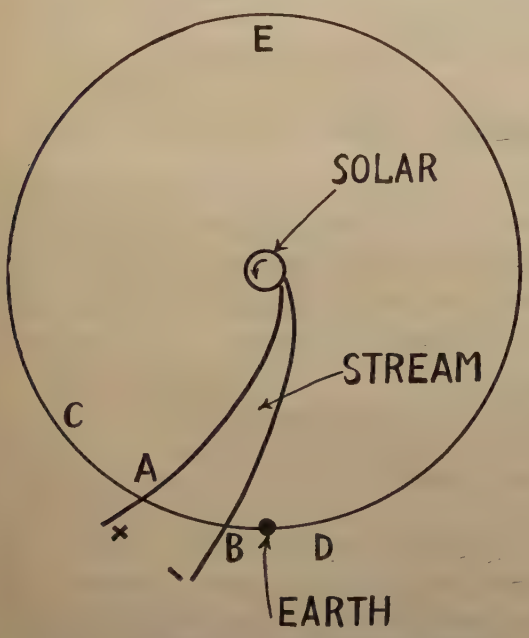

Fig. 1 Polarization of the neutral ionized stream by the solar magnetic field.

Prior to this, we must examine the influence of an electric field upon the cosmic ray intensity.

§ 2. *On the Motion of Charged Particles in the Electro-Magnetic Field*

In a magnetic field, from the extended Liouville's theorem,[9],[19] the intensity of cosmic rays in an allowed direction, defined as the number of particles of given energy crossing unit solid angle per unit time, is the same as it is at infinity and therefore, if the distribution of cosmic particles at infinity, is assumed to be isotropic, the intensity is precisely the same in all allowed directions. So that we can easily obtain a direc-

tional intensity of cosmic rays at any point on the earth by only knowing the intensity spectrum of primary cosmic rays and the minimum energy at that point (cut-off energy).

On the other hand, there is a different appearance in an electro-magnetic field. The intensity of cosmic rays in space[9] is

$$I=\frac{P^3}{m}\cdot D, \tag{2.1}$$

where m and P are mass and momentum of cosmic ray respectively, and not constants, and

$$D=\frac{\delta N}{\delta V} \quad \text{with} \quad \delta V=\delta x\cdot\delta y\cdot\delta z\cdot\delta P_x\cdot\delta P_y\cdot\delta P_z. \tag{2.2}$$

δN is the number of particles in δV. From the extended Liouville's theorem, D is constant in an electro-magnetic field,[19] but P and m are varied from point to point by the influence of the electric field, then the intensity changes as follows,

$$\Delta I=D\cdot\left(\frac{3P^2}{m}\cdot\Delta P-\frac{P^3}{m^2}\cdot\Delta m\right). \tag{2.3}$$

From Eqs. (2.1) and (2.3)

$$\frac{\Delta I}{I}=3\cdot\frac{\Delta P}{P}-\frac{\Delta m}{m}=\frac{3W\cdot\Delta W}{W^2-(m_0c^2)^2}-\frac{\Delta W}{W}, \tag{2.4}$$

where m_0 and W are rest mass and total energy of the particle respectively and c is the velocity of light. With the relation $W=E+m_0c^2$, Eq. (2.4) becomes

$$\Delta I=L(E)\cdot\Delta E\cdot I, \tag{2.5}$$

where

$$L(E)=\frac{2}{E}-\frac{2(m_0c^2)}{E^2}+\frac{5(m_0c^2)^2}{E^3}-\frac{11(m_0c^2)^3}{E^4}+\cdots\cdots. \tag{2.6}$$

Then, the intensity of cosmic particles changes from I to $I-\Delta I$, when its kinetic energy E decreases by an amount ΔE. This is most important fact for the explanation of the decrease of intensity, as to be mentioned in the next section. Thus, taking this effect into consideration, we can obtain a directional intensity at a given point on the earth by getting the cut-off energy and intensity spectrum of primary cosmic rays, as well as in the case of the magnetic field.

The equation of a charged particle in the electro-magnetic field is

$$\frac{d}{dt}(m\boldsymbol{V})=e\boldsymbol{E}+\frac{e}{c}[\boldsymbol{VH}]. \tag{2.7}$$

As the current system produced during the magnetic storm seems to be symmetry about the axis of the earth's magnetic dipole moment, so the electro-magnetic field produced by this system is also symmetry about this axis. Moreover, let us assume this field to be static.[25]

It is most desirable to examine the orbit of a charged particle in such a field and the earth's magnetic dipole field, and how the cut-off energy varies at a given point on the earth. Unfortunately, Eq. (2.7) cannot be solved analytically and so we are gratified with the first approximotion as follows: Some variation of cut-off

energ, caused by the electro-magnetic field of the current system, seems to be too small to strongly influence the variation of cosmic ray intensity on the earth's surface.[20] So we will neglect the influence of the variation of the cut-off energy and use that of the earth's magnetic dipole field.[21]

§ 3 *Variation of the Intensity Spectrum and Decrease of the Cosmic Ray Intensity by the Electric Field*

Let us suppose that primary cosmic rays are all positive protons, whose differential intensity spectrum is $I(E)dE$, where E is the energy of cosmic rays. From the investigations by many workers, next two types are adovocated as the spectrum.

$$I(E)\,dE=J\cdot E^{-\alpha}\cdot dE, \qquad (3.1)^{(9)}$$

and

$$I(E)\,dE=J\cdot e^{-\alpha E}\cdot dE. \qquad (3.2)^{(8),(22)}$$

In the present state, as it is impossible to decide which is the true representation, we might as well adopt both.[26]

In a static electro-magnetic field, mentioned in Section 2, the variation of the energy of cosmic rays at any point in space is determined by the scalar potential V alone, and does not depend upon their paths. Let us assume a potential at any point on the earth to be V_p, then, arriving at this point from infinity, cosmic ray suffers an energy loss ΔE, where

$$\Delta E=eV_p. \qquad (3.3)$$

So, the primary energy E changes to $E-\Delta E$.

Thus, taking Eq. (2.5) into consideration, the intensity spectrum $I(E)\,dE$ varies to (c.f. Fig. 2)

$$I(E+\Delta E)\cdot\{1-L(E+\Delta E)\cdot\Delta E\}\cdot dE. \qquad (3.4)$$

If we neglect the variation of the cut-off energy of cosmic rays at any point of the earth, as mentioned in the previous section, the decrease of cosmic ray intensity in a given direction by this variation of spectrum is easily obtained at the top of the atmosphere, i.e.,

$$y_v(\%)=\left(1-\frac{\int_{E_\lambda}^{\infty}I(E+\Delta E)\cdot\{1-L(E+\Delta E)\cdot\Delta E\}dE}{\int_{E_\lambda}^{\infty}I(E)dE}\right)\times 100, \qquad (3.5)$$

where E_λ is the cut-off energy in a given direction at geomagnetic latitude λ^0.

But on the earth's surface, how the intensity of cosmic rays varies is not simply determinable by the atmospheric effects. So I will estimate this order in the next.

[A] In the case of $I(E)=J\cdot E^{-\alpha}\cdot dE$

(i) From Eq. (3.5), at the top of the atmosphere, the decrease of intensity becomes

$$y_v(\%)=100\cdot\left[1-\left(\frac{E_\lambda}{E_\lambda+\Delta E}\right)^{\alpha+1}\right]$$
$$+100\,(\alpha-1)\left(\frac{\Delta E}{E_\lambda}\right)\left(\frac{E_\lambda}{E_\lambda+\Delta E}\right)^{\alpha}\cdot\left[\frac{2}{\alpha}-\frac{2}{\alpha+1}\left(\frac{m_0c^2}{E_\lambda+\Delta E}\right)\right.$$

$$+\frac{5}{\alpha+2}\left(\frac{m_0c^2}{E_\lambda+\Delta E}\right)^2-\frac{11}{\alpha+3}\left(\frac{m_0c^2}{E_\lambda+\Delta E}\right)^3+\cdots\cdots\Big]. \quad (3.6)$$

(ii) The decrease of intensity on the ground:—In the case of the variation of the earth's magnetic field, there yields only the variation of the cut-off energy, so we can make the order estimation of the decrease from the latitude effect of the field-sensitive rays at sea-level.

But in the present case, the situation is slightly different from the former, due to variation of the differential intensity spectrum, as in Fig. 2. Let us make two assumptions as follows:

(a) From the latitude effect, when field-sensitive primary cosmic rays with an interval of 1 Bev. arrive on the ground, they correspond to 0.7 per cent of the total intensity on the ground. Let us expand this experimental evidence up to the region of non-field-sensitive rays.

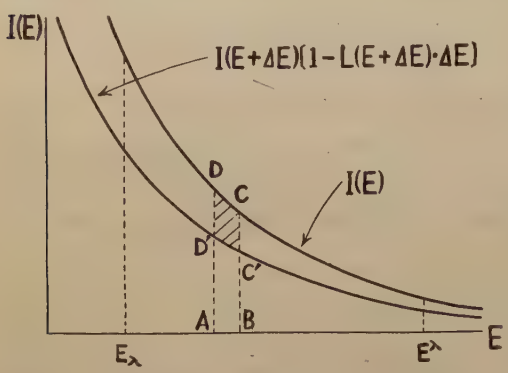

Fig. 2 Variation of the differential intensity spectrum of primary cosmic rays by the electric field. E_λ: cut-off energy at geomagnetic latitude λ^0, and $E^\lambda = E_\lambda + \frac{100}{0.7}\cdot 1\,Bev.$

(b) As a result of this expansion, the primary cosmic rays have an effect of infinite per cent on the ground. This irrationality is avoided by cutting off the spectrum at the suitable energy E^λ, where

$$E^\lambda = E_\lambda + \frac{100}{0.7}\cdot 1\,Bev. \quad (3.7)$$

From these assumptions, area ABCD in Fig. 2 has an effect of dy' per cent on the ground, where

$$dy'(\%) = \frac{0.7}{1\,Bev.}\cdot dE. \quad (3.8)$$

Then the decrease of area DCC'D' by the influence of the electric field brings the decrease of dy per cent, where

$$dy(\%) = \frac{0.7}{1\,Bev.}\cdot\left[1-\frac{I(E+\Delta E)\cdot\{1-L(E+\Delta E)\cdot\Delta E\}}{I(E)}\right]\cdot dE. \quad (3.9)$$

Integrating Eq. (3.9), extending over the interval between E_λ and E^λ, we get the decrease of total intensity on the ground.

$$y(\%) = \int_{E_\lambda}^{E^\lambda} dy = \frac{0.7\,\Delta E}{1\,Bev.}\cdot\Big[(\alpha+2)\,ln\frac{E^\lambda+\Delta E}{E_\lambda+\Delta E} - A\cdot\left(\frac{1}{E_\lambda+\Delta E}-\frac{1}{E^\lambda+\Delta E}\right)$$
$$+\frac{B}{2}\left\{\frac{1}{(E_\lambda+\Delta E)^2}-\frac{1}{(E^\lambda+\Delta E)^2}\right\}-\frac{C}{3}\left\{\frac{1}{(E_\lambda+\Delta E)^3}-\frac{1}{(E^\lambda+\Delta E)^3}\right\}+\cdots\cdots\Big], \quad (3.10)$$

where

$$A = 2(m_0c^2)+\frac{(\alpha+3)\cdot\alpha}{2!}\cdot\Delta E$$

$$B = 5(m_0c^2)^2+2\alpha(m_0c^2)\cdot\Delta E+\frac{(\alpha+4)\cdot\alpha\cdot(\alpha-1)}{3!}(\Delta E)^2$$

$$C = 11(m_0c^2)^3+5\alpha(m_0c^2)^2\cdot\Delta E+\alpha(\alpha-1)(m_0c^2)(\Delta E)^2+\frac{(\alpha+5)\cdot\alpha(\alpha-1)(\alpha-2)}{4!}(\Delta E)^3\cdots \quad (3.11)$$

[B] In the case of $I(E)\,dE=J\cdot e^{-\alpha K}\cdot dE$

(i) From Eq. (3.5), the decrease of cosmic ray intensity at the top of the atmosphere becomes

$$y_U(\%)=100(1-e^{-\alpha\Delta K})+100\alpha\cdot A\Delta E\cdot e^{\alpha K_\lambda}\left[-E_i\{-\alpha(E_\lambda+\Delta E)\}\right]$$
$$+100\,\alpha\cdot\Delta E\cdot e^{-\alpha\Delta K}\cdot\left[-\frac{B}{(E_\lambda+\Delta E)}+\frac{C}{(E_\lambda+\Delta E)^2}-\frac{D}{(E_\lambda+\Delta E)^3}+\cdots\cdots\right], \quad (3.12)$$

where E_i denotes Logarithmic Integral, and

$$A=2+2\,(m_0c^2)\cdot\alpha+5\,(m_0c^2)^2\cdot\frac{\alpha^2}{2\,!}+11\,(m_0c^2)^3\cdot\frac{\alpha^3}{3\,!}+\cdots\cdots$$

$$B=2\,(m_0c^2)+5\,(m_0c^2)^2\cdot\frac{\alpha}{2\,!}+11\,(m_0c^2)^3\cdot\frac{\alpha^2}{3\,!}+23\,(m_0c^2)^4\cdot\frac{\alpha^3}{4\,!}+\cdots\cdots$$

$$C=5\,(m_0c^2)^2\cdot\frac{1}{2}+11\,(m_0c^2)^3\cdot\frac{\alpha}{3\cdot2}+23\,(m_0c^2)^4\cdot\frac{\alpha^2}{4\cdot3\cdot2}+47\,(m_0c^2)^5\cdot\frac{\alpha^3}{5\cdot4\cdot3\cdot2}+\cdots\cdots$$

$$D=11\,(m_0c^2)^3\cdot\frac{1}{3}+23\,(m_0c^2)^4\cdot\frac{\alpha}{4\cdot3}+47\,(m_0c^2)^5\cdot\frac{\alpha^2}{5\cdot4\cdot3}+93\,(m_0c^2)^6\cdot\frac{\alpha^3}{6\cdot5\cdot4\cdot3}+\cdots\cdots \quad (3.13)$$

(ii) The decrease of intensity on the ground:—By the same consideration as in the case of [A], the decrease of intensity becomes

$$dy\,(\%)=\frac{0.7}{1\,Bev.}\left[1-\frac{I(E+\Delta E)\{1-L\,(E+\Delta E)\cdot\Delta E\}}{I(E)}\right]\cdot dE$$
$$=\frac{0.7}{1\,Bev.}\left[1-\frac{I(E+\Delta E)}{I(E)}\right]\cdot dE+\frac{0.7}{1\,Bev.}\cdot\frac{L\,(E+\Delta E)\cdot I(E+\Delta E)\cdot\Delta E}{I(E)}\cdot dE. \quad (3.14)$$

The first term on the right hand side of Eq. (3.14) is not necessary to be calculated under the above mentioned assumptions. For,

$$I(E+\Delta E)=J\cdot e^{-\alpha(K+\Delta K)}=(J\cdot e^{-\alpha\Delta K})\cdot e^{-\alpha K}. \quad (3.15)$$

From this equation, we see that the spectrum of cosmic rays is not influenced by the presence of the electric field, and only its coefficient J changes to $J\cdot e^{-\alpha\Delta K}$. In the other words, the intensity of the primary cosmic rays decreases without varying its intensity distribution at infinity, therefore this effect is transmitted at any point in the atmosphere, regardless of the atmospheric effects upon the cosmic rays. So that the decrease on the ground is

$$y_I(\%)=100\,(1-e^{-\alpha\cdot\Delta K}). \quad (3.16)$$

But the second term cannot be solved by such consideration, so we must use the above mentioned two assumptions.

$$y_{II}(\%)=\frac{0.7\cdot\Delta E}{1\,Bev.}\cdot\int_{K_\lambda}^{K^\lambda}\frac{L\,(E+\Delta E)\cdot I(E+\Delta E)}{I(E)}\cdot dE$$
$$=\frac{0.7\cdot\Delta E}{1\,Bev.}\cdot e^{-\alpha\cdot\Delta K}\cdot\left[2\,ln\frac{E^\lambda+\Delta E}{E_\lambda+\Delta E}-2\left\{\left(\frac{m_0c^2}{E_\lambda+\Delta E}\right)-\left(\frac{m_0c^2}{E^\lambda+\Delta E}\right)\right\}\right.$$
$$\left.+\frac{5}{2}\left\{\left(\frac{m_0c^2}{E_\lambda+\Delta E}\right)^2-\left(\frac{m_0c^2}{E^\lambda+\Delta E}\right)^2\right\}-\frac{11}{3}\left\{\left(\frac{m_0c^2}{E_\lambda+\Delta E}\right)^3-\left(\frac{m_0c^2}{E^\lambda+\Delta E}\right)^3\right\}+\cdots\cdots\right]. \quad (3.17)$$

Then the decrease of total intensity on the ground is

$$y = y_I + y_{II}. \tag{3.18}$$

Figs. 3 and 4 represent the decrease of the vertical intensity in per cent, calculated from Eqs. (3.6), (3.10), (3.12) and (3.18) respectively.

From these figures, we see that the latitude effect of the decrease of cosmic ray intensity is larger in the case of [A] than [B]. We may also conclude that the influence upon the decrease on the ground is more effective in the case of [B] than [A].

In conclusion, we may expect the decrease of intensity of about one or two per cent on the ground by an electric field which makes cosmic rays lose their energies of about 10^8 ev. On the other hand, in the case of the magnetic field, the variation of the cut-off energy of about 10^9 ev. or more is necessary to produce such a decrease on the ground. So the decrease of cosmic ray intensity on the ground is more influenced by the electric field than by the magnetic field.

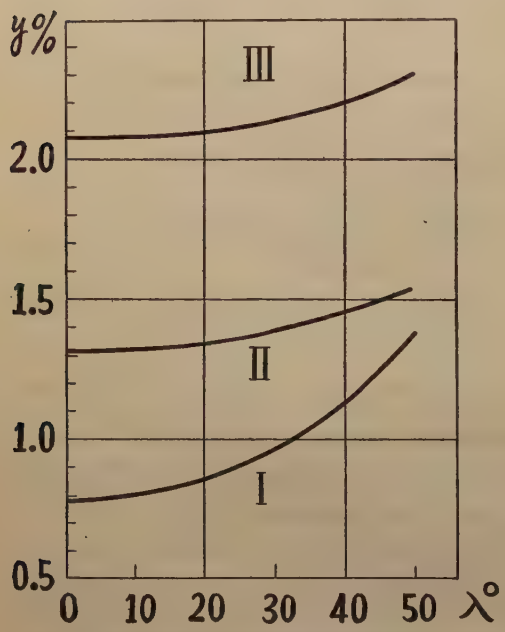

Fig. 3 Decrease of vertical intensity on the ground in per cent, in the case of $\Delta E = 10^8$ ev., as a function of geomagnetic latitude, for various energy spectrums.
Curve I: $I(E)dE = J \cdot E^{-\alpha} \cdot dE$, $\alpha = 2.75$,
Curve II: $I(E)dE = J \cdot e^{-\alpha E} \cdot dE$, $\alpha = 0.1\ Bev.^{-1}$,
Curve III: $I(E)dE = J \cdot e^{-\alpha E} \cdot dE$, $\alpha = 0.176\ Bev.^{-1}$.

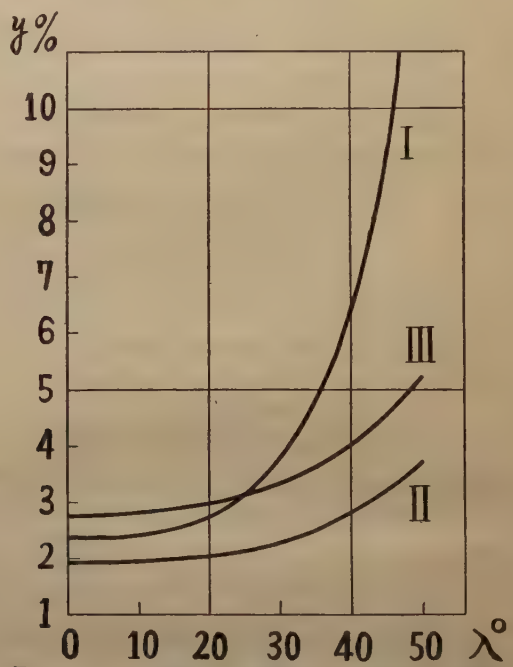

Fig. 4 Decrease of vertical intensity at the upper atmosphere, in per cent, in the case of $\Delta E = 10^8$ ev., as a function of geomagnetic latitude, for various energy spectrums. Curves I, II and III correspond to the Curves in Fig. 3, respectively.

§ 4. *The Magnetic Storm Model*

From the above calculation, the intensity of cosmic rays is decreased by the amount of about one or two per cent on the ground by the influence of the potential of about 10^8 volts. But we cannot adopt the electric field of the stream, adovocated

by H. Alfvén, to explain the cosmic ray storm, because it is difficult to interpret experimental evidence (A) by this hypothesis. It is necessary to assume an electric field, growing with the current system.

Of many theories of magnetic storm, it seems most appropriate to adopt that of S. Chapman and V.C.A. Ferraro.[16] They suppose a neutral ionized stream, emitted from the sun with a velocity of about $2 \cdot 10^8$ cm/sec. The earth entering into this stream, a westward current is produced. Its shape is uncertain, and for mathematical simplicity, it is said to be an equatorial ring current, spherical current or cylindrical current.

It seems to be hopeless at present to determine more clearly the current system from the observations of the magnetic field alone. To examine the auroral phenomena during the magnetic storm[14],[18],[28] is another way to determine the current system. Also, cosmic ray phenomena during the magnetic storm may be able to determine it.

In the next, I will examine the current system from the point of view that the cosmic ray storm will be explained by the electric field.

As pointed out by S. Chapman and V.C.A. Ferraro,[17] or recently by D.F. Martyn,[18] there must exist a radial electric field in the current system to stabilize itself. If an equatorial ring current is adopted, the potential difference, produced between the outer and the inner side of the ring current, is necessary to be more than 10^8 volts in order to produce the potential of about 10^8 volts on the earth. Then the energy of charged particle, incident upon the auroral zone from the ring[27], is much larger than the observed one. But, if a closed current system, surrounding the earth, is adopted, the above difficulty is avoided, and furthermore the electric field of this system influences most effectively upon the cosmic rays. But as we have no knowledge about the current system, produced practically, we must be satisfied with the next approximation as follows: An infinite cylindrical current is adopted as an idealized current system for a mathematical simplicity to estimate the electric field of the

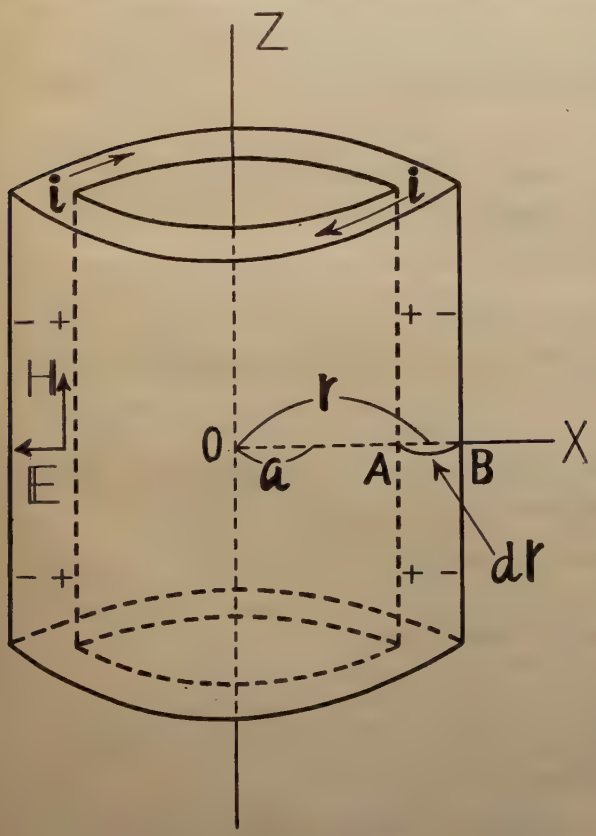

Fig. 5 Cylindrical current system as an idealized magnetic storm model.

current, as shown in Fig. 5. We will then consider the effects produced by the difference between the idealized system and the practical one.

In conclusion, the current system, required from the stand-point of the electric field hypothesis of the cosmic rays storm, is that which produces a potential of the order of about 10^8 volts on the earth.

§ 5. *Estimation of Electric Field connected with Magnetic Storm*

Let us examine the electric field produced by the current system by using the above-mentioned idealized model. As pointed out in previous section, a radial electric field is required in the cylindrical current system for the stability of itself, as shown in Fig. 5. According to the storm theory of Chapman and Ferraro,[17] the equations of the motion of charged particles in the current are

$$-m_i u_i^2/r = eE - eu_i H, \tag{5.1}$$

$$-m_e u_e^2/r = -eE + eu_e H. \tag{5.2}$$

where

m_e, m_i: masses of electron and ion respectively,

u_e, u_i: velocities of electron and ion respectively, (west-ward positive),

E: polarized electric field,

H: magnetic field.

Adding Eq. (5.1) and (5.2),

$$m_i u_i^2 \fallingdotseq m_i u_i^2 + m_e u_e^2 = reH(u_i - u_e). \tag{5.3}$$

From Eq. (5.3), $u_i > u_e$.

Moreover, Chapman and Ferraro also deduce the next relation,

$$(u_i - u_e) \ll u_i \text{ or } u_e.$$

The distance between the center of the earth and the current system is

$$Z = (\beta/Nm_i u_i^2)^{\frac{1}{6}}, \tag{5.4}$$

$$Z = r/a, \tag{5.5}$$

where

a: earth's radius,

r: distance between the earth's center and the current system,

N: numbers of electrons or ions per c.c.,

$$\beta = \text{constant} = \begin{cases} \dfrac{2H_a^2}{4\pi} & \text{(Chapman's estimation[17])}, \\ \dfrac{H_a^2}{4\pi} & \text{(Martyn's estimation[18])}, \end{cases} \tag{5.6}$$

H_a: earth's magnetic field at the earth's surface.

Let the current denote i, flowing in the unit length of the cylindrical shell, then

$$i = Ne(u_i - u_e) \cdot dr. \tag{5.7}$$

Also, the decrease of the horizontal component of earth's magnetic field by this current is

$$\Delta H = 4\pi i. \tag{5.8}$$

If we neglect the magnetic field produced by the charged particles, and adopt approximately the equation $H=H_a/Z^3$, we get the next relation from Eqs. (5.3), (5.4), (5.7) and (5.8).

$$dr=\frac{H_a\cdot\Delta H\cdot a}{4\pi}\cdot\frac{Z^4}{\beta}. \tag{5.9}$$

The electric field, produced in the current shell, is approximately

$$\boldsymbol{E}\fallingdotseq u_i\cdot\boldsymbol{H}=u_i\cdot\frac{H_a}{Z^3}. \tag{5.10}$$

From Eqs. (5.9) and (5.10), the potential difference between A and B becomes (c.f. Fig. 5)

$$V=\boldsymbol{E}\cdot dr=u_i\cdot\frac{H_a^2\cdot\Delta H\cdot a}{4\pi}\cdot\frac{Z}{\beta}$$

$$\frac{H_a^2\cdot\Delta H\cdot a}{4\pi}\cdot u_i\cdot\frac{(\beta/Nm_iu_i^2)^{\frac{1}{6}}}{\beta}. \tag{5.11}$$

Table I Calculated values of ΔE and Z

Case (i) $\beta=\frac{H_a^2}{4\pi}$. (Martyn's estimation)

N	$\Delta H(\gamma)$	u_i (cm/sec.)	$1\cdot10^8$	$2\cdot10^8$	$3\cdot10^8$	$4\cdot10^8$
20	100	ΔE(e.v.) =	$3.5\cdot10^6$	$5.6\cdot10^6$	$7.3\cdot10^6$	$8.9\cdot10^6$
		Z =	5.5	4.4	3.9	3.5
20	200	ΔE(e.v.) =	$7.1\cdot10^6$	$1.1\cdot10^7$	$1.5\cdot10^7$	$1.8\cdot10^7$
		Z =	5.5	4.4	3.9	3.5
100	100	ΔE(e.v.) =	$2.7\cdot10^6$	$4.3\cdot10^6$	$5.6\cdot10^6$	$6.8\cdot10^6$
		Z =	4.2	3.4	2.9	2.7

Case (ii) $\beta=\frac{1}{20}\cdot\frac{H_a^2}{4\pi}$. (1/20 of Martyn's estimation)

N	$\Delta H(\gamma)$	u_i (cm/sec.)	$1\cdot10^8$	$2\cdot10^8$	$3\cdot10^8$	$4\cdot10^8$
20	100	ΔE(e.v.) =	$4.3\cdot10^7$	$6.8\cdot10^7$	$8.9\cdot10^7$	$1.1\cdot10^8$
		Z =	3.4	2.7	2.3	2.1
100	100	ΔE(e.v.) =	$3.3\cdot10^7$	$5.2\cdot10^7$	$6.9\cdot10^7$	$8.3\cdot10^7$
		Z =	2.6	2.1	1.8	1.6

Case (iii) $\beta=\frac{1}{50}\cdot\frac{H_a^2}{4\pi}$. (1/50 of Martyn's estimation)

N	$\Delta H(\gamma)$	u_i (cm/sec.)	$1\cdot10^8$	$2\cdot10^8$	$3\cdot10^8$	$4\cdot10^8$
20	100	ΔE(e.v.) =	$9.2\cdot10^7$	$1.5\cdot10^8$	$1.9\cdot10^8$	$2.3\cdot10^8$
		Z =	2.9	2.3	2.0	1.8
100	100	ΔE(e.v.) =	$7.0\cdot10^7$	$1.1\cdot10^8$	$1.5\cdot10^8$	$1.8\cdot10^8$
		Z =	2.2	1.8	1.5	1.4

In this case, the potential, produced on the earth by this current system, equals to V in Eq. (5.11). Therefore, cosmic rays, arriving to the earth from infinity, lose their energies by an amount of ΔE, respectively, where

$$\Delta E = eV. \tag{5.12}$$

Table I shows the calculated values of Eq. (5.12) for various values of ΔH, N, u_i and β, where proton's mass is adopted as the value of m_i.

But, it is for a mathematical simplicity and not essential to adopt such an infinite cylindrical current system. I will show this in the next. It is clear that the practical current system has no infinite length, but we have no knowledge about its shape or its dimensions. Therefore, by using an eqatorial ring current which is extremely different in shape from the infinite cylindrical current, let us estimate the potential produced on the earth and compare with that of the cylindrical current. If the difference of both potentials will be small, it will be able to say that the potential produced on the earth by the practical current system will be not different very much from that of the infinite cylindrical current system.

In the case of the ring current, the potential difference, produced between the outer and the inner side of the ring current, is

$$V_R = \frac{\sqrt{2}\cdot H_a^{\frac{3}{2}}\cdot \Delta H^{\frac{1}{2}}\cdot a}{\pi}\cdot u_i \cdot \frac{(\beta/N m_i u_i^2)^{-\frac{1}{12}}}{\beta^{\frac{1}{2}}}. \tag{5.13}$$

In a case of $N=20$, $\Delta H = 10^{-3}$ Gauth, $u_i = 2\times 10^8$ cm/sec., and $\beta = H_a^2/4\pi$,

$$V_R = 1.44\times 10^7 \text{ volts}. \tag{5.14}$$

The potential produced on the earth by this ring current becomes approximately to one-sixth of V_R in Eq. (5.13) after some calculation. Then

$$V = 2.4\times 10^6 \text{ volts}. \tag{5.15}$$

From Table I, in the infinite cylindrical current,

$$V = 5.6\times 10^6 \text{ volts}. \tag{5.16}$$

Therefore, the potential produced on the earth in the case of the ring current equals to about a half or one-third of that of the infinite cylindrical current. From the above calculation, it can be said that the practical current system produces about the same potential on the earth as the infinite cylindrical current system.

§ 6. *Explanation of the Cosmic Ray Phenomena during the Magnetic Storm by the Electric Field*

From the standpoint of the electric field hypothesis, let us examine how the cosmic rays phenomena, connected with the magnetic storm, can be explained.

(i) Exp. Evi. (A) is explainable by the potential, produced on the earth by the current system. Quantitatively, the decrease of cosmic ray intensity, expected theoretically from the electric field of Chapman's storm theory, is one-tenth or one-twentieth of the observed value, as seen from Fig. 4 and Table I.

From Eq. (5.11) and Table I, this theoretical value is proportional to $u_i^{\frac{2}{3}}$, $N^{-\frac{1}{6}}$ and $\beta^{-\frac{5}{6}}$ respectively, so it is not influenced by the variation of N, but largely by the

variations of u_i and β.

It is undesirable to adopt such a large value of u_i as 2×10^9 cm/sec., for its value is supposed to 2×10^8 cm/sec. from the magnetic storms. Decreasing of the value of β is a way to increase the energy loss of cosmic ray, as shown in Table I. β is a parameter for determining, to what distance from the earth's center arrives the solar stream, and is given different values by Chapman and Martyn, respectively. If we can expect β to be one-twentieth or one-fiftieth of Martyn's estimation, the decrease of the cosmic ray intensity will be explainable by such an electric field. But it may not be necessary for β to be ievested with such a small value because we are quite ignorant about the current system, so there may be something which makes the potential larger.

(ii) As mentioned above, we cannot get a satisfactory result quantitatively, but it seems to be very reasonable to account for other phenomena by this electric field.

(a) It seems to be suitable in explaining Exp. Evi. (C), because there are no cosmic rays arriving at any earth's surface without suffering their energy losses by the electric field. This discussion holds true only if the potential of the earth is higher than that of infinity and does not depend upon the shape of the current system. But also in this case, the closed current system is most effective.

(b) S.E. Forbush[4] pointed out that the decrease of cosmic ray intensity had latitude effect of several per cent on the ground. Theoretically, if $J\cdot E^{-\alpha}$ is adopted, the calculated latitude effect is too large, compared with the observed one. But if $J\cdot e^{-\alpha K}$ is adopted, the calculated effect seems to be very reasonable to account for the observations, as in Fig. 3.

(c) As for Exp. Evi. (D), the interpretation is quite contrary to that of the magnetic field hypothesis,[23] as stated in Sect. 1. From Eq. (5.11), the larger the radius of the current system, the smaller the decrease of cosmic ray intensity. But, we must not forget, the above expression only holds in the case of N=constant.

(d) There is no explanation for Exp. Evi. (F) at present, but it does not seem to me to be impossible to search for it.

(e) Although the cause of the diurnal variation of cosmic rays is obscure at present, it may be sure that the diurnal variation is produced by the low energy region of cosmic rays. When the intensity of cosmic rays decreases with the growth of the electric field of the current system, the ratio of the low energy part to the total intensity decreases, i.e., the amplitude of the diurnal variation decreases slightly (c.f. Fig. 2). Although this decrease will be far smaller than that of the variation of magnetic field, we cannot explain the increase of the amplitude of the diurnal variation of cosmic rays by the electric field of the current system. It is necesssary to assume another cause to explain this phenomenon.

In conclusion, it seems to be very reasonable to account for the cosmic ray phenomena during the magnetic storm by such an electric field, except for the insufficiency of the decrease of intensity.

§ 7. *Observations which will determine the True Cause of Cosmic Storm*

As mentioned in a previous section, everything is working smoothly, in the case of the electric field hypothesis than the magnetic one. But we must not forget that the observations at the higher atmosphere during the magnetic storms play important roles, in judging the relative merits of these hypotheses.

If the decrease of cosmic ray intensity should be explained by an improved Chapman's magnetic field hypothesis, what should be the decrease at the upper atmosphere? This is estimated from the latitude effect on the ground, as the variation of magnetic field will cause only that of the cut-off energy. In Fig. 6, the decreases of intensity at the upper atmosphere are shown for various energy spectrums and latitudes, when that of the ground is just one per cent. At the same time, Fig. 6 also contains that of the electric field hypothesis. But the latter is a rough approximation for we neglect the variation of the cut-off energy.[20]

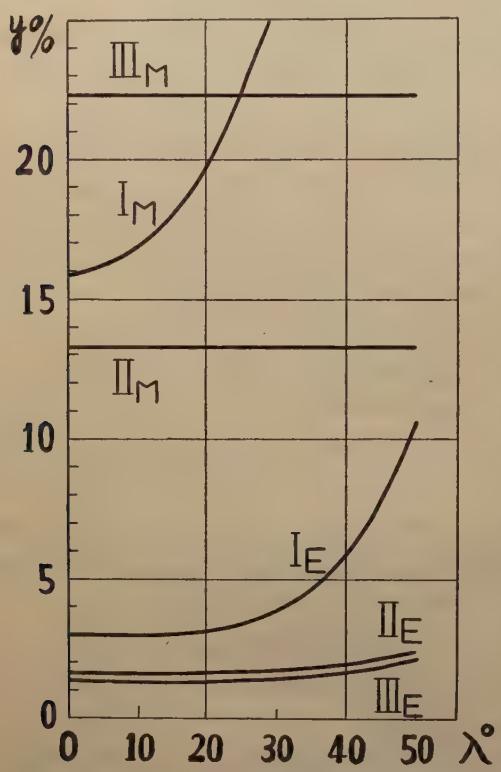

Fig. 7 Assumed decrease of vertical intensity at the upper atmosphere, in per cent, as a function of geomagnetic latitude, for various energy spectrums, when that of the ground is just one per cent.
Curve I: $I(E)dE=J\cdot E^{-\alpha}\cdot dE$, $\alpha=2.75$,
Curve II: $I(E)dE=J\cdot e^{-\alpha K}\cdot dE$, $\alpha=0.1$ *Bev.*$^{-1}$
Curve III: $I(E)dE=J\cdot e^{-\alpha K}\cdot dE$, $\alpha=0.176$ *Bev.*$^{-1}$
and subscripts M and E represent the curves, obtained from the magnetic field hypothesis and the electric one, respectively.

From these figures, we see that the decrease of intensity at the upper atmosphere is larger in the case of the magnetic field hypothesis than the electric one. If we are able to know the decreases at various altitudes from the observations, it will be decided which is the true cause.

There is another way to decide the true cause. In the case of the magnetic field hypothesis, it is low energy region of cosmic rays that is prevented to arrive at the earth by the increase of the earth's magnetic dipole-moment, and therefore there is no variation on the higher energy region.

On the other hand, in the case of the electric field hypothesis, the decrease of intensity occurs not only in a region of low energy but also in that of high energy (c.f. Fig. 2). So the observation of high energy region of cosmic rays during the magnetic storm is a key to determine the true cause.

Unfortunately, we cannot do it at

once for the absence of such data, so it is most desirable to make such observations in future.

§ 8. *Conclusion*

It must be emphasized that adopting the infinite cylindrical current as the west-ward current system during the magnetic storm is only for a mathematical simplicity and is never essential. The discussions mentioned in the previous hold good also strictly in the case of the practical current system, because the electric field in the current system produces a potential on the earth, though less effective than the idealized one, as stated in Sect. 5.

The difficulty with which this electric field hypothesis is confronted at present, is that the decrease of cosmic ray intensity is of the order ten or twenty times too large to be accounted for by the electric field, deduced from the Chapman's storm theory.

Except for this, it seems to be very reasonable to account for the cosmic ray phenomena, connected with the magnetic storm, by this electric field hypothesis. Thus, the relation between the magnetic and cosmic ray storm seems to be accounted for from the standpoint of the electric field, but the connection of the auroral phenomena with them remains obscure.

Lastly, next two observations of the cosmic rays;—(i) the decrease of the high energy component of cosmic rays during the magnetic storm, and (ii) the decreases of the cosmic rays at higher altitudes during the magnetic storm,—are most important for determining the true cause of the cosmic ray storm. It is most desirable to make such observations and determine the cause of the cosmic ray storm.

Acknowledgements

In conclusion, the writer wishes to express his hearty thanks to Prof. Dr. M. Hasegawa, for his constant interest in and encouragement to, the present research, and to Dr. Y. Tamura and Dr. M. Ota for their kind advices, and also to Dr. T. Nagata, Dr. Y. Sekido and Mr. J. Nishimura for their many valuable criticisms and discussions in relation to this work.

References

(1) S. Chapman, Nature, **140**, 425 (1937).
(2) S.E. Forbush, Phys. Rev., **51**, 1108 (1937).
(3) V.F. Hess and A. Demmelmair, Nature, **140**, 310 (1937).
(4) S.E. Forbush, Terr. Mag., **43**, 203 (1938).
(5) D.H. Loughridge and P.F. Gast, Phys. Rev., **57**, 937 (1940).
(6) Y. Sekido and S. Yoshida, Rep. Ionos. Res. in Japan, **4**, 37 (1950).
(7) See for example, M.S. Vallarta, "On the allowed cone of cosmic radiation," Toronto Univ. Press (1938).
(8) T.H. Johnson, Rev. Mod. Phys., **10**, 193 (1938).

(9) See for example, L. Jánossy, "Cosmic Rays," Oxford, (1950).

(10) T. Yagi, Journal of the Cosmic Ray Institute, Nagoya Univ. in Japan, Vol. **3**, no. 2, 1 (1949).

(11) T.H. Johnson, Terr. Mag., **43**, 1 (1938).

(12) J. Clay and E.M. Bruin, Physica, **5**, 111 (1938).

(13) E. Bruche, Terr. Mag., **36**, 41 (1931).

(14) T. Nagata, J. Geophys. Res., **55**, 127 (1940)

(15) S. Hayakawa J. Nishimura, T. Nagata and M. Sugiura, J. of Sci. Res. Inst. in Japan, **44**, 121 (1950).

(16) S. Chapman and V.C.A. Ferraro, Terr. Mag., **36**, 77 and 171 (1931); Terr. Mag., **37**, 147 (1932).

(17) S. Chapman and V.C.A. Ferraro, Terr. Mag., **38**, 79 (1933).

(18) D.F. Martyn, Nature, **167**, 92 (1951).

(19) W.F.G. Swann, Phys. Rev., **44**, 224 (1933).

(20) This effect becomes large and cannot be neglected on the upper atmosphere. But on the earth's surface, such assumption will be held approximately. I will consider this elsewhere.

(21) See for example, R.A. Alpher, J. of Geophys. Res., **55**, 437 (1950).

(22) Hu Chien Shan, Phys. Rev., **60**, 614 (1941).

(23) For example, Y. Katô and T. Kanno, Sci. Rep. Tôhoku Univ. in Japan, Series 5, Vol. 2, 1 (1949).

(24) H. Alfvén, Phys. Rev., **75**, 1732 (1949); and "Cosmical electro-dynamics," Oxford (1940).

(25) The influence of a variable field upon the cosmic rays is not so large in the case of the magnetic storm. I will consider this elsewhere.

(26) Recently, a new type of the intensity spectrum of cosmic rays was adovocated, which had a maximum in the low energy region. But the effect, which this new type of spectrum will influence upon the cosmic ray variation, will not be much different from that of the spectrum employed here.
H.V. Neher, Phys. Rev., **83**, 649 (1951),
Chang-Yun Fan, Phys. Rev., **82**, 211 (1951).

(27) This idea was suggested by D.F. Martyn. (c.f. Ref. 19.)

(28) H. Alfvén, Kungl. Svenska Vet. Hand. Tredje Serien Band 18. N:o 3.

Letters to Editor

On a self-exciting process in magneto-hydrodynamics

Recently, a simple and plausible explanation of the non-dipole part of the earth's magnetic field and its secular variations was proposed by W. M. Elsasser and E. C. Bullard. The variations are attributed to hydrodynamical eddies in the earth's core and to changes in electric current systems in the outer part of the core caused by the eddies. This success leads to the idea that the whole magnetic field of the earth is ultimately produced and maintained by a mechanism of induction. Elsasser discusses the relation between the field and motion in a very general way and concludes that there may exist chains of relations in which a field H_1 interacts with a motion V_1 to produce a field H_2 which, in turn, interacts with another motion V_2 to reproduce H_1. If it is possible to show the existence of such a "self-exciting dynamo" in the earth's core, the main field might also be explained. All that is necessary is a weak initial field to start with, and the field will then grow automatically until the energy dissipated as Joule's heat becomes equal to that supplied.

On the other hand, T. G. Cowling showed that the self-exciting process is impossible if the motion of the fluid is rotationally symmetrical about an axis and is confined to meridian planes. In addition, Elsasser showed that the same is also true for purely toroidal flow. Many believe that these theorems are foretastes of a stronger theorem that will prove the self-exciting process is impossible at all. In this connection, Bullard proposed a convection current model, which does not violate the above theorems, and by which the self-exciting dynamo may be possible. We have examined the problem whether the magneto-hydrodynamical equations have a solution representing the self-exciting process which is appropriate to the Bullard's model.

The problem is reduced to solve the following differential equations for the radial parts of the magnetic fields S_1^0, T_2^0, T_2^{2c} and T_2^{2s}.

$$
\begin{aligned}
&(16/3)\cdot[d^2S_1^0/dr^2+4/r\cdot dS_1^0/dr]-(48\times24/5)\cdot r^2V_2^{2c}T_2^{2s}=0\\
&(24/5)\cdot[r\cdot d^2T_2^0/dr^2+6\cdot dT_2^0/dr]-(16/5)\cdot4\pi\kappa\cdot dV_1^0/dr\cdot S_1^0\\
&\quad-(288\times6/35)\cdot4\pi\kappa\cdot r^{-2}[d(r^4V_2^{2c}T_2^{2c})/dr+d(r^3V_2^{2c})/dr\cdot rT_2^{2c}]=0,\\
&(48\times6/5)\cdot[r\cdot d^2T_2^{2c}/dr^2+6\cdot dT_2^{2c}/dr]+(96\times6/5)\cdot4\pi\kappa\cdot V_1^0rT_2^{2s}\\
&\quad-(288\times6/35)\cdot4\pi\kappa\cdot r^{-2}[d(r^4V_2^{2c}T_2^0)/dr+d(r^3V_2^{2c})/dr\cdot rT_2^0]=0,\\
&(48\times6/5)\cdot[r\cdot d^2T_2^{2s}/dr^2+6\cdot dT_2^{2s}/dr]-(96\times6/5)\cdot4\pi\kappa\cdot V_1^0rT_2^{2c}-(96\times2/5)\cdot\\
&4\pi\kappa\cdot r^{-2}[3r^3V_2^{2c}\cdot d(dS_1^0/dr+2/r\cdot S_1^0)/dr+d\{d(r^3V_2^{2c})/dr\cdot S_1^0\}/dr]=0,\quad(1)
\end{aligned}
$$

where κ is the electric conductivity of the earth's core and r is the distance from the center of the earth. The radial parts of the fluid velocity fields V_1^0 and V_2^{2c} are put tentatively

$$V_1^0(r)=a^{-1}V_{1.0}[1-(r/a)],\quad V_2^{2c}(r)=a^{-1}V_{2.2c}[1-(r/a)]^2,\quad(2)$$

where a is the radius of the earth's core and $V_{1.0}$ and $V_{2.2c}$ are undetermined cons-

tants of the dimensions of velocity. The boundary conditions imposed on the radial functions S_1^0, T_2^0, T_2^{2c} and T_2^{2s} are $T_2^0(r)=T_2^{2c,s}(r)=0$ (3), $S_1^0(r)+r/3\cdot dS_1^0/dr=0$ (4) at $r=a$. The radial functions should also be finite at $r=0$. Thus our problem is reduced to solve (1) with (2) under the boundary conditions (3) and (4). It is easily seen that this is an eigen-value problem for $V_{1,0}$ and $V_{2,2c}$. If we get real eigen-values for $V_{1,0}$ and $V_{2,2c}$ by solving the problem, we can thus prove that the process proposed by Bullard is self-exciting. An approximate method is used to obtain the eigen-values, and later this approximate method is shown to be good enough for studying the present problem. The eigen-values $4\pi\kappa aV$ (where V's denote the maximum values of the velocities concerned) thus obtained are of the orders of 10^2 c.g.s. e.m.u. These results are to be compared with those obtained by Elsasser and Bullard in their discussions on the secular variation of the earth's magnetic field, i.e., $\kappa=3.\ 10^{-6}$ e.m.u., $V\sim10^{-2}$, $a=3.\ 10^8$, $4\pi\kappa aV\sim10^2$. The results obtained by us show that a self-exciting dynamo is possible by which the earth's magnetic field is produced and maintained. The self-exciting dynamo is considered to have the similar structure as supposed by Elsasser and Bullared in their studies on the secular variation of the earth's magnetic field.

H. Takeuchi and Y. Shimazu

Geophysical Institute, Faculty of Science,
Tokyo University, Tokyo, Japan.

Drifting of *Es* Ionic Clouds

Drifting of *Es* ionic clouds in Japan was already discussed by the author (1). It was obtained in the study that the direction of the drifting changed semi-diurnally with a mean speed of about 100 m/s and that southward drifting during 19-01h. was the most frequently and conspicuous. From an estimation for relations between the drifting and terrestrial magnetism, it was assumed in the report that the southward drifting during this period of 19–01h., in the northern hemisphere, might occur in region of higher latitudes than the center of an electric current that produced geomagnetic daily variation, and that northward drifting might occur in the lower latitudes during this period,—in the southern hemisphere, these relations would be reverse.

In this report, some examples surporting this estimation are obtained from observational data in foreign stations besides Japanese stations.

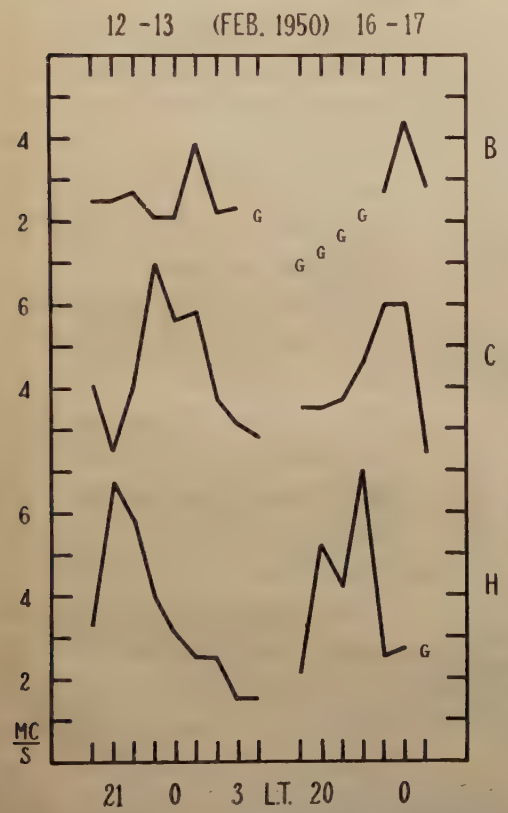

Fig. 1 *fEs* variations representing northward drifting of *Es* at Brisbane, Canberra and Hobart.

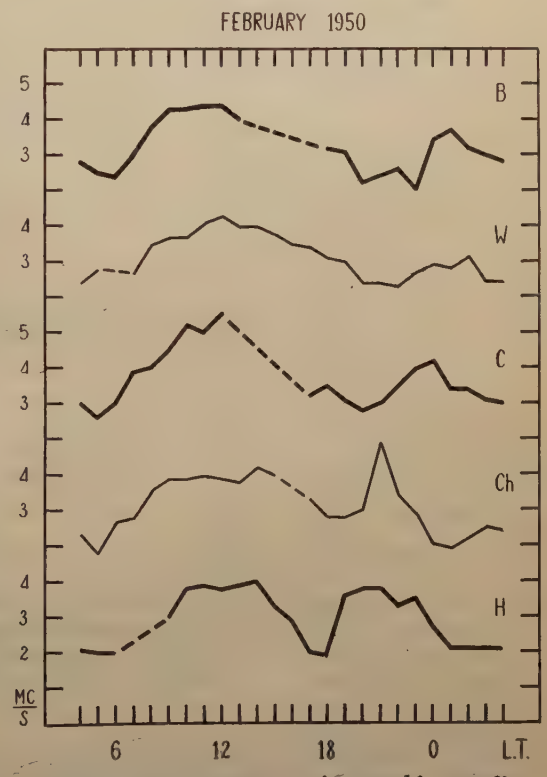

Fig. 2 Variation-curves of monthly median values of *fEs* representing northward drifting of *Es* during 19–01h.. B, C and H of big lines are respectively Brisbane, Canberra and Hobart situated on almost same meridian, and W and Ch of fine lines are Watheroo and Christchurch situated in the neighbourhood of those three stations.

Northward drifting of *Es* at three stations situated on almost same meridian, Brisbane (153.0°E, 27.5°S), Canberra (149.°E, 35.3°S) and Hobart (147.4°E,

42.8°S) in Australia, as shown in Fig. 1, may occur frequently during 19–01h. in summer.

This tendency is seen in variation-curves of monthly median values of *fEs* too, at these stations and Watheroo (115.9°E, 30.3°S) and Christchurch (172.6°E, 43.5°S), as shown in Fig. 2. Its mean speed in these examples is about 100–150 m/s. As these stations seem to situate in higher latitudes than the center of the dynamo-current of the southern hemisphere in summer, such northward drifting is favourable to above-mentioned estimation.

On the other hand, variation-curves of monthly median values of *fEs* at Wakkanai (141.7°E, 45.4°N), Fukaura (139.9°E, 40.6°N), Shibata (139.3°E, 37.9°N), Lanchow (103.8°E, 36.1°N), Kokubunji (139.5°E, 35.7°N), Yamagawa (130.6°E, 31.2°N), Chungking (106.8°E, 29.4°N), Okinawa (127.8°E, 26.3°N), Guam (144.8°E, 13.5°N) and Leyte (125.0°E, 11.0°N) are compared in Fig. 3, and their remarkable variations during 19–01h. extracted from the figure will be seen in Fig. 4. Southward drifting at first seven stations is conspicuous in the figure as already reported, and northward drifting seems to occur at Guam and Leyte with a speed of comparable order abovementioned, though fine variations of drifting in each day at these two stations can not be obtained because of lack of values in each day. These examples also may be favourable to the above-estimated relations.

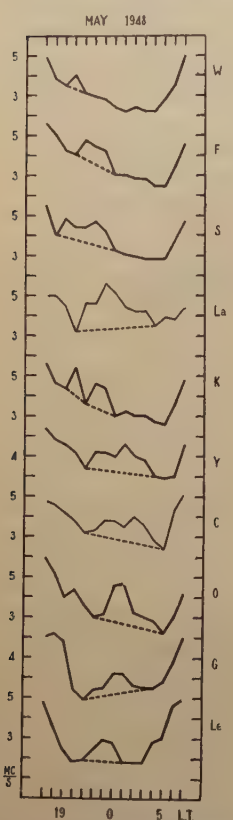

Fig. 3 Variation-curves of monthly median values of *fEs*. Stations are Wakkanai, Fukaura, Shibata, Kokubunji, Yamagawa, Okinawa, Guam and Leyte (big lines) located near same meridian, and Lanchow and Chungking (fine lines) located in the neighbourhood of those stations.

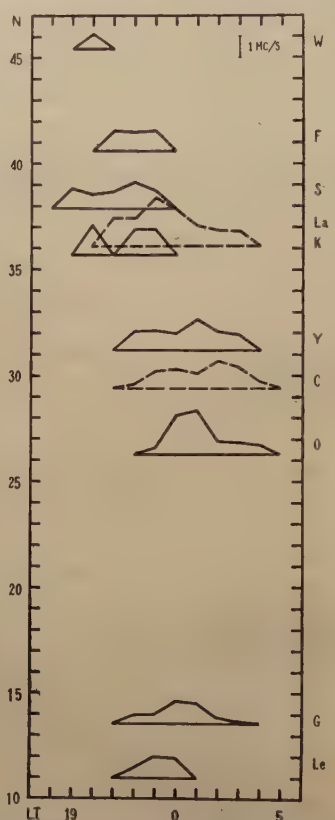

Fig. 4 Deviations from dotted lines in each variation-curve of Fig. 3, concerning the geographic latitude of each station.

In conclusion, the author wishes to express his sincere thanks to Prof. M. Hasegawa for helpful suggestions, and also to Miss M. Kato for her assistance.

By Sadami MATSUSHITA
Geophysical Institute, Kyoto University

(1) S. Matsushita, J. Geomag. Geoelect., **1**, 35, 41 (1949), **2**, 9 (1950).

Errata

K. MAEDA and M. IZAKI, Some Applications of Modern Mathematical Statistics to the Lunar Tidal Analysis of Ionospheric Height.
(Vol. III, No. 1, April, 1951)

Page	Line	In Place of	Read
1	title	Application	Applications
1	title	Statistic	Statistics
1	1	lunnar	lunar
1	1	anlyses	analyses
1	11	significince	significance
1	17	importants	important
1	6*	find and	find an
2	11*	scaling skill	scaling and the scaling skill
2	5*	rhe	the
3	23	abserved	observed
3	6*	discribed	described
3	5*	normol	normal
4	1	$F=\frac{\frac{1}{2}[(\hat{a}_r-a_r)^2+\cdots}{2}\ \frac{\frac{1}{2}\sum_{t=1}^{N}u_t{}^2-\left(\frac{1}{N}\sum_{t=1}^{N}u_t\right)^2\cdots}{N-2h-1}$	$F=\frac{\frac{1}{2}[(\hat{a}_r-a_r)^2+\cdots}{2}\Big/\frac{\frac{1}{2}\sum_{t=1}^{N}u_t{}^2-\left(\frac{1}{N}\sum_{t=1}^{N}u_t\right)^2\cdots}{N-2h-1}$
5	2	obtain.	obtain F_0.
6	2*	$e^{-\frac{2m^2\pi^2\sigma^2}{k^2}}$	$e^{-\frac{2n^2\pi^2\sigma^2}{k^2}}$
7	21	ebuation	equations

* As counted from the bottom

The Meeting of the Society of Terrestrial Magnetism and Electricity.

The 10h General Meeting. Held at Kyoto University on Oct. 21–23, 1951.

54 Reports were read, about 100 Members assembled.

JOURNAL OF GEOMAGNETISM AND GEOELECTRICITY

Vol. III, 1951

INDEX OF AUTHORS

JOURNAL OF GEOMAGNETISM AND GEOELECTRICITY
TABLE OF CONTENTS

Vol. III, No. 1, 1951

Vol. III, No. 2, 1951

Vol. III, No. 3–4, 1951

昭和27年3月15日　印刷
昭和27年3月20日　發行
第3卷第3, 4號　定價300圓
（國外定價360圓）

編輯兼發行者　日本地球電氣磁氣學會
代表者　長谷川万吉

印刷者　京都市下京區上鳥羽學校前
田中幾治郎

賣捌所　丸善株式會社京都支店
丸善株式會社　東京・大阪・名古屋・仙台・福岡

JOURNAL OF GEOMAGNETISM AND GEOELECTRICITY

Vol. III No. 3–4

1951

CONTENTS

JOURNAL
OF
GEOMAGNETISM
AND
GEOELECTRICITY

VOL. IV

1952

SOCIETY
OF
TERRESTRIAL MAGNETISM AND ELECTRICITY
OF
JAPAN

KYOTO